The Relative Importance of CYP26A1 and CYP26B1 in Mediating Retinoid Homeostasis: Studies on the Formation, Elimination and Biological Activity of All-*trans*-Retinoic Acid Metabolites

Ariel R. Topletz

A dissertation submitted in partial fulfillment of the requirements for the degree of

Doctor of Philosophy
University of Washington
2013

Reading Committee:
Nina Isoherranen, Chair
Jashvant D Unadkat
Joanne Wang

Program Authorized to Offer Degree:
Department of Pharmaceutics

University of Washington

Abstract

Ariel R. Topletz

Chair of the Supervisory Committee:
Associate Professor Nina Isoherranen
Department of Pharmaceutics

All-trans-retinoic acid (*at*RA), the active metabolite of Vitamin A (retinol), is an essential nutrient during both fetal development and adult life. The concentration of *at*RA within a cell is tightly regulated by the synthesis and elimination of *at*RA. One of the major elimination pathways for *at*RA is oxidation, predominantly by the cytochrome P450s CYP26A1 and CYP26B1 that efficiently hydroxylate *at*RA. The role of both CYP26A1 and CYP26B1 is believed to be to inactivate *at*RA, and both are essential for correct fetal development. It is not known whether both enzymes play crucial roles during adult life.

In this work, the differences in the catalytic efficiency of CYP26A1 and CYP26B1 and the metabolites formed from *at*RA by CYP26A1 and CYP26B1 were explored. The subsequent metabolism and the activity of *at*RA metabolites were also evaluated. CYP26A1 was determined to form 4-OH-RA from *at*RA more efficiently (K_m = 50 nM, Cl_{int} = 190 µL/min/pmoles P450) than CYP26B1 (K_m = 19 nM, Cl_{int} = 43 µL/min/pmoles P450). In addition, formation of 4-OH-RA by CYP26A1 was stereoselective resulting in formation of (4S)-OH-RA whereas no significant stereoselectivity in 4-OH-RA formation by CYP26B1was observed. The primary hydroxylated metabolites of *at*RA, (4S)-OH-RA, (4R)-OH-RA and 18-OH-RA, and the secondary metabolite, 4-oxo-RA, were all found to be substrates of CYP26A1 and CYP26B1. However, formation of 4-oxo-RA from 4-OH-RA was not P450 mediated in cells or in human fetal livers and was mediated by a yet to be identified enzyme. CYP26A1

mRNA was induced by *at*RA, 4-oxo-RA, (4S)-OH-RA, (4R)-OH-RA, and 18-OH-RA in HepG2 cells. Based on measured cell exposure to the retinoids, 4-oxo-RA is the most potent retinoid in terms of RAR activation.

Since *at*RA is an important signaling molecule during pregnancy and fetal development, the metabolism of *at*RA in maternal liver during pregnancy was measured in a mouse model and the metabolism in human fetal liver was characterized. It was determined that during mouse pregnancy CYP26A1 activity was significantly increased in the liver, suggesting increased activation of RARs and increased *at*RA clearance during pregnancy, and decreased *at*RA concentration. The increased CYP26A1 activity in the maternal liver may function as a first-pass barrier to protect the developing fetus from excess *at*RA exposure. The human fetal liver also metabolized *at*RA, but the overall extraction ratio of *at*RA by the human fetal liver was predicted to be minimal (0.01-0.05), suggesting that CYP26 expression in other fetal tissues is critical for regulating *at*RA concentration. In conclusion the results of this study show that CYP26A1 and CYP26B1 are important enzymes regulating *at*RA clearance during pregnancy and adult life, and CYP26A1 and CYP26B1 have specific kinetic characteristics that likely explain their different roles in *at*RA clearance.

Table of Contents

LIST OF TABLES

LIST OF FIGURES

LIST OF NON-STANDARD ABBREVIATIONS

*at*RA — all-*trans* retinoic acid

GD — gestational day

KPi — potassium phosphate

MLH — mouse liver homogenates

PMSF — phenylmethylsulfonyl fluoride

P450 — cytochrome P450

RA — retinoic acid

RAR or Rar — retinoic acid receptor

RARE — retinoic acid response element

*at*RA-d_5 — deuterated all-*trans*-retinoic acid

AUC — Area under the curve

4-oxo-RA — 4-oxo-all-*trans*-retinoic acid

4-OH-RA — 4-hydroxy-all-*trans*-retinoic acid

(4R)-OH-RA — (4R)-hydroxy-all-*trans*-retinoic acid enantiomer

(4S)-OH-RA — (4S)-hydroxy-all-*trans*-retinoic acid enantiomer

18-OH-RA — 18-hydroxy-all-*trans*-retinoic acid

4-oxo-RA-d_3 — deuterated 4-oxo-all-*trans*-retinoic acid

HepG2 — Fetal Hepatocarcinoma Cells

RDH — Retinol Dehydrogenase

RALDH — Retinal Dehydrogenase

RAR — Retinoic Acid Receptor

RXR — Retinoid “X” Receptor

IS — Internal Standard

LOQ— Limit of Quantification

LOD— Limit of Detection

4OH-Ox— 4-OH-RA Oxidase

hFL— human fetal liver

ACKNOWLEDGEMENTS

I would like to first and foremost acknowledge and express gratitude to my advisor, Dr. Nina Isoherranen for all of her guidance and support, and for teaching me how to work in many different facets while demanding nothing less than excellence. I would also like to thank Dr. Wendel Nelson for being my mentor through a very difficult and lengthy organic synthesis. He not only gave me invaluable guidance in my labwork, but also taught me to fully understand how to scientifically question each experiment I perform. My committee members, Dr. Rheem Totah, Dr. Jashvant Unadkat, and Dr. Joanne Wang were essential in helping me to cultivate the ideas behind my thesis. Finally, I would like to thank all of my lab members and friends here at UW; their support and tough love were instrumental to my maturation both as a scientist and as a person.

DEDICATIONS

I would like to dedicate this thesis in part to my parents, Bruce and Judith and especially to my loving and encouraging husband, Adam.

Chapter 1 : Introduction

1.1 Identification and Biological Activity of all-*trans*-retinoic Acid (*at*RA)

Vitamin A (retinol) was first identified in 1913 as a fat-soluble factor in eggs and butter vital for maintaining growth in rats (Davis, 1913). The acid form of retinol, all-*trans*-retinoic acid (Figure 1.1), was synthesized in 1946 (Arens and Van Dorp, 1946), and it was subsequently determined to be an active *in vivo* metabolite of retinol in rats (Emerick et al., 1967). Subsequently, *at*RA has been shown to regulate intestinal homeostasis by inducing differentiation in epithelial cells, and reducing keratinization (Logan, 1972). All-*trans*-retinoic acid (*at*RA) was also shown to have a prophylactic effect in papillomas and carcinomas of the skin, prompting its use as a drug, Tretinoin (Bollag, 1972). *at*RA is also a crucial signaling molecule in embryonic patterning and limb generation (Maden, 1982).

The expression of specific transcription factors and the concentration of *at*RA within a cell regulate cell-specific responses to *at*RA (McBurney, 1993; Rhinn and Dolle, 2012). *at*RA binds to Retinoic Acid Receptors (RARs), that are heterodimerized with Retinoid X Receptors (RXRs), to induce gene transcription via Retinoic Acid Repsonse Elements (RAREs, Figure 1.2). There are three isoforms of RARs and RXRs (α, β, and γ), each of which have been shown to play different functional roles (Krust et al., 1989). In mice, knock-out of RARα resulted in sterility in males (Lufkin et al., 1993), RARβ$^{-/-}$ mice had eye formation abnormalities and impaired locomotion (Ghyselinck et al., 1997), and RARγ$^{-/-}$mice had skeletal and epithelial defects (Lohnes et al., 1993). In addition to the receptor specific differences, the magnitude of RAR activation in target cells is also *at*RA concentration dependent. For example, in murine P19 embryonic carcinoma stem cells, aggregates treated with *at*RA at concentrations around 100 nM were shown to develop into neuronal and astroglial cells (McBurney, 1993; Sonneveld et al., 1999). Those treated with 10 nM *at*RA differentiated predominantly into skeletal muscle, and at

concentrations around 1 nM *at*RA cardiac muscle was formed while differentiation into skeletal muscle decreased (McBurney, 1993). These concentration gradients have been proposed to be maintained by a combined effect of *at*RA elimination and synthesis (White and Schilling, 2008).

1.2 Elimination Pathways of *at*RA

Retinoic acid concentration in cells is tightly regulated by both synthesis of *at*RA from retinal and metabolism of *at*RA (Figure 1.1). *at*RA has been shown to undergo four types of biotransformations in vivo: decarboxylation, isomerization, oxidation and glucuronidation (Hanni et al., 1976; Frolik et al., 1978). Of these, the primary elimination pathway is believed to be cytochrome P450-mediated oxidation. Isomerization of *at*RA and other RA isomers, 9-*cis*, 13-*cis*, or 9,13-di*cis*RA, has been shown to occur in vivo, with recent evidence to support that the 9,13-di*cis*RA and *at*RA are the primary isomers that circulate in mouse serum (Kane et al., 2008; Muindi et al., 2008). In non-fasting humans, *at*RA (3.0 ± 0.1 nM), 13-*cis*RA (3.9 ± 0.2 nM), 9-*cis*RA (0.09 ± 0.01 nM), 9,13-di*cis*-RA (0.3 ± 0.1 nM), and their secondary metabolites 4-oxo-RA (~2 nM) and 4-oxo-13-*cis*RA (11.9 ± 1.6 nM) were detected in human serum, with 4-oxo-13-*cis*RA circulating at the highest concentration (Arnold et al., 2012).

Oxidation of *at*RA has been shown to be mediated by P450 enzymes (P450), of which CYP3A, CYP2C8 and CYP26 appear to be the most important in 4-OH-RA formation (Thatcher et al., 2010) (Figure 1.3). There are three members of the CYP26 family, CYP26A1, CYP26B1, and CYP26C1, that are all spatiotemporally (i.e., time and tissue type-dependent) expressed during development and in adult tissues. CYP26A1 mRNA and/or protein have been found in the human liver, placenta, and fetal brain, and CYP26A1 expression in the fetal chick has been shown to vary depending on time during gestational stage and tissue type (Swindell et al., 1999; Xi and Yang, 2008; Thatcher et al., 2010). Previous mRNA data has suggested that CYP26B1 is

the predominant CYP26 enzyme present in tissues other than the human fetal brain and adult liver, such as the kidney and testes (Xi and Yang, 2008). CYP26C1 mRNA was shown to be present in the human adult lung, brain, and spleen (Xi and Yang, 2008). Knocking out either CYP26A1 or CYP26B1 in mice was shown to be lethal during fetal development, but the two knock-outs had very different phenotypes (Abu-Abed et al., 1998; Yashiro et al., 2004). For example, CYP26A1$^{-/-}$ mice had neural tube defects, truncation of tails, and died during mid-gestation, whereas CYP26B1$^{-/-}$ mice had shorter limb growth and impaired lung formation and died either during gestation or shortly after birth (Abu-Abed et al., 1998; Yashiro et al., 2004).

CYP26A1 and CYP26B1 have been shown to be highly specific towards *at*RA metabolism, while CYP26C1 preferentially metabolizes 9-c*is*RA (White et al., 2000; Taimi et al., 2004). Interestingly, homology between the two *at*RA hydroxylases (CYP26A1 and CYP26B1) is low, but the homology between species for CYP26 enzymes is high. mCYP26A1 and hCYP26A1 are 98% homologous, whereas hCYP26A1 is only 42% homologous to hCYP26B1 (Thatcher and Isoherranen, 2009). The low overall sequence homology between CYP26A1 and CYP26B1 would suggest that the two enzymes are functionally different although they both appear to prefer *at*RA as a substrate. Substrate recognition sites (SRS) are the portions of an enzyme where a substrate (such as *at*RA) interacts with the active site residues of the enzyme (such as in proximity to the heme in a P450 enzyme) to facilitate biotransformation (Kuhnel et al., 2008). Only 40 % of the SRS sequences were homologous between hCYP26A1 and hCYP26B1 (Figure 1.4). The low homology in the overall sequences and SRSs between CYP26A1 and CYP26B1 suggests that there are functional differences between the two enzymes.

The first primary metabolite of *at*RA identified and isolated was 5,6-epoxide-RA formed in rat intestinal mucosa (McCormick et al., 1978), soon followed by the detection of 4-oxo(keto)-RA and 18-hydroxy-RA (18-OH-RA) in rat feces (Hanni and Bigler, 1977), and 4-hydroxy-RA (4-OH-RA) in hamster liver microsomes (Frolik et al., 1979). The formation of a hydroxylated product at the C-16 position of *at*RA (16-OH-RA) was shown to occur by the bacterial *at*RA hydroxylase, CYP120A1 and by CYP26A1 (Alder et al., 2009; Thatcher et al., 2011). Incubations of *at*RA in rat liver, kidney, lung and testis microsomes produced metabolite profiles differing depending on the type of tissue. 4-OH-RA was generated in all four tissues (26-44% of all metabolites analyzed), but 4-oxo-RA was found only in the kidney and the liver (12-37%), and 18-OH-RA was predominantly formed in the testis (11-14%) (Fiorella et al., 1993). The differences between the metabolite profiles are likely due to the different CYP26 enzymes found in each tissue.

*at*RA was determined to have a very high affinity for CYP26A1, with a K_m of 9.4 nM and substrate depletion V_{max} of 11.3 pmol/min/pmol P450 (Lutz et al., 2009). CYP26A1 has been shown to be the predominant CYP26 enzyme in the human liver and was predicted to be the primary enzyme responsible for hepatic oxidation of *at*RA based on the high *in vitro* intrinsic clearance values of *at*RA with CYP26A1 as compared to other P450 enzymes (Thatcher et al., 2010). In He-La cells transfected with hCYP26A1, formation of 4-oxo-RA, 4-OH-RA and 18-OH-RA from *at*RA was observed (Chithalen et al., 2002). However, incubations of *at*RA and 4-OH-RA with CYP26A1 microsomes showed that 4-oxo-RA was not formed by CYP26A1 (Lutz et al., 2009). The discrepancy between the metabolite profile in the cell system and CYP26 microsome incubations is likely due to a non-P450-mediated oxidation of 4-OH-RA to 4-oxo-RA in whole cell systems. This observation is supported by data that an unknown enzyme (likely an

alcohol dehydrogenase) catalyzes the formation of the 4-oxo-RA and is NAD^+ dependent (Roberts et al., 1980). Preliminary incubations using a deuterated standard of *at*RA (*at*RA-d_5 labeled with 2 deuteriums at the C-4 and 3 deuteriums at the C-18 positions) showed that 4-OH-RA, 16-OH-RA, and 18-OH-RA are formed by CYP26A1 (Thatcher et al., 2011). An oxo-metabolite with the loss of a second deuterium atom, determined to be 4-oxo-RA, was also detected after incubating CYP26A1 with *at*RA-d_5 (Thatcher et al., 2011). One of the aims of this thesis was to characterize the formation and elimination of *at*RA metabolites by CYP26A1 and CYP26B1.

1.3 Activity of *at*RA Metabolites

Theoretically, if *at*RA is the active form of Vitamin A, isomerization or oxidative metabolism should result in inactive metabolites. However, the 9-*cis*RA and 13-*cis*RA, 4-OH-RA, 18-OH-RA and 5,6-epoxy-RA metabolites have been shown to bind to all three RAR isoforms and induce RARE-luciferase with differing levels of affinity and preference (Idres et al., 2002) (Table 1-1). Promyelocytic leukemia cells (NB4) treated with 4-oxo-RA, 4-OH-RA, 18-OH-RA and 5,6-epoxy-RA showed that these metabolites had similar potency as *at*RA based on differentiation of NB4 cells into mature neutrophils (Idres et al., 2001). When CYP26A1 expression in P19 EC cells was knocked out, a loss of *at*RA-dependent differentiation was observed, suggesting that *at*RA metabolites formed by CYP26A1 may play a role in regulating differentiation into various cell types, including neuronal, endodermic, and smooth muscle cells (Langton and Gudas, 2008). Alternatively, the loss of differentiation could have been due to increased *at*RA concentrations leading to apoptosis of the cells. The tight regulation of *at*RA metabolism along with evidence that the metabolites bind RARs with differing affinities suggests that some of the metabolites have a specific biological role.

*at*RA has been shown to induce its own metabolism via induction of specific CYP26 enzymes in certain cell types (Tay et al., 2010; Takeuchi et al., 2011). Resistance to *at*RA treatment that frequently occurs in APL patients is believed to be due to increased clearance of *at*RA due to CYP26A1 induction in the liver (Ozpolat et al., 2002). Similarly in HepG2 cells, *at*RA has been shown to induce CYP26A1 and RARβ mRNA in a time and concentration-dependent manner (Tay et al., 2010; Zhang et al., 2010). In HepG2 cells, CYP26A1 and RARβ mRNA induction was shown to be regulated by RARα activation. This was based on the fact that AM580, an RARα agonist, induced CYP26A1 and RARβ mRNA but AC55649, a RARβ agonist did not (Tay et al., 2010). RARγ was not expressed in HepG2 cells. In agreement with the HepG2 cells, CYP26A1 mRNA in the rat liver was shown to increase upon *at*RA treatment, confirming that *at*RA-mediated induction of CYP26A1 occurs in vivo (Yamamoto et al., 2000). Since the *at*RA metabolites have been shown to bind to RARα (Idres et al., 2002), 4-oxo-RA, (4R)-OH-RA, (4S)-OH-RA, and 18-OH-RA may also induce CYP26A1 and RARβ expression via RARα-mediated transcription.

1.4 Roles of the Maternal and Fetal Livers in *at*RA Metabolism

*at*RA is a key signaling molecule (morphogen) during fetal development. The concentration of *at*RA in the fetus is tightly regulated both by synthesis of *at*RA from retinol by alcohol and aldehyde dehydrogenases (ALDHs and RALDHs) and metabolism of *at*RA by CYP26 enzymes (Duester, 2008). In maternal plasma, retinol is highly bound to retinol binding protein (RBP). The RBP-retinol complex interacts through a substrate channeling-type transfer of retinol from RBP to Stra6, an uptake transporter specific for retinol (Kawaguchi et al., 2007). Specific mutations in Stra6 (D333A, Y336A, G340L, and G342L) have been found to reduce retinol uptake and cause severe birth defects or even lethality of the fetus consistent with

disruption of vital *at*RA signaling pathways during development and a lack of *at*RA in the fetus (Kawaguchi et al., 2007). The deformities due to Stra6 mutations strongly suggest that uptake of maternal retinol by Stra6 is important and supply of *at*RA from maternal circulation is not sufficient to support fetal development. It is likely that retinol from maternal sources is metabolized to *at*RA in the fetus and hence the main source of *at*RA to the developing fetus is fetal *at*RA synthesis, not *at*RA from maternal plasma. However, it is not clear whether the placenta and fetal liver provide an efficient barrier for *at*RA distribution from the mother to the fetus via P450-mediated metabolism or via transport. Also, ALDHs and RALDHs are spatiotemporally expressed in fetal tissues presumably to regulate synthesis of retinoic acid from retinol.

The current standard of care during pregnancy encourages consumption of daily vitamin supplements containing Vitamin A either in the form of retinyl palmitate or β-carotene. The dose of Vitamin A varies highly among commercially available supplements, ranging from 500 IU (0.15 mg retinol equivalents (RAE)) to 5000 IU (1.5 mg RAE). The daily recommended dose is 0.7 mg RAE, with a maximum daily intake of 3 mg RAE (IOM, 2001). As foods in many countries such as the United States are already fortified with Vitamin A, there exists a growing concern that additional supplement consumption during pregnancy may pose a risk of toxicity to the fetus via overexposure to retinoids (Rothman et al., 1995). Thus, changes in the capacities of the maternal and fetal livers to metabolize *at*RA are of interest and understanding of maternal retinoid metabolism will be useful in estimating the safety of maternal vitamin A supplementation.

The maternal and fetal livers together with the placenta are effective first-pass barriers to compounds entering into fetal circulation. Hence, understanding of *at*RA metabolism during

pregnancy is important. Expression of the CYP26 enzymes at different stages of gestation in maternal and fetal tissues has yet to be determined. However, as CYP26 is shown to be the predominant enzyme responsible for oxidative metabolism of *at*RA, expression even in low levels may be sufficient to effectively clear endogenous *at*RA in the maternal plasma after maternal Vitamin A consumption and prior to reaching fetal circulation. CYP26 enzymes are believed to form predominantly non-bioactive metabolites from *at*RA; however, the secondary metabolite of *at*RA, 4-oxo-RA, appears to have an effect on the developing fetus. 4-oxo-RA has been shown to be teratrogenic in Xenopus laevis, and also to induce Hox4 and Hox9 genes at higher levels than *at*RA (Pijnappel et al., 1993). In the mouse, administration of 4-oxo-RA resulted in malformations such as cleft palate and short fibula in the developing fetus at a similar extent as that seen after administration of *at*RA, although certain malformations were specific to *at*RA-induced teratogenicity, such as short humerus and bent tibia (Creech Kraft et al., 1989). Hence better understanding of the formation of 4-oxo-RA in maternal and fetal tissues is needed.

1.5 Thesis Hypotheses and Aims

Throughout this thesis, the functional differences between CYP26A1 and CYP26B1, the relative differences in the biological activity of identified *at*RA metabolites and the regulation of *at*RA metabolism during pregnancy, both in the maternal mouse liver and in the human fetal liver, were explored. Also of interest was to clarify the role of CYP26 in the formation and elimination of 4-oxo-RA, a known bioactive *at*RA metabolite and the only *at*RA metabolite shown to circulate in human plasma. The overall hypotheses of this thesis were that there are functional differences in the metabolism of *at*RA between CYP26A1 and CYP26B1, and that the CYP26 enzymes ultimately function as a deactivating pathway for *at*RA and its primary hydroxylated metabolites. These hypotheses were tested via the following four specific aims.

Aim 1: to characterize the functional differences between CYP26A1 and CYP26B1 in formation and elimination of *at*RA metabolites. Aim 2: to determine if *at*RA oxidative metabolites induce CYP26A1 mRNA, using HepG2 cells. Aim 3: to establish the changes in Cyp26a1 expression and activity in the maternal mouse liver during pregnancy. Aim 4: To determine the role of CYP26 and CYP3A7 in *at*RA clearance in the human fetal liver during the first and second trimesters of pregnancy.

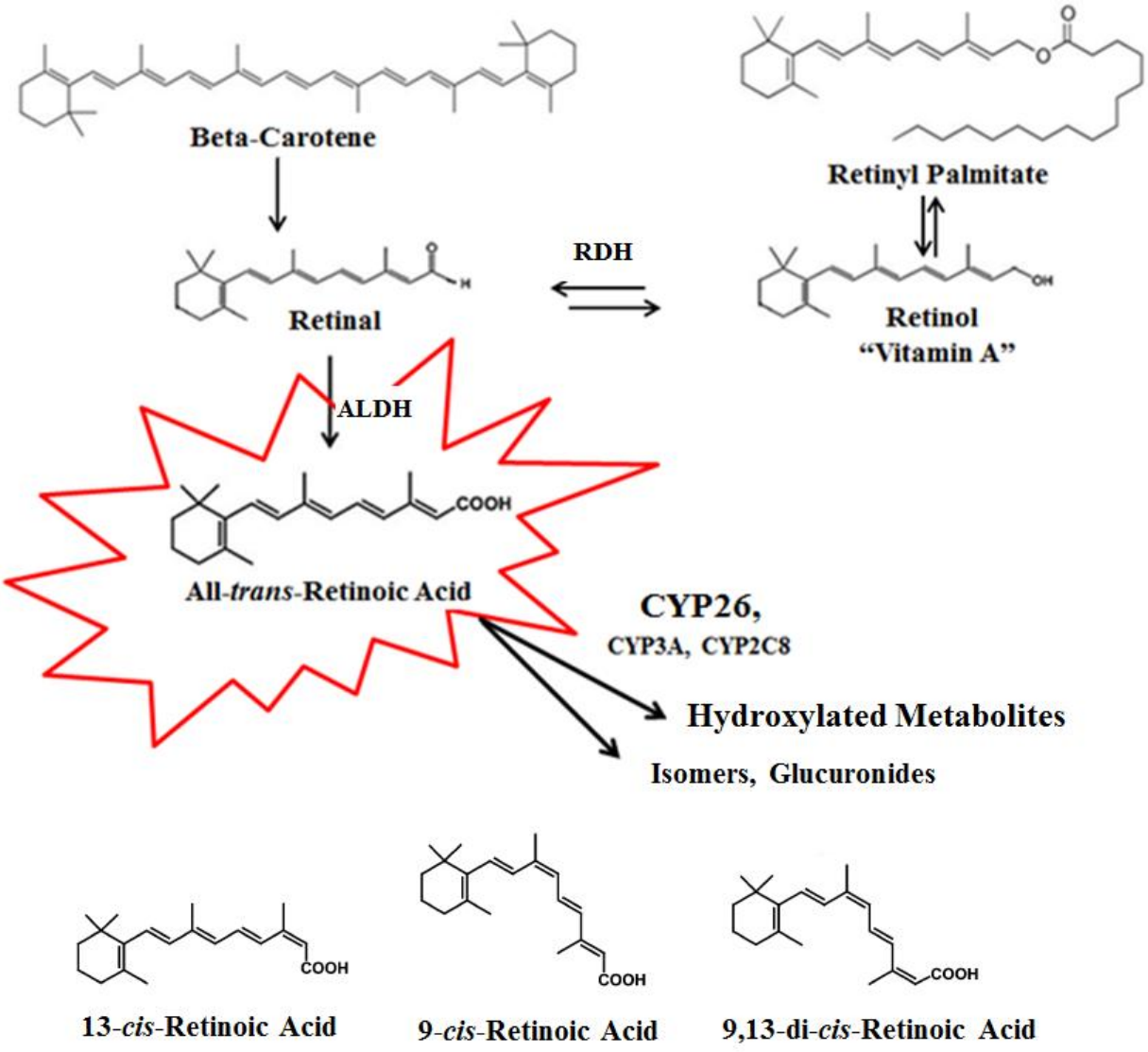

Figure 1.1 Synthesis of *at*RA from Retinol or β-carotene and *at*RA elimination pathways are shown. 13-cis-RA, 9-cis-RA, and 9,13-di-cis-RA, are the isomerization products of *at*RA detected in human plasma.

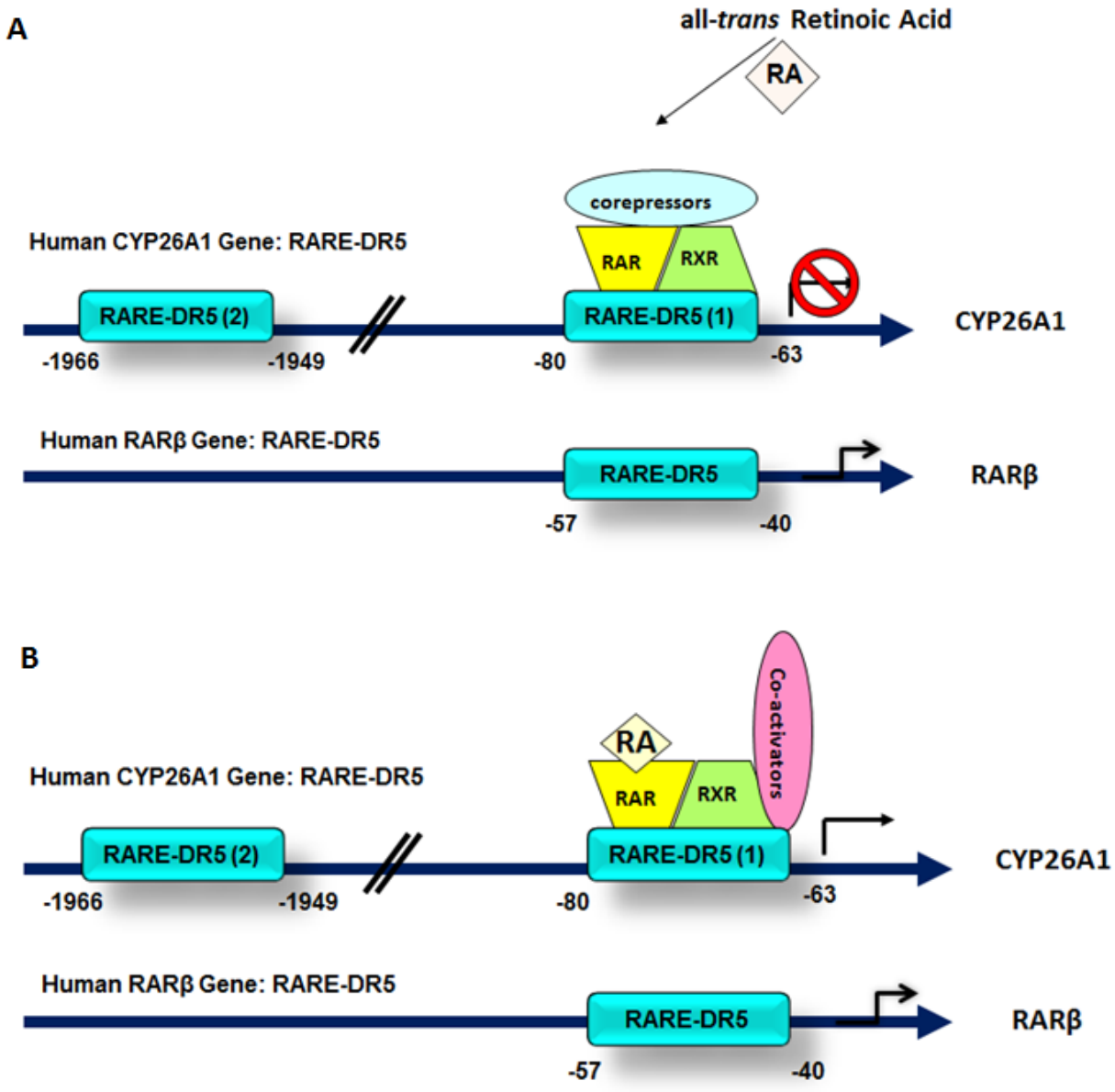

Figure 1.2: Regulation of gene transcription by *at*RA. (A) RAR-RXR complex co-localized with corepressors on the RARE-DR5 located in the promoter sequence of *CYP26A1* and *RARβ* in the absence of *at*RA. The RAR-RXR complex is present for all three RARE-DR5 sequences, though is shown on only one RARE-DR5. (B) When *at*RA binds to the RAR-RXR complex; corepressors are removed and transcriptional co-activators are recruited to induce CYP26A1 and RARβ mRNA transcription.

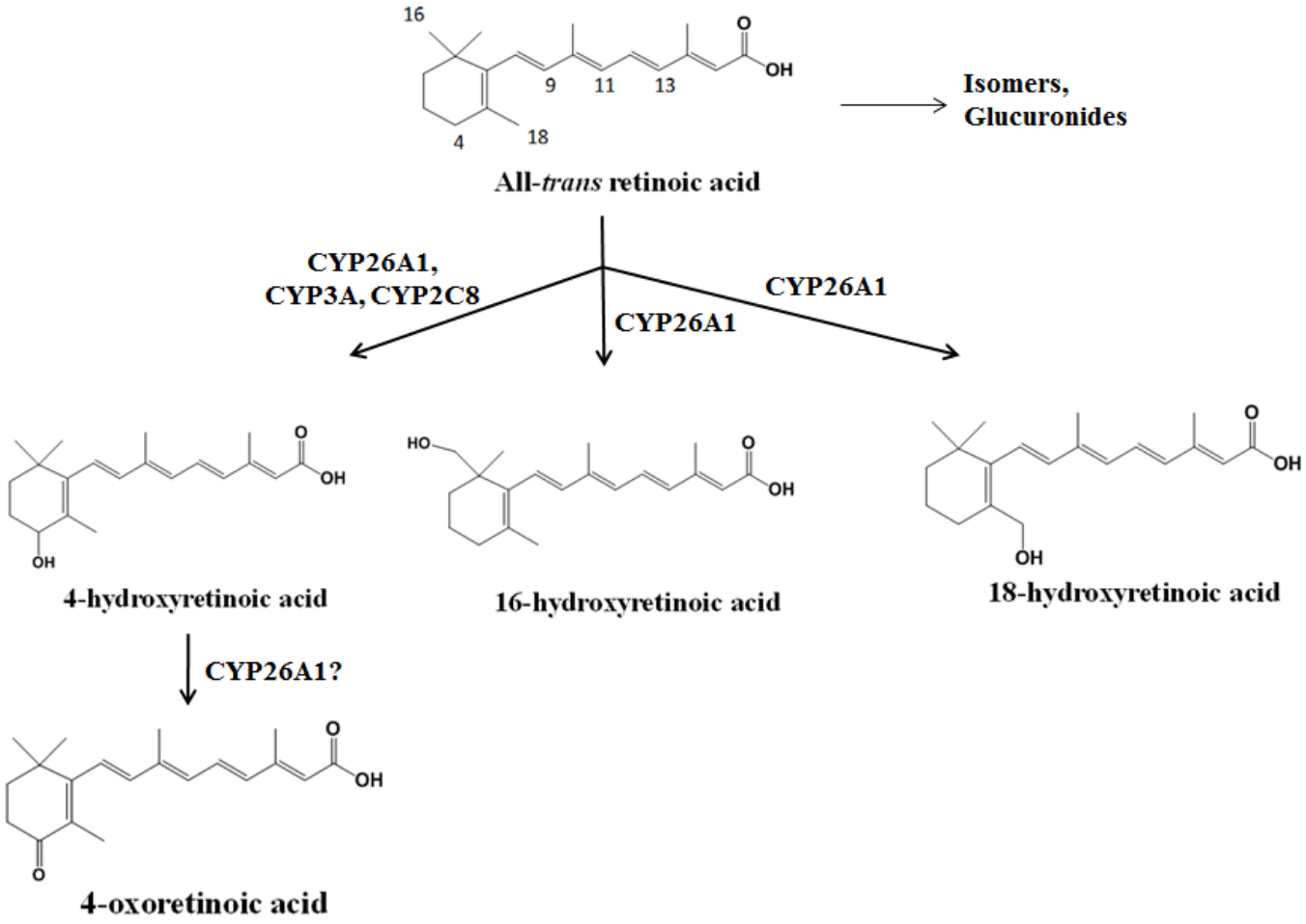

Figure 1.3: Structures of *at*RA metabolites formed by CYP26A1

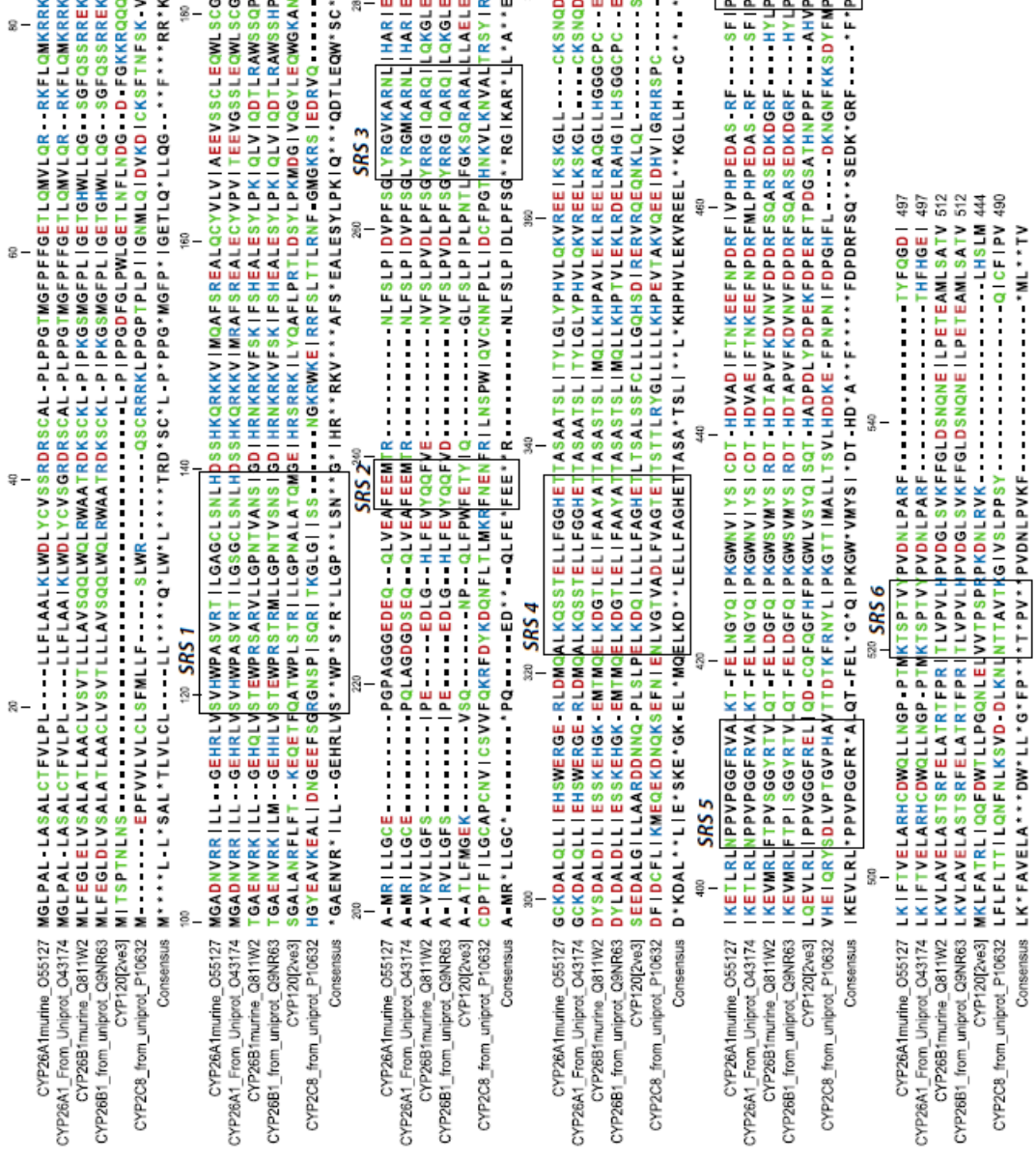

Figure 1.4: Sequence alignment and substrate recognition sites (SRS) in CYP26A1 and CYP26B1. The sequences of human and mouse CYP26A1 and CYP26B1 were aligned with the sequences of CYP120A1 and CYP2C8 which have both been crystallized with RA in the active site. SRSs are designated by black boxes.

Table 1-1: The EC_{50} values of RAR activation for *at*RA and its metabolites. COS-7 cells overexpressing RARα, RARβ, or RARγ were transfected with RARE-tk-Luc and treated with *at*RA and its metabolites. Luciferase activity was measured to determine the EC_{50} values (Idres et. al., 2002).

	EC_{50} (nM)		
Retinoid	**RARα**	**RARβ**	**RARγ**
*at*RA	169	9	2
4-oxo-RA	33	8	89
4-OH-RA	791	64	94
18-OH-RA	162	14	14

Chapter 2 : Characterization of the Functional Differences between CYP26A1 and CYP26B1: Metabolite Formation and Catalytic Efficiency

Portions of this chapter have been published in:

Biochemical Pharmacology (2012) Vol. 83:149-163

and

The Journal of Biological Chemistry (2012) Vol. 287 No. 50: 42223-42232

2.1 Introduction

Vitamin A and its metabolite, all-*trans* retinoic acid (*at*RA), have been shown to be vital dietary components for many types of cells, with pronounced concentration dependent effects (McBurney, 1993; Thatcher and Isoherranen, 2009; Napoli, 2012). A deficiency or excess of *at*RA has been shown to be attributed to incorrect gene regulation and even cellular death (Langton and Gudas, 2008). Hence, the concentration of *at*RA within a cell at any given time is tightly regulated and dependent on both synthesis of *at*RA from retinal and further elimination of *at*RA. One of the major elimination pathways for *at*RA is oxidation, predominantly by the cytochrome P450 enzymes in the CYP26 family of enzymes (CYP26A1, CYP26B1, and CYP26C1) (Ross and Zolfaghari, 2011).

CYP26A1 and CYP26B1 have both been shown to metabolize *at*RA (White et al., 2000). However, clear differences in the spatiotemporal expression, phenotype of knock-out animals, and in the sequence homology have been shown between CYP26A1 and CYP26B1 (Abu-Abed et al., 1998; Yashiro et al., 2004; White and Schilling, 2008). The expression of CYP26A1 and CYP26B1 mRNA has been shown to differ between human tissue types (Xi and Yang, 2008). CYP26A1 mRNA is predominantly detected in the liver, and CYP26A1 has been shown to be inducible upon treatment with *at*RA (Ray et al., 1997; Xi and Yang, 2008; Tay et al., 2010). Conversely, CYP26B1 mRNA is detected mostly in extrahepatic tissues, such as the testes, brain, and lymphocytes, and is also inducible upon *at*RA treatment in granulocytes (Xi and Yang, 2008; Takeuchi et al., 2011). Clear phenotypic differences were observed between cyp26a1 and cyp26b1 knock-out mice. For example, cyp26a1$^{-/-}$ mice had neural tube defects whereas cyp26b1$^{-/-}$ mice had malformed limbs and lungs (Abu-Abed et al., 1998; Yashiro et al., 2004) suggesting the two enzymes are not functionally redundant. Whether the lack of

redundancy is due to biochemical differences between CYP26A1 and CYP26B1 or due to differences in their regulation of *at*RA is currently unknown.

Three primary metabolites of *at*RA have been shown to be formed by CYP26A1; 4-OH-RA, 16-OH-RA, and 18-OH-RA (Figure 2.1), as well as a plethora of secondary and subsequent metabolites (Chithalen et al., 2002; Thatcher et al., 2011). The abundance of the metabolites formed was shown to be depend on the CYP26A1 content and cell type; high enzyme content and low *at*RA concentrations resulted in greater formation of secondary metabolites (Chithalen et al., 2002). Conversely, high *at*RA concentrations and low CYP26A1 expression resulted in formation of mostly primary metabolites and 4-oxo-RA in cells (Chithalen et al., 2002). These data suggest that the primary metabolites are subsequently also metabolized by the CYP26 enzymes after the *at*RA is depleted and that 4-oxo-RA is not formed by CYP26A1. In agreement with this, it was shown that 4-oxo-RA is not formed by CYP26A1 (Lutz et al., 2009). However, the metabolites formed by CYP26B1 and the differences in the kinetics of metabolite formation between CYP26A1 and CYP26B1 have not been previously characterized.

The primary metabolite formed by the CYP26, CYP3A and CYP2C8 enzymes, 4-OH-RA, has a chiral center (Figure 2.1B). The 4-OH-RA enantiomers preferentially formed by CYP26A1 and CYP26B1 as well as subsequent metabolites formed from each enantiomer by CYP26A1 and CYP26B1 have yet to be elucidated, as well as the biological implications of forming one enantiomer over another. However, characterization of the stereochemistry of 4-OH-RA formation may provide additional insight to the understanding of CYP26 active site features.

It is likely that CYP26A1 and CYP26B1 metabolize *at*RA to different preferential metabolites. Incubations of *at*RA in the adult rat liver, kidney, lung and testis microsomes

resulted in different metabolite profiles in the different types of tissues (Fiorella et al., 1993). 4-OH-RA was generated in all four tissues (26-44% of all metabolites analyzed), but 4-oxo-RA only in the kidney and the liver (12-37%), and 18-OH RA was predominantly made in the testis (11-14%) (Fiorella et al., 1993), suggesting that different enzymes contribute to the metabolism of *at*RA in different tissues. However, the expression of CYP26A1 and CYP26B1 in the different tissues is not known.

The necessity of both highly conserved enzymes suggests that CYP26A1 and CYP26B1 are functionally different or have different biological roles. We hypothesized either that the kinetics of *at*RA metabolism or the qualitative metabolic profiles of *at*RA between CYP26A1 and CYP26B1 are different, leading to different biological functions of the two enzymes. The first aim of this study was to determine the qualitative and quantitative differences in the formation of the primary metabolites of *at*RA by CYP26A1 and CYP26B1, as well as the stereoselective formation of 4-OH-RA enantiomers. Secondly, we aimed to characterize the qualitative and quantitative differences in the metabolism of *at*RA, (4S)-OH-RA, (4R)-OH-RA, 4-oxo-RA and 18-OH-RA between CYP26A1 and CYP26B1. The results were used to better understand the biological role of CYP26A1 and CYP26B1 and evaluate the active site differences between CYP26A1 and CYP26B1 using homology models of the two enzymes.

2.2 Materials and Methods

Chemicals and Enzymes. 4-oxo-RA-d_3 and *at*RA-d_5 (Figure 2.1) were purchased from Toronto Research Chemicals (North York, Ontario). (4R)-OH-RA, (4S)-OH-RA and 4-oxo-RA were synthesized as previously described (Samokyszyn et al., 2000; Shimshoni et al., 2012; Topletz et al., 2012). All chemicals for synthesis of 18-OH-RA were purchased from Sigma Aldrich Company. Optima-grade water, optima-grade acetonitrile, ethanol and ethyl acetate were

purchased from Fisher Scientific (Pittsburgh, PA). CYP26A1 and CYP26B1 were expressed in Sf9 cells and microsomes were prepared as previously described (Lutz et al., 2009; Thatcher et al., 2010). Rat P450 reductase was expressed in *Escherichia coli* and purified as previously reported (Lutz et al., 2009).

Analytical Instruments and Methods Used for 18-OH-RA Synthesis. Analytical instruments utilized to determine chemical purity of 18-OH-RA and preceding steps included NMR, HPLC-UV, UV absorption, and HPLC-MS/MS. NMR analysis was done using either a 300 MHz or 500 MHz instrument, and all samples were dissolved in $CDCl_3$. HPLC–UV analysis was performed using an Agilent Technologies (Palo Alto, CA) 1200 series HPLC system with an Agilent Technologies Extend C18 3.5 mm column (2.1 mm x 100 mm). mm). The analytes were separated over a 28 min gradient elution using mobile phases of aqueous 50 mM ammonium acetate buffer (pH 4.5) and acetonitrile. The initial conditions were 90:10 buffer:acetonitrile. Acetonitrile was increased linearly over 15 min to reach a final condition of 10:90 buffer:acetonitrile, which was then held for another 13 min before returning to the initial conditions. Analytes were detected using a multiple wavelength UV detector, monitoring wavelengths at 342 nm and 360 nm. Accurate mass analysis was performed using a Waters ACQUITY UPLC and autosampler coupled to a Waters Micromass Synapt Ion Mobility Q/TOF hybrid MS/MS mass spectrometer operated in negative electrospray mode (Milford, MA). UV analysis was done using a Nanodrop 2000c spectrophotometer, Thermofisher Scientific (Wilmington, DE); all samples were dissolved in absolute EtOH.

Incubation, Extraction, HPCL-UV and HPLC-MS/MS Analysis Protocol for Kinetic Experiments. Samples from kinetic experiments were extracted using ethyl acetate as previously described (Thatcher et al., 2010). Modifications and internal standards used are indicated in the

specific method sections for each experiment. HPLC-UV analysis was performed as described above. For mass spectrometry analysis, analytes were separated with an Agilent Zorbax C18 column (3.5µm, 2.1mm x 100mm) or a Chiralcel OD-RH column (5 µm, 2.1 x 150 mm) (chiral separation) and analyzed using an AB Sciex API 5500 Q/LIT mass spectrometer equipped with an Agilent 1290 Infinity UHPLC and operated under either positive or negative ion electrospray as described in the method section for each specific experiment.

Synthesis of 18-OH-RA. The synthesis of 18-OH-RA (Figure 2.2) as described below was performed using modified methods previously developed (Rosenberger, 1982; Kawanobe, 1984).

2-Formyl-6,6-dimethylcyclohexanone (**2**) To a stirred suspension of NaH, 60 % in mineral oil (5.8 g, 0.145 mol) in dry toluene (180 mL), 2-methyl cyclohexanone (13.5 g, 0.12 mol) was added dropwise over 2 hours at reflux (100 °C). The temperature was lowered to 60 °C, and methyl iodide (20.6 g, 0.15 mol) was added dropwise over 2 hours. The reaction mixture was then stirred for another 2 hours at 60 °C. After 2 hours, the temperature was lowered to 5 °C in an ice bath, and a slurry of NaOMe (11.0 g, 0.204 mol) and HCO_2Me (16.3 g, 0.22 mol) was added all at once. The reaction mixture was then brought to room temperature, allowed to stir overnight, and monitored by TLC (ethyl acetate/chloroform, 2:8). The reaction was quenched by pouring the reaction mixture directly into cold water (250 mL), and the aqueous toluene mixture was acidified with 20 % HCl (60 mL). Without removing the toluene layer, the product in the acidified aqueous phase was extracted with ether (3 x 100 mL). The extract was washed with brine (3 x 100 mL), dried over $MgSO_4$ and concentrated. The concentrate was a dark red liquid which was distilled to give a honey-colored liquid product, bp: 85-87 °C at 15 mm Hg. Yield: 24 % (4.45 g, 0.029 mol). ^{1}H NMR ($CDCl_3$, 300 MHz) δ 14.71

(d, 1, J= 3 Hz, OH), 8.7 (d, 1, J= 3 Hz, vinyl H), 2.34 (t, 2, J= 6 Hz, C-3), 1.69 (m, 2, C-4), 1.58 (m, 2, C-5), 1.21 (s, 6, C-6 CH_3).

Isopropyl ether **(3a**) To a 100 mL roundbottom flask, **2** (4.45 g, 0.029 mol) was dissolved in acetone (33 mL), and treated with potassium carbonate (7.8 g, 0.056 mol) and isopropyl iodide (9.8 g, 0.058 mol). The reaction mixture was allowed to stir at reflux for 5 hours and monitored by TLC (ethyl acetate/hexanes, 1:9). After the reaction had run to completion, the residual solids were filtered off, and the acetone was evaporated in vacuo. The resulting liquid product was then extracted with ether (3 x 100 mL), washed with water (2 x 50 mL) and aqueous $NaHCO_3$, 5 % (2 x 50 mL), dried over $MgSO_4$, and concentrated via rotary evaporation to yield the honey-colored liquid product **3**, bp: 72-78 °C at 0.2 mm Hg. Yield: 87 % (4.98 g, 0.0254 mol). ^{1}H NMR ($CDCl_3$, 300 MHz) δ 7.38 (t, 1, J=1.5 Hz, vinyl H), 4.19 (septet, 1, **CH**$(CH_3)_2$), 2.43 (m, 2, C-3), 1.68 (d, 2, J=3 Hz, C-4), 1.31 (d, 6, J=6 Hz, CH (**CH**$_3)_2$), 1.2 (s, 2, C-5), 1.12 (s, 6, C-6 CH_3).

3-(1-Ethoxyethoxy)-3-methyl-1-penten-4-yne (**3b**) Ethyl vinyl ether (13.1 g, 0.182 mol) was cooled in a 100 mL round bottom flask to 5 °C in an ice bath and carefully treated with *p*-toluenesulfonic acid (50.1 mg, 0.291 mmol). 3-Hydroxy-3-methyl-1-penten-4-yne (10.0 g, 0.104 mol) was slowly added, and solution was kept in the ice bath a further 10 minutes until the initial exothermic reaction had subsided. The reaction mixture was then brought to room temperature and allowed to stir for a further 10 minutes. The reaction was quenched with the addition of triethylamine (0.26 mL, 1.86 mmol). The product was purified via distillation to give **3b**, a colorless liquid containing two diastereomers with chiral centers at the C-3 and O**C**H(CH_3)OEt positions. bp: 67-71°C at 0.2mm Hg. Yield: 81.4% (14.25 g, 0.084 mol). ^{1}H NMR ($CDCl_3$, 300 MHz) δ 5.90, 5.80 (dd, 1, J = 10 Hz, 17, OC**H**(CH_3)OEt,), 5.59, 5.56 (dd, 1,J = 1 Hz, 4, vinyl *cis* H), 5.21, 5.19 (d, 1, J = 1 Hz, vinyl *trans* H), 4.96, 4.89 (q, 1, J = 5 Hz,

C**H**=CH_2), 3.75, 3.60, 3.53, 3.41 (double sextets, 1, OC**H**$_2$$CH_3$), 2.63, 2.62 (s, 1, alkyne H), 1.58, 1.55 (s, 3, CH_3), 1.36, 1.28 (d, 3, J = 5 Hz), OCH(C**H**$_3$)OEt), 1.20, 1.15 (t, 3, J = 7 Hz, OCH_2C**H**$_3$).

rac-5-(6,6-Dimethyl-2-formyl-1-cyclohexene-1-yl)-3-methyl-3-hydroxy-1-penten-4-yne (**4**) In a round bottom flask, THF (80 mL) was cooled to -50 °C in a dry ice bath containing acetone. *n*-Butyllithium, 2.5 M (12.0 mL, 0.03 mol) was carefully added under nitrogen using a dry syringe. The reaction mixture was cooled to -65 °C and a solution of **3b** (5.55 g, 0.033 mol) in THF (10.5 mL) was added. The reaction mixture was brought to 0 °C for 15 minutes to initiate selective deprotonation of alkyne. The temperature was then dropped back to -65 °C, a solution of **3a** (4.98 g, 0.025 mol) in THF (10.5 mL) was added, then brought to room temperature and allowed to stir for one hour. The reaction was monitored by TLC (ethyl acetate/chloroform, 5:95). After 1 hour, the mixture was clear and had turned deep red-orange in color. The reaction was then quenched by the careful addition of 5.0 mL water using a Pasteur pipette. The THF layer was removed, the water layer extracted with ether (100 mL x 3), the extract washed with brine (100 mL x 3), dried over $MgSO_4$, and concentrated to yield a viscous dark yellow crude product. The product was then re-dissolved in 80 mL acetone, and treated with H_2SO_4 (1 N, 20 mL) for 0.5 hours to remove the protecting groups. The aqueous layer was then extracted with ether, washed with brine and saturated $NaHCO_3$, dried over $MgSO_4$ and concentrated via rotavap. The crude product **4** was purified via flash chromatography. A total of 8.06 g crude product was added to a column containing 100 g silica gel that had a column volume of 115 mL. The eluent used for flash chromatography was a gradient of 0-4% ethyl acetate in chloroform, and 500 mL per each additional 1 % ethyl acetate was processed through the column for a total of ~22 column volumes. Yield: 58.8 % (3.47 g, 0.015 mol). ^{1}H NMR

($CDCl_3$, 300 MHz) δ 10.17 (s, 1, CHO), 6.02 (dd, 1, J = 7 Hz, H-2), 5.56 (d, 1, J=17 Hz, H-1), 5.18 (d, 1, J = 9.6 Hz, H-1), 2.25 (t, 2, C-3), 1.65 (s, 3, H-3, CH_3), 1.218 (s, 6, C-6 CH_3).

rac-(4E)-5-[2-(Acetoxymethyl)-6,6-dimethyl-1-cyclohexen-1-yl]-3-hydroxy-1,3-pentadiene (**5**) In a 250 mL roundbottom flask, a slurry of lithium aluminum hydride powder (1.70 g, 0.045 mol) in THF (58 mL) was cooled to 0 °C in an ice bath. The slurry was carefully added to a solution of **4** (3.47 g, 0.015 mol) in THF (29 mL) over 20 minutes. The mixture was then stirred at reflux for 5 hours. The reaction mixture was then cooled to -10 °C, and a saturated Na_2SO_4 solution (8.8 mL) was added dropwise using a Pasteur pipette. After the addition of Na_2SO_4, the reaction mixture was warmed to room temperature, was allowed to stir for an additional 1 hour, and became white and cloudy. The aqueous layer was then extracted with ether (100 mL x 3). The combined ether extracts were dried over sodium sulfate, filtered and concentrated via rotary evaporation to yield a light-yellow colored oil.

The crude diol product was then re-dissolved in ether (16 mL) and cooled to 10 °C in an ice bath. The solution was treated for 30 minutes with a 1:1 mixture of acetic anhydride and pyridine (10.1 g), brought to room temperature and stirred for a further 2 hours. More ether (100 mL) was added to the reaction mixture, and then washed with water (2 x 25 mL), sodium bicarbonate (5 %, 2 x 25 mL), and brine (2 x 25 mL) to remove acetic anhydride and pyridine. The ether layer was then dried over sodium sulfate and concentrated via rotary evaporation to yield **5**. Yield: 63 % (2.64 g, 9.5 mmol). ^{1}H NMR ($CDCl_3$, 300 MHz) δ 6.14 (d, 1, J = 16 Hz, H-4), 5.80 (d, 1, J = 15 Hz, H-5), 6.00 (dd, 1, J = 11,17 Hz, H-2), 5.60 (d, 1, J = 16 Hz), 5.28 (d,1, J = 17 Hz, trans H-1), 5.11 (d, 1, J = 11, cis H-1), 4.58 (s, 2, C-2 C**H**$_2$OAc), 2.07 (s, 3, OAc), 1.43 (s, 3, C-3 CH_3), 1.02 (s, 6, C-6 CH_3).

Phosphonium Salt (**6**) A solution of triphenylphosphinehydrobromide (3.30 g, 9.6 mmol) in dichloromethane (8.3 mL) was added to a roundbottom flask and cooled to 5 °C. A solution of **5** (2.64 g, 9.5 mmol) in dichloromethane (8.3 mL) was added, allowed to warm to room temperature, and stirred 1 hour. The reaction was quenched by slowly pouring the solution into an Erlenmeyer flask containing ether (165 mL) and cooled overnight at 2 °C. The reaction was monitored by TLC (ethyl acetate/hexanes, 2:8). The ether was then decanted from the residual precipitate, the orange precipitate product **6** re-dissolved in methylene chloride, and dried via rotary evaporation. Yield: 26 % (1.52 g, 2.5 mmol). ^{1}H NMR ($CDCl_3$, 300 MHz) δ 7.5 (m, 15, phenyl H), 5.80 (q, 2, J = 16, 29 Hz, H-4, H-5), 5.31 (m, 1, H-2), 4.70 (dd, 1, J = 8, 15 Hz, H-1), 4.34 (s, 2, C-2 C**H**$_2$OAc), 1.98 (s, 3, OAc), 1.95 (m, 2, C-3), 1.74 (s, 3, C-3 C**H**$_3$), 1.49 (m, 2, C-4), 1.34 (m, 2, C-5), 0.95 (s, 6, C-6 C**H**$_3$).

Ethyl (2E, 4E, 6E, 8E)-9-[2-(Acetoxylmethyl)-6,6-dimethyl-1-cyclohexen-1-yl]-3,7-dimethyl-2,4,6,8-nonatetraenoate (**7**) In a 25 mL roundbottom flask, phosphonium salt **6** (1.52 g, 2.5 mmol) was dissolved in 10 mL methylene chloride containing ethyl-3-methyl-4-oxocrotonate (0.31 g, 2.2 mmol) and cooled to -20 °C. Sodium methoxide in MeOH (1.01 mL, 3.2 M, 3.23mmol, 1.5meq) was added dropwise over 15 minutes to the reaction solution, which then darkened into a deep red color. The mixture was allowed to stir for another 3.5 hours at 0-5 °C in an ice bath, as the mixture faded into a dark orange color. The reaction progress was monitored by TLC (ethyl acetate/hexanes, 1:9); RF = 0.9 (reactant), RF = 0.25 (product) and product was a bright yellow. To the completed reaction mixture, a mixture of hexanes/ethyl acetate (7:3, 26.7 mL) was added. The resulting mixture was washed twice with water, dried over $MgSO_4$, filtered and concentrated via rotary evaporation. The crude product (mixture of 4Z and 4E isomers; equivalent to the C-11 position on retinoic acid) was purified via flash

chromatography (33.4 g silica gel, column volume = 72 mL) using a gradient of 0-5 % ethyl acetate in hexanes. Yield: 17.2 % (150 mg, 0.38 mmol. ^{1}H NMR ($CDCl_3$, 300 MHz) *4E isomer*: δ 6.97 (dd, 1, J = 11, 15 Hz, H-11), 6.30 (d, 1, J = 15 Hz, H-12), 6.15 (d, J = 11 Hz, H-10), 6.23 (d, 1, J = 16 Hz, H-8), 6.11 (d, J = 16 Hz, H-7), 5.85 (s, 1, H-14), 4.61 (s, 2, 18-CH_2OAc), 4.18 (q, 1, J = 7 Hz, OC**H**$_2$$CH_3$), 2.36 (s, 3, 20-$CH_3$), 2.08 (s, 3, 18-OC(O)C**H$_3$**), 2.00 (m, 2, 4-CH_2), 1.99 (s, 3, 19-CH_3), 1.67 (m, 2, 3-CH_2), 1.59 (m, 2, 2-CH_2), 1.31 (t, 3, J = 7 Hz, OCH_2C**H**$_3$), 1.06 (s, 6, 16,17-CH_3).

4Z isomer: δ 6.53 (d, 1, J = 7 Hz, H-11), 6.30 (d, 1, J = 15 Hz, H-12), 6.23 (d, 1, J = 16 Hz, H-8), 6.15 (d, J = 11 Hz, H-10), 6.11 (d, J = 16 Hz, H-7), 5.79 (s, 1, H-14), 4.60 (s, 2, OC**H**$_2$$CH_3$), 4.18 (q, 1, J = 7 Hz, OC**H$_2$**CH_3), 2.35 (s, 3, 20-CH_3), 2.08 (s, 3, 18-OC(O)C**H**$_3$), 1.95 (s, 3, 19-CH_3) 1.67 (m, 2, 3-CH_2), 1.59 (m, 2, 2-CH_2), 1.31 (t, 3, J = 7 Hz, OCH_2C**H**$_3$), 1.06 (s, 6, 16,17-CH_3).

Palladium nitrate catalyzed isomerization (**7b**). To a solution of 18-OH-retinoic acid diester (18-acetate, 15-ethyl ester) (91 mg, 0.24 mmol) in acetonitrile (1 mL) 50 °C, 18.2 µL from a solution of palladium nitrate (5.0 mg, 22 µmol) and triethylamine (4.8 mg, 47 µmol) in acetonitrile (1 mL) was added (retinoid to palladium catalyst ratio of 1:1000, w/w). The reaction mixture was kept at 50 °C overnight, and the conversion from the 11-*cis*- to all-*trans*-isomer was monitored by HPLC-UV. HPLC-UV analysis was performed as described above. Retention times for the 18-acetoxy regioisomers of the all-*trans*-, 11-*cis*- and 9-*cis*-retinoic acid esters were 24.9 min, 25.3 min, and 25.6 min, respectively.

At completion, the organic solvents were evaporated and the residue dissolved in 10mL of methylene chloride. Palladium nitrate was extracted with 2 x 5 mL water, and the organic

phase was dried over sodium sulfate, filtered and evaporated to dryness. Yield: 92 % (84 mg, 0.22 mmol).

Hydrolysis to18-hydroxyretinoic acid (**8**). To a solution of the all-*trans*-18-OH-retinoic acid diester (18-acetate, 15-ethyl ester) (84 mg, 0.22 mmol) in methanol (5 mL) at 0 °C (ice bath) was added 5 mL of a 2 M KOH solution in methanol:water (1:9), also at 0 °C. Hydrolysis was monitored by TLC (1 % acetic acid, ethyl acetate/hexanes, 25:75); RF = 0.75 (diester) and RF = 0.10 (product). After 5 hours, an additional 3 mL of the 2 M KOH solution was added and the mixture was stirred for an additional 8.5 hours at room temperature. The reaction mixture was adjusted to pH 6 using 1 M pH 6 citrate buffer and 1 M citric acid at -10 ºC (ice $CaCl_2$bath). The 18-OH-RAwas extracted with ethyl acetate (2 x 100 mL). After NaCl was added to the remaining aqueous layer, the mixture was extracted with additional ethyl acetate (2 x 100 mL). The combined organic extracts were washed with brine, dried over sodium sulfate, and evaporated to dryness. 18-OH-RA was isolated by HPLC-UV, using conditions as previously described (retention time of 18-OH-RA = 16.8 min). ^{1}H NMR ($CDCl_3$, 500 MHz): δ 6.96 (dd, 1, J = 15, 12 Hz, H-11), 6.26 (d, 1, J = 15 Hz, H-12), 6.12 (d, 1, J = 11.5 Hz, H-10), 6.20 (d, 1, J = 16 Hz, H-8), 6.10 (d, 1, J = 16 Hz, H-7), 5.75 (s, 1, H-14), 4.07 (s, 2, 18-CH_2O), 2.30 (s, 3, 20-CH_3), 2.15 (m, 2, 4-CH_2), 1.94 (s, 3, 19-CH_3), 1.60 (m, 2, 3-CH_2),1.44 (m, 2, 2-CH_2), 0.97 (s, 6, 16,17-CH_3). Accurate mass of the synthetic product was obtained using mass spectrometry as described above. Ten microliters of a 100 nM sample in 50:50 acetonitrile:water was injected into a 50:50 acetonitrile:water isocratic flow (50 μL/min). The detection settings utilized were as follows: a Capillary Voltage of -3.3 kV, a Trap Collision Energy of -6.0 V and a Transfer Collision Energy of -4.0 V. An MS spectra was obtained over a range of 50-1000 m/z. Leucineenkephalin (M-1 = 554.2615 m/z) was infused at 5 μL/min and utilized as an internal

calibrant (Lock Mass) at an interval of 1 scan every 10 sec. The accurate mass of the product was 315.1966 m/z (calc 315.1960 m/z, 1.9 ppm accuracy).

Characterization of formation of 4-OH-RA and 18-OH-RA by CYP26A1 and CYP26B1 from atRA. The formation kinetics for 4-OH-RA and 18-OH-RA catalyzed by CYP26A1 and CYP26B1 were determined. Two pmoles of CYP26 and 4 pmoles of reductase were incubated at room temperature in 1 mL KPi buffer for 5 minutes to allow for reductase incorporation into the membrane. *at*RA was then added to each vial, and samples were incubated in a 37 °C water bath in the presence of NADPH for 2 min (CYP26A1) or 5 min (CYP26B1). Incubations were terminated with the addition of 3 mL of ethyl acetate and acitretin (10 µL of a 5 µM stock) was added as an internal standard prior to extraction. Samples were extracted as previously described (Thatcher et al., 2010) and HPLC–UV analysis was performed using an Agilent Technologies (Palo Alto, CA) 1200 series HPLC system with an Agilent Technologies Extend C18 3.5 mm column (2.1 mm x 100 mm). *at*RA concentrations ranged from 10 to 250 nM. To determine the V_{max} and K_m for formation of 4-OH-RA and 18-OH-RA, the substrate concentration was corrected for depletion, the measured velocities were plotted as a function of *at*RA concentration and the Michaelis–Menten equation fitted to the data using GraphPad Prism v.5 (La Jolla, CA).

Characterization of Stereoselective Formation of 4-OH-RA by CYP26A1 from atRA. The stereoselective formation of (4R)-OH-RA and (4S)-OH-RA by CYP26A1 and CYP26B1 from *at*RA was characterized qualitatively. *at*RA was incubated with CYP26A1 (2 pmoles with 4 pmoles P450 reductase) and CYP26B1 (4 pmoles with 8 pmoles P450 reductase) for 2 (CYP26A1) or 10 (CYP26B1) minutes as described above. To determine any concentration dependent effects, product formation was analyzed at two concentrations of *at*RA, at and above

K_m (20 and 300 nM, respectively). Samples were extracted as previously described (Thatcher et al., 2010) then reconstituted in 100 µL acetonitrile for mass spectrometry analysis. The 4-OH-RA enantiomers were separated and analyzed using mass spectrometry as described below.

The kinetics of (4S)-OH-RA and (4R)-OH-RA formation from *at*RA catalyzed by CYP26A1 and CYP26B1 were determined. *at*RA (20 to 300 nM) was incubated with CYP26A1 and CYP26B1 as described above. An internal standard of 4-oxo-RA-d_3 (20 µL of a 2.5 µM stock solution) was added to all samples prior to ethyl acetate extraction. Samples were extracted as previously described and reconstituted in 100 µL acetonitrile for mass spectrometry analysis.

The 4-OH-RA enantiomers (Figure 2.1) were separated using a Chiralcel OD-RH column (5 µm, 2.1 x 150 mm) and analyzed using positive ion electrospray. The mobile phase flow was 0.17 mL/min. A linear gradient from initial 50:50 water:acetonitrile for 14 min to 20:80 over 10 min was used, followed by 20:80 water:acetonitrile for 10 min. Analytes were detected using positive ion electrospray mass spectrometry, with the declustering potential of 80 V, collision energy of 33 eV ((4S)-OH-RA and (4R)-OH-RA) and 35 eV (4-oxo-RA-d_3); and collision exit potential of 13 V ((4S)-OH-RA and (4R)-OH-RA) and 2 V (4-oxo-RA-d_3). The parent-fragment MS/MS transitions of *m/z* 299 → 121 Da ((4S)-OH-RA and (4R)-OH-RA) and 300 → 226 Da (4-oxo-RA-d_3) were monitored.

Identification of metabolites formed by CYP26A1 and CYP26B1 from atRA, 4-OH-RA (rac), (4S)-OH-RA and (4R)-OH-RA: To identify metabolites formed from (4S)-OH-RA and (4R)-OH-RA by CYP26A1 and CYP26B1, (4S)-OH-RA and (4R)-OH-RA (1 µM) were incubated with CYP26A1 (5 pmoles with 10 pmoles reductase) or CYP26B1 (7 pmoles with 14 pmoles reductase) for 30 min. The incubation mixtures were extracted with ethyl acetate (no internal standard added) as previously described (Thatcher et al., 2010) and analyzed using an

AB Sciex API 5500 Q/LIT mass spectrometer equipped with an Agilent 1290 Infinity UHPLC and Agilent Zorbax C18 column (3.5 μm, 2.1 x 100 mm). The metabolites were separated using gradient elution from 10 % acetonitrile and 90% aqueous ammonium acetate (50 mM) to 90 % acetonitrile over 30 minutes. The column was maintained at 25°C and the injection volume was 2 μL. Metabolites were monitored by negative ion electrospray mass spectrometry with the ion source voltage (IS) and source temperature (TEM) set at -4500 V and 400° C, respectively. The MRM transitions of *m/z* 313 → 269 Da, 315 → 241 Da, 315 → 253 Da, 329 → 255 Da, 329 → 267 Da, 331 → 239 Da and 331 → 269 Da were monitored in incubations with unlabeled *at*RA and its metabolites. The declustering potential, collision energy, and collision exit potential were set to -90 V, -25 V, and -10 V, respectively. Formation of all the identified metabolites was determined to be NADPH dependent.

Depletion of (4S)-OH-RA, (4R)-OH-RA, 4-oxo-RA and 18-OH-RA by CYP26A1 and CYP26B1. Incubations with (4S)-OH-RA, (4R)-OH-RA, 4-oxo-RA and 18-OH-RA were performed in 8 x 13 mm borosilicate glass test tubes as previously described (Thatcher et al., 2010). For full depletion curves, samples were run in duplicate with CYP26A1 (2 pmol/mL enzyme and 4 pmol/mL rat reductase) or CYP26B1 (4 pmol/mL enzyme and 8 pmol/mL rat reductase) using at least five substrate concentrations ranging from 5 to 150 nM (CYP26A1) or 10 to 300 nM (CYP26B1) in an initial volume of 2 mL in KPi buffer. Standard curves for each substrate were constructed in 100 mM KPi buffer (pH 7.4) containing enzyme. Rat P450 reductase was added to CYP26A1 and CYP26B1 membrane preparations in a 2:1 reductase to P450 ratio and pre-incubated for 5 min at room temperature to allow for reductase incorporation into the membrane before being added to each sample. Samples containing enzyme and substrate in buffer were pre-incubated for 5 min at 37ºC before the addition of NADPH (final

concentration of 1 mM) to initiate the reaction. At designated time points for incubations with CYP26A1 (0.5, 1, 2, and 5 min) and CYP26B1 (1, 2, 5, and 10 min), aliquots of 0.5 mL were collected and immediately quenched into a test tube containing 3 mL of cold ethyl acetate. For the final time point, ethyl acetate was added directly into the incubation vial. An internal standard of 4-oxo-RA-d_3 (20 µL of a 2.5 µM solution in ethanol) was added to all samples, and samples were extracted as described above.

For determination of Cl_{int} by substrate depletion, the metabolites were incubated at a concentration << K_m. The concentrations were 2.5 nM ((4S)-OH-RA and (4R)-OH-RA) and 5nM (4-oxo-RA and 18-OH-RA) with CYP26A1 and 2.5 nM (all substrates) with CYP26B1. Samples were incubated in triplicate with CYP26A1 (2 pmol/mL and 4 pmol/mL P450 rat reductase) or CYP26B1 (1 pmol/mL and 2 pmol/mL P450 rat reductase). Incubations were initiated with NADPH (final concentration of 1 mM) for an initial volume of 4.5 mL KPi buffer. One mL aliquots were removed at designated time points for CYP26A1 incubations (0.5, 1, 1.5, and 2 min) or CYP26B1 incubations (2, 5, 10, and 20 min). For depletion experiments, the analytes were separated over a linear 10 min gradient using an initial mobile phase condition of 5:95 acetonitrile: 0.1% aqueous formic acid (optima grade water) to a final condition of 95:5 acetonitrile: 0.1% aqueous formic acid. Analytes were detected using positive ion electrospray mass spectrometry, with declustering potentials of 80 V (18-OH-RA and 4-oxo-RA), collision energies of 20 eV (18-OH-RA) and 37 eV (4-oxo-RA) and a collision exit potential of 13 V (18-OH-RA and 4-oxo-RA). The parent-fragment MS/MS transitions of *m/z* 317 → 253 Da (18-OH-RA) and 315 → 121 Da (4-oxo-RA) were monitored. Mass spectrometry parameters for (4R)-OH-RA, (4S)-OH-RA, and 4-oxo-RA-d_3 were performed as described in the characterization of 4-OH-RA enantiomer formation from *at*RA.

Data Analysis. Data analysis from HPLC-UV was performed using HP Chemstation software. Mass spectrometry data was analyzed using Analyst software (AB Sciex, Foster City, CA). Peak heights were used to determine the ratio of substrate to the internal standard (4-oxo-RA-d_3).

For depletion analyses, substrate concentrations were plotted against time to determine the concentration-dependent depletion rates (k_{dep}) (Eq. 1).

$C = C_0 e^{-k_{dep} t}$ equation 1

The k_{dep} values were then plotted in GraphPad Prism v.5 (La Jolla, CA) against the respective average concentration over the entire time interval during the depletion experiment and fitted using Eq. 2 to determine K_m.

$k_{dep} = k_{dep,max} * (1 - \frac{[S]}{[S] + K_m})$ equation 2

Intrinsic clearances (Cl_{int}) for each metabolite by CYP26A1 and CYP26B1 were calculated using $k_{dep,max}$ values obtained from substrate depletion at concentrations << K_m (Eq. 3).

$Cl_{int} = \frac{V_{rxn} * k_{dep,max}}{pmoles\ CYP}$ equation 3

Symbols used in the equations above included the following abbreviations: reaction volume (V_{rxn}), depletion rate (k_{dep}), concentration (C), initial concentration (C_0), and substrate concentration (S).

2.3 Results

2.3.1 Synthesis of 18-OH-RA. The 18-OH-RA was synthesized from 2-formyl-6,6-dimethylcyclohexanone as previously described with two important modifications (Rosenberger, 1982; Kawanobe, 1984) (Figure 2.2). The isomerization of the mixture of 11-*cis*- and 11-*trans*-isomers of the intermediate 18-acetate ester of ethyl retinoate to the 11-all-*trans*diester was effectively accomplished using palladium nitrate, a water soluble catalyst more easily removed

than bis(benzonitrile)palladium dichloride, and the final product was obtained by alkaline hydrolysis of both the 18-acetate and 15-ethyl esters under mild conditions, a one-step procedure that avoids the multi-step exchange of protecting groups (Rosenberger, 1982).

2-Methylcyclohexanone, **1**, was selectively methylated at the 2-position using sodium hydride and iodomethane. Then, the methylated ketone was formylated in the 6-position using sodium methoxide and methyl formate to produce **2**, during which the mixture became thick and clumpy and was light yellow in color. The formyl group was then protected as an enol ether, **3a**, by the addition of an isopropyl group using iodopropane and potassium bicarbonate**.**

The acetal **3b** was synthesized by the addition of ethyl vinyl ether to 3-hydroxy-3-methyl-1-penten-4-yne using *p*-toluenesulfonic acid. Compound **3b** was then adducted to **3a** using *n*-butyllithium, forming the acetylenic anion. The ethyl ether and isopropyl protecting groups were then removed via acid catalyzed hydrolysis using aqueous H_2SO_4 (1 N) to form the aldehyde **4**.

Aldehyde **4** contains 15 of the 20 carbons of 18-hydroxyretinoic acid, including the essential hydroxyl group adjacent to the alkyne. The alkyne and aldehyde groups were reduced using three equivalents of lithium aluminum hydride. The resulting carbinol was then re-protected via acetylation using acetic anhydride and pyridine to provide **5.** The reduction was modified from Rosenberger's method, in which 1.5 equivalents of lithium aluminum hydride were used (Rosenberger, 1982). However, using only 1.5 equivalents of lithium aluminum hydride afforded reduction of the aldehyde group but not the alkyne. It was also found that running the reaction in ether resulted in a large clumping of material out of the solution. Thus, THF was used in place of ether following a modified protocol.

The phosphonium salt **6** (ylid) was formed by the addition of triphenylphosphinehydrobromide to the acetylated **5**. The Rosenberger procedure was slightly modified. The liquid layer was decanted instead of removing the salt via filtration, yielding an orange residue that was soluble in methylene chloride but not in ether.

The Wittig reaction was performed to selectively add ethyl-3-methyl-4-oxocrotonate to the C-11 position of the phosphonium salt ylid. The di-ester product **7** was a mixture of 11-*cis* and 11-*trans* isomers. About 60% of the material was lost due to technical error, and therefore the percent yield is indicative of recovered product, not total product formed.

In the method described by Rosenberger, bis(benzonitrile)palladium dichloride was used to selectively complex the 11-*cis* hydroxyl-ester and convert it to its all-*trans* isomer (Rosenberger, 1982). However, removal of the palladium dichloride catalyst was of a concern due to similarities in the lipophilic nature of the catalyst and the di-ester. Instead, a palladium nitrate catalyst was used to convert any 11-*cis* isomers to all-*trans* prior to hydrolysis. Both the di-ester and hydrolyzed forms of **7** efficiently complex with the catalyst. However, as the palladium nitrate was water soluble, the di-ester was used in order to facilitate the aqueous extraction of the palladium catalyst. HPLC/UV was used to monitor the reaction over time. There were three main peaks that were less than 1 min apart in the reactant material, determined by NMR to be the all-*trans*-hydroxyl-ester, 11-*cis*-hydroxyl-ester, and 9-*cis*-hydroxyl-ester, respectively. After the reaction had run overnight, the middle peak (11-*cis*-hydroxyl-ester) disappeared and the area of the first peak (all-*trans*-hydroxyl-ester) increased. NMR analysis was used to confirm that >95% of the material from the reaction was the all-*trans* isomer.

The hydrolysis procedure was also modified from Rosenberger's method, in which the hydroxyl group on the C-18 position was deprotected and reprotected using ethyl vinyl ether

before hydrolyzing the ethyl ester on the aliphatic chain of the molecule at reflux. Instead, hydrolysis of **7** was done using dilute potassium hydroxide (1 M) in methanol/water (1:9) for 8.5 hours at room temperature, yielding the 18-hydroxy all-*trans* retinoic acid **8**. The reaction was monitored by TLC. Purification of the crude **8** was done by crystallization followed by further HPLC fraction collecting from the mother liquor. The final product yielded an orange-yellow powder.

Analysis of **8** by NMR, HPLC and negative ion electrospray MS/MS showed one major peak (> 95% of the total peak areas detected) to be of the correct mass. Based upon NMR shifts (Table 2-1), retention time, an *m/z* of 315 (negative ion electrospray, M-1) and fragmentation patterns matching the literature values (Rosenberger, 1982; Chithalen et al., 2002). Calculation of the extinction coefficient via UV analysis ($\varepsilon_{experimental}$ = 24,000 1/M*cm in EtOH) differed from the reported value (ε = 49,400 1/M*cm in EtOH) (Rosenberger, 1982). Melting point analysis determined **8** to completely melt at 147.1°C (lower than the reported value of 185-188°C) with the melting range spanning 30 degrees.

2.3.2 Formation Kinetics of 4-OH-RA and 18-OH-RA by CYP26A1 and CYP26B1 from *at*RA

. The kinetics of *at*RA metabolism by CYP26A1 and CYP26B1 were measured using the formation of 4-OH-RA and 18-OH-RA. The Michaelis–Menten plots and HPLC–UV chromatograms of the kinetic characterization are shown in Figure 2.3. Based on 4-OH-RA formation, CYP26A1 had greater catalytic activity (V_{max}) than CYP26B1 but lower affinity for *at*RA than did CYP26B1 (Table 2-2). Based on the HPLC–UV traces, 4-OH-RA was the most abundant metabolite formed by both enzymes. The predominant formation of 4-OH-RA was also supported by the 45 % lower V_{max} for 18-OH-RA formation compared to 4-OH-RA formation by CYP26A1 (Table 2-2). With CYP26B1, 18-OH-RA formation could be detected

but the formation was insufficient to determine kinetic constants. Based on the overall intrinsic clearances, CYP26A1 had a significantly higher catalytic efficiency towards *at*RA metabolism than does CYP26B1.

2.3.3 Stereoselective Formation of 4-OH-RA enantiomers by CYP26A1 and CYP26B1 from *at*RA.

The stereoselectivity in the formation of 4-OH-RA enantiomers by CYP26A1 and CYP26B1was first qualitatively determined from *at*RA. Metabolism of *at*RA by CYP26A1 preferentially resulted in the formation of (4S)-OH-RA enantiomer over the (4R)-OH-RA enantiomer (Figure 2.4). When *at*RA was incubated with CYP26B1, an *at*RA concentration-dependent formation of both 4-OH-RA enantiomers was observed. At a low concentration of *at*RA (20 nM, Figure 2.4) (4R)-OH-RA and (4S)-OH-RA were formed by CYP26B1 in a 1:2 ratio, whereas at higher concentrations of *at*RA (300 nM), the formation of (4R)-OH-RA increased to a relative ratio of 1:1 ((4R)-OH-RA to (4S)-OH-RA). Thus, CYP26B1 is less stereospecific than is CYP26A1 in formation of 4-OH-RA enantiomers.

Separation of the 4-OH-RA enantiomers formed from *at*RA by CYP26A1 using a chiral column enabled the quantification of the Michaelis-Menten parameters for stereoselective formation of (4S)-OH-RA and (4R)-OH-RA. The k_{cat} for (4S)-OH-RA formation by CYP26A1 was 2.1 ± 0.2 pmol/min/pmoles of P450 and K_m was 10 ± 6 nM. The K_m and k_{cat} of (4R)-OH-RA formation could not be determined due to the very low formation of this enantiomer by CYP26A1 and the lack of concentration dependence in its formation. Quantification of Michaelis-Menten parameters of (4S)-OH-RA and (4R)-OH-RA formation by CYP26B1 was not possible due to the low K_m of *at*RA, low catalytic activity of CYP26B1 and significant substrate and product depletion (data not shown). The detection limit for (4S)-OH-RA and (4R)-OH-RA

using the method involving chiral separation was significantly higher than that with the other detection methods (wide peak width due to constrained acceptable column flow parameters).

2.3.4 Identification of sequential metabolites from *at*RA, 4-OH-RA (racemic), (4S)-OH-RA and (4R)-OH-RA by CYP26A1 and CYP26B1. To characterize the sequential metabolites formed by CYP26 from *at*RA, *at*RA, 4-OH-RA (rac), (4S)-OH-RA and (4R)-OH-RA were incubated with CYP26A1 (Figure 2.5, left panels) and CYP26B1 (Figure 2.5, right panels) and metabolite formation was determined by LC-MS/MS. Three major metabolites that were formed from all substrates by CYP26A1 and CYP26B1 were identified. Two were dihydroxylated products identified as 4,16-OH_2-RA (*m/z* 331 → 239 Da, retention time 10.4 min) and 4,18-OH_2-RA (*m/z* 331 → 269 Da, retention time 13.7). The other metabolite was an oxo-OH product identified as 4-oxo-16-OH-RA (*m/z* 329 → 255 Da, retention time 12.3 min) based on mass spectrometry and fragmentation patterns.

The major product formed by CYP26A1 from *at*RA (Figure 2.5A) and racemic 4-OH-RA (Figure 2.5C) was 4,16-OH_2-RA, whereas less specificity towards the formation of a major metabolite was observed with CYP26B1 (Figure 2.5B,D). Mass spectrometric analysis of the metabolic products formed from (4S)-OH-RA by CYP26A1 showed that the dihydroxylated product, 4,16-OH_2-RA, was the predominant metabolite formed from (4S)-OH-RA and 4-oxo-RA was a minor metabolite (Figure 2.5E). In contrast, 4-oxo-RA was a major product formed from (4R)-OH-RA by CYP26A1 along with multiple dihydroxylated metabolites including 4,16-OH_2-RA, 4,18-OH_2-RA, 4-oxo-16-OH-RA and 4-oxo-18-OH-RA (Figure 2.5G). These products were also detectable from (4S)-OH-RA but were quantitatively minor. The predominant formation of 4,16-OH_2-RA from (4S)-OH-RA by CYP26A1 was similar to that seen from *at*RA, further confirming that the enantiomer formed directly from *at*RA is (4S)-OH-RA. Similarly to

CYP26A1, the primary metabolic product formed from (4S)-OH-RA by CYP26B1 was 4,16-OH_2-RA (Figure 2.5F). However, incubations with (4R)-OH-RA and CYP26B1 yielded dihydroxylated products 4,16-OH_2-RA, 4,18-OH_2-RA, and 4-oxo-16-OH-RA, the formation of none distinctively preferred over another (Figure 2.5H). Unlike with CYP26A1, 4-oxo-RA was not detectable as a metabolite formed from either 4-OH-RA enantiomer by CYP26B1.

2.3.5 Kinetics of Metabolism of (4S)-OH-RA, (4R)-OH-RA, 18-OH-RA and 4-oxo-RA by CYP26A1 and CYP26B1. To determine the catalytic efficiency of CYP26A1 in metabolizing 4-OH-RA enantiomers, substrate depletion experiments were conducted. To calculate the relative affinities (K_m) of (4R)-OH-RA and (4S)-OH-RA with CYP26A1 and CYP26B1, the depletion rates were analyzed at different concentrations. The depletion curves as well as the relationship between k_{dep} and 4-OH-RA concentration are shown in Figure 2.6A and B; depletion curves for CYP26B1-mediated metabolism are shown in Figure 2.6C and D. The affinity of (4S)-OH-RA (K_m = 5.2 ± 1.3 nM) towards CYP26A1 was not significantly different from that of (4R)-OH-RA (K_m = 11.0 ± 5.2 nM) (Table 2-3). In contrast to CYP26A1, the K_m of (4R)-OH-RA (31 ± 19 nM) with CYP26B1 was 7.7-fold higher than that for (4S)-OH-RA (4.0 ± 2.5 nM) (Table 2-3).

When (4S)-OH-RA and (4R)-OH-RA were incubated with CYP26A1 at 2.5 nM concentrations (< K_m), the depletion of (4S)-OH-RA was significantly faster (***$P < 0.001$, Cl_{int} = 1450 ± 150 µL/min/pmol P450) than that of (4R)-OH-RA (Cl_{int} = 740 ± 12 µL/min/pmol P450) (Figure 2.8A, Table 2-3). In contrast, the depletion of (4R)-OH-RA by CYP26B1 at 2.5 nM concentration (<< K_m) was significantly faster (*$P < 0.05$, Cl_{int} = 104 ± 19 µL/min/pmol P450) than that of (4S)-OH-RA (Cl_{int} = 46 ± 18 µL/min/pmol P450) (Figure 2.8B, Table 2-3). Overall, the depletion rates by CYP26A1 were much faster than those by CYP26B1.

Full concentration-dependent depletion curves were also constructed to determine 4-oxo-RA and 18-OH-RA depletion by CYP26A1 (Figure 2.7A,B) and CYP26B1 (Figure 2.7C,D). The K_m estimates for 4-oxo-RA and 18-OH-RA with CYP26A1 were 63 ± 24 nM and 39 ± 25 nM, respectively (Table 2-3). The K_ms for 4-oxo-RA (29 ± 6.6 nM) and 18-OH-RA (4.8 ± 6.3 nM) depletion by CYP26B1 were significantly lower than those for CYP26A1 (Table 2-3). The intrinsic clearances of 18-OH-RA and 4-oxo-RA by CYP26A1 were calculated from the lowest point on the depletion curve and were 2.5-fold higher for 18-OH-RA (290 ± 98 µL/min/pmol P450) than for 4-oxo-RA (91 ± 16 µL/min/pmol P450) (Figure 2.8A, Table 2-3). The overall Cl_{int} values of 18-OH-RA and 4-oxo-RA by CYP26B1 (33 ± 10 µL/min/pmol P450 for 18-OH-RA) and (15 ± 4.0 µL/min/pmol P450 for 4-oxo-RA) were lower than those measured for CYP26A1 (Figure 2.8B, Table 2-3).

2.4 Discussion

Based on the biological necessity of two enzymes highly conserved and specific for *at*RA metabolism and the low sequence homology between the two enzymes (40-50 %), we hypothesized that CYP26A1 and CYP26B1 are functionally different with regards to the oxidative metabolism of *at*RA and its subsequent metabolites. Differences were indeed observed in the formation of the primary metabolites of *at*RA by CYP26A1 and CYP26B1, both in the catalytic efficiencies and relative metabolic profiles, although the same metabolites were formed by both enzymes (Figure 2.3 and Figure 2.5). The ratio between 4-OH-RA and 18-OH-RA formed was 7.7-fold greater with CYP26B1 than CYP26A1 (Figure 2.3). Also, the formation of 4-OH-RA enantiomers was less stereoselective by CYP26B1 than by CYP26A1. CYP26A1 was shown to predominantly favor formation of (4S)-OH-RA (Figure 2.4A), while CYP26B1 formed both stereoisomers, with a ratio between 1:1 and 1:2 (Figure 2.4B). The stereoselective

formation of (4S)-OH-RA by CYP26A1 from *at*RA is in agreement with the proposed orientation of *at*RA within the active site of CYP26A1 (Shimshoni et al., 2012). A homology model of *at*RA in the active site of CYP26A1 depicted the β-ionone ring of *at*RA to reside in an angle that the C-4, C-16 and C-18 positions were at similar distances from the heme, but that the (4S)-hydrogen is positioned 1.5Å closer than the (4R)-hydrogen (Shimshoni et al., 2012). It is likely that within the CYP26B1 active site, the β-ionone ring is in a different angle in relation to the heme position such that both C-4S and C-4R hydrogens are close to the heme but the C-18 and C-16 hydrogens are further away from the heme.

In incubations of *at*RA with CYP26A1 and CYP26B1, metabolites that were more polar than 4-OH-RA were detected (Figure 2.3A and B) suggesting that some primary oxidation products of *at*RA are also substrates of CYP26A1 and CYP26B1. Indeed, when 4-OH-RA, 18-OH-RA and 4-oxo-RA were incubated with CYP26A1 and CYP26B1, depletion of all three substrates was observed and formation of more polar metabolites detected (Topletz et al., 2012). Due to the formation of multiple dihydroxylated metabolites from 4-OH-RA, 18-OH-RA and 4-oxo-RA for which no synthetic standards are available, substrate depletion was used to characterize and compare metabolism of these compounds by CYP26A1 and CYP26B1. Also, as both 4-OH-RA enantiomers were formed by CYP26B1 and have been shown to be formed by CYP3A and CYP2C8 enzymes (Shimshoni et al., 2012), it is possible that both 4-OH-RA enantiomers are formed in tissues containing CYP26B1 or other P450 enzymes. Thus, the depletion and subsequent metabolite formation of (4R)-OH-RA and (4S)-OH-RA by both CYP26A1 and CYP26B1 was characterized.

Of particular interest was that the predominant metabolite formed from (4S)-OH-RA by CYP26A1 was 4,16-OH_2-RA, whereas from (4R)-OH-RA, CYP26A1 formed mainly 4-oxo-RA,

which is found in human plasma and known to be an active retinoid (Pijnappel et al., 1993; Idres et al., 2002). Since (4S)-OH-RA is the preferentially formed enantiomer from *at*RA by CYP26A1 (Figure 2.4A), this data suggests that CYP26A1 is an enzyme that deactivates retinoids. Similarly, CYP26B1 was shown to form only dihydroxylated products from both enantiomers, inactivating both 4-OH-RA enantiomers it forms. However the predominant metabolite (4,16-OH_2-RA) was formed from (4S)-OH-RA by CYP26B1 whereas it was not formed from (4R)-OH-RA. (4S)-OH-RA has a much higher affinity (87% lower K_m) but lower rate of catabolism (55.7% lower Cl_{int}) than (4R)-OH-RA by CYP26A1. These differences between 4-OH-RA enantiomer elimination provide further insight into the differences in structure-function between CYP26A1 and CYP26B1.

*at*RA had a higher affinity and intrinsic clearance (1220 µL/min/pmoles CYP26A1) with CYP26A1 than of all the metabolites tested except (4S)-OH-RA (1450 ± 150 µL/min/pmoles CYP26A1), the 4-OH-RA enantiomer formed by CYP26A1. Between the metabolites, (4S)-OH-RA exhibited the lowest K_m (5.2 ± 1.3 nM) and 4-oxo-RA the highest K_m (63 ± 24 nM) towards CYP26A1. The intrinsic clearance of (4S)-OH-RA (1450 ± 150 µL/min/pmoles CYP26A1) by CYP26A1 was 13.5-fold and 5.1-fold higher than that of 4-oxo-RA (91 ± 16 µL/min/pmoles CYP26A1) and 18-OH-RA (290 ± 98 µL/min/pmoles CYP26A1), respectively (Table 2-3). Metabolism of 4-oxo-RA by recombinant CYP26A1 was shown to be > 90 % slower than that reported for *at*RA (Table 2-3) (Lutz et al., 2009). Conversely to CYP26A1, (4R)-OH-RA (Cl_{int} = 104 ± 19 µL/min/pmol P450) metabolism by CYP26B1 was about 2-fold more efficient than (4S)-OH-RA (Cl_{int} = 46 ± 18 µL/min/pmol P450) (Table 2-3) and the Cl_{int} of *at*RA by CYP26B1 was greater than that for any of the four metabolites. Overall, CYP26A1 had a higher catalytic

activity than CYP26B1 towards all substrates, with clearance values by CYP26B1 being 7 to 31-fold lower than those observed with CYP26A1.

The data shown here suggests that CYP26B1 is a high affinity low capacity RA hydroxylase with a specific biological role and CYP26A1 is a lower affinity, higher capacity RA hydroxylase. As shown here, *at*RA binds both CYP26A1 and CYP26B1 with high affinity with 2-fold greater K_m value for CYP26A1. In accordance with the high affinity low capacity definition, the V_{max} for CYP26B1 mediated 4-OH-RA formation was only 10% of that determined for CYP26A1 (Table 2-2). In addition, formation of other metabolites was not efficient enough by CYP26B1 to allow determination of kinetic constants. Thus, in the overall depletion of *at*RA, CYP26A1 is approximately 20-fold more efficient than CYP26B1 due to rapid formation of multiple primary metabolites (4-OH-RA, 18-OH-RA and 16-OH-RA) (Figure 2.3). This supports the role of CYP26A1 as a high capacity *at*RA hydroxylase. CYP26A1 was also more efficient in depleting the metabolites of *at*RA than CYP26B1 supporting the identification of CYP26B1 as a high affinity low capacity CYP26 enzyme. The higher capacity and efficiency of CYP26A1 as an *at*RA hydroxylase compared to CYP26B1 appears consistent with its expression in the human liver where it presumably contributes to the first pass metabolism of *at*RA obtained from the diet (Thatcher et al., 2010). Based on mRNA data, CYP26B1 on the other hand is expressed in tissues with much lower metabolic activity such as cerebellum (Xi and Yang, 2008; Topletz et al., 2012).

Despite the lower catalytic efficiency of CYP26B1 than CYP26A1, it has approximately 100-fold higher intrinsic clearance towards *at*RA than common drug metabolizing P450s such as CYP3A4 and CYP2C8. The intrinsic clearance of *at*RA metabolism by CYP26B1 was 43 mL/min/pmol P450 (Table 2-2), whereas the intrinsic clearances by CYP3As and CYP2C8 are

0.2 to 0.4 mL/min/pmol P450 (Thatcher et al., 2010). It is not clear why CYP26B1 has a much lower V_{max} (0.8 pmol/min/pmol P450) for *at*RA hydroxylation than other P450s (2 to 5 pmol/min/pmol P450 for CYP3As and CYP2C8, 10 pmol/min/pmol P450 for CYP26A1) (Thatcher et al., 2010). It is possible that CYP26B1 is not as well coupled for the P450 cycle as the other P450s or that P450 reductase is not the only electron transfer partner, nor the optimal one for CYP26B1. If an alternative electron transfer partner is preferred, the catalytic activity observed in this study does not reflect the maximum catalytic rate of CYP26B1 in vivo. In addition, the recombinant system used here does not include other cellular soluble or membrane bound proteins that may affect CYP26B1 activity and *at*RA metabolism.

In conclusion, clear differences were observed in the metabolic profiles and catalytic efficiencies of *at*RA and its metabolites between CYP26A1 and CYP26B1. The *at*RA metabolites, (4S)-OH-RA, (4R)-OH-RA, 4-oxo-RA and 18-OH-RA were found to be substrates of both CYP26A1 and CYP26B1 and CYP26 enzymes mostly formed dihydroxylated products except from (4R)-OH-RA, from which 4-oxo-RA was formed by CYP26A1. Based on this data, the enzyme responsible for 4-oxo-RA formation in vivo remains to be identified. CYP26A1 metabolized all substrates tested faster than CYP26B1, although CYP26B1 preferred (4R)-OH-RA over (4S)-OH-RA as a substrate, conversely to CYP26A1. CYP26B1 appeared to be less stereospecific than CYP26A1 though it preferentially oxidized *at*RA at the C-4 position whereas CYP26A1 oxidized *at*RA at the C-4, C-16, and C-18 positions. Based on the localization of CYP26A1 (predominantly in the liver) and CYP26B1 (extrahepatically) it is likely that the two enzymes function in concert to regulate the tissue and cell specific exposure of *at*RA and its metabolites.

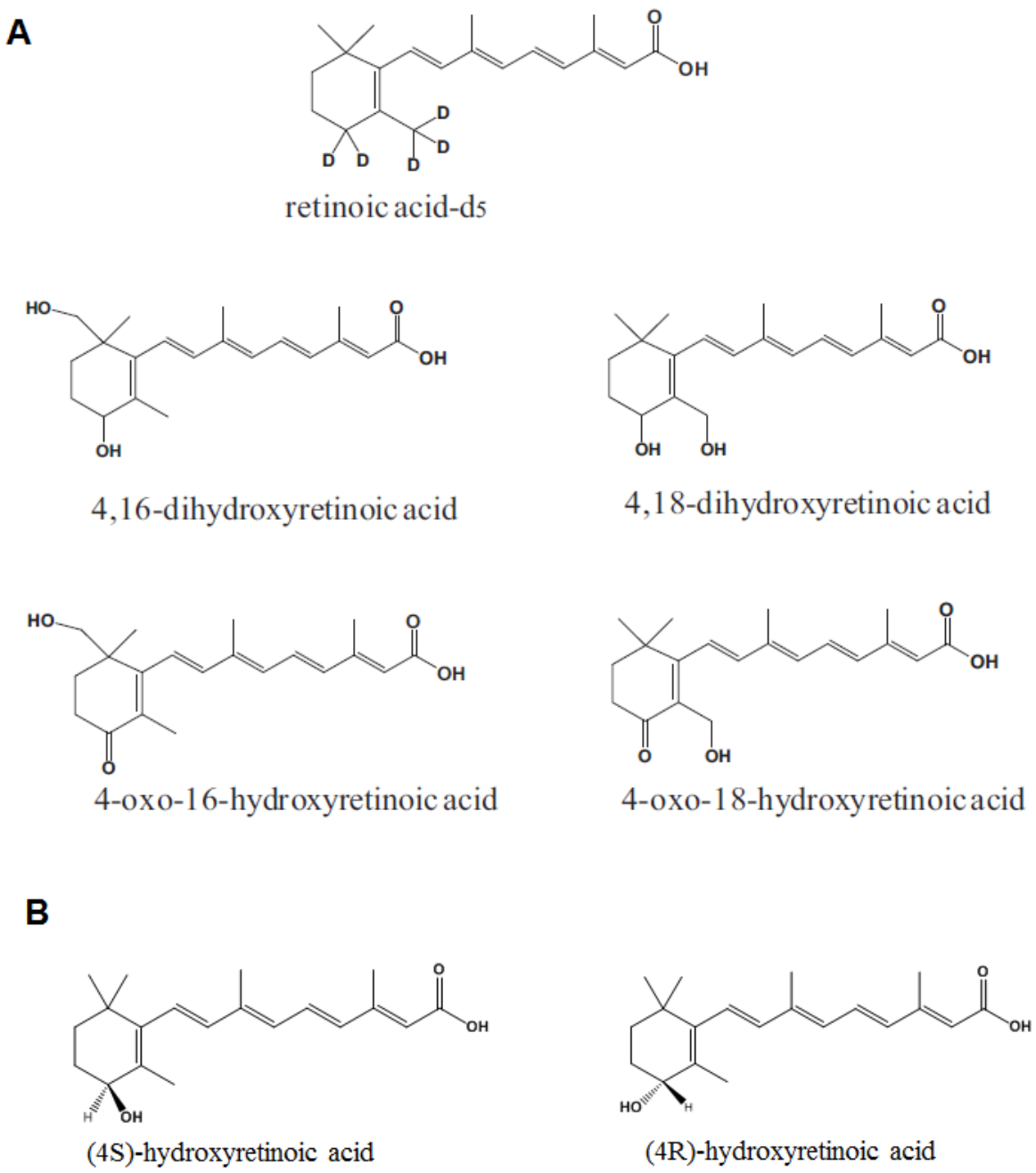

Figure 2.1: Chemical structures of (A) *at*RA-d_5 and *at*RA secondary oxidative metabolites by CYP26A1 and CYP26B1 (B) Enantiomers of 4-OH-RA

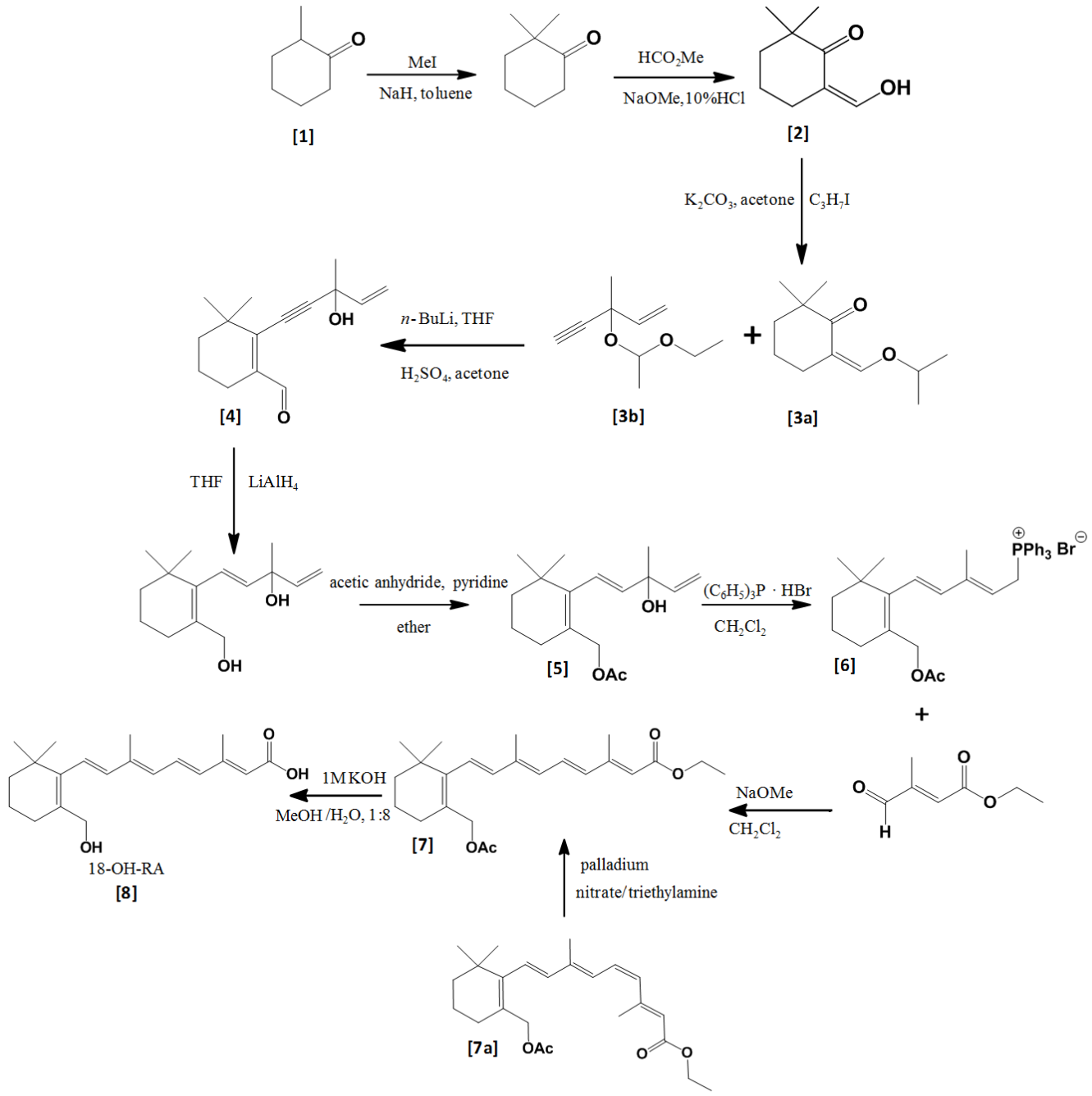

Figure 2.2: Scheme of total synthesis of 18-OH-RA [8]

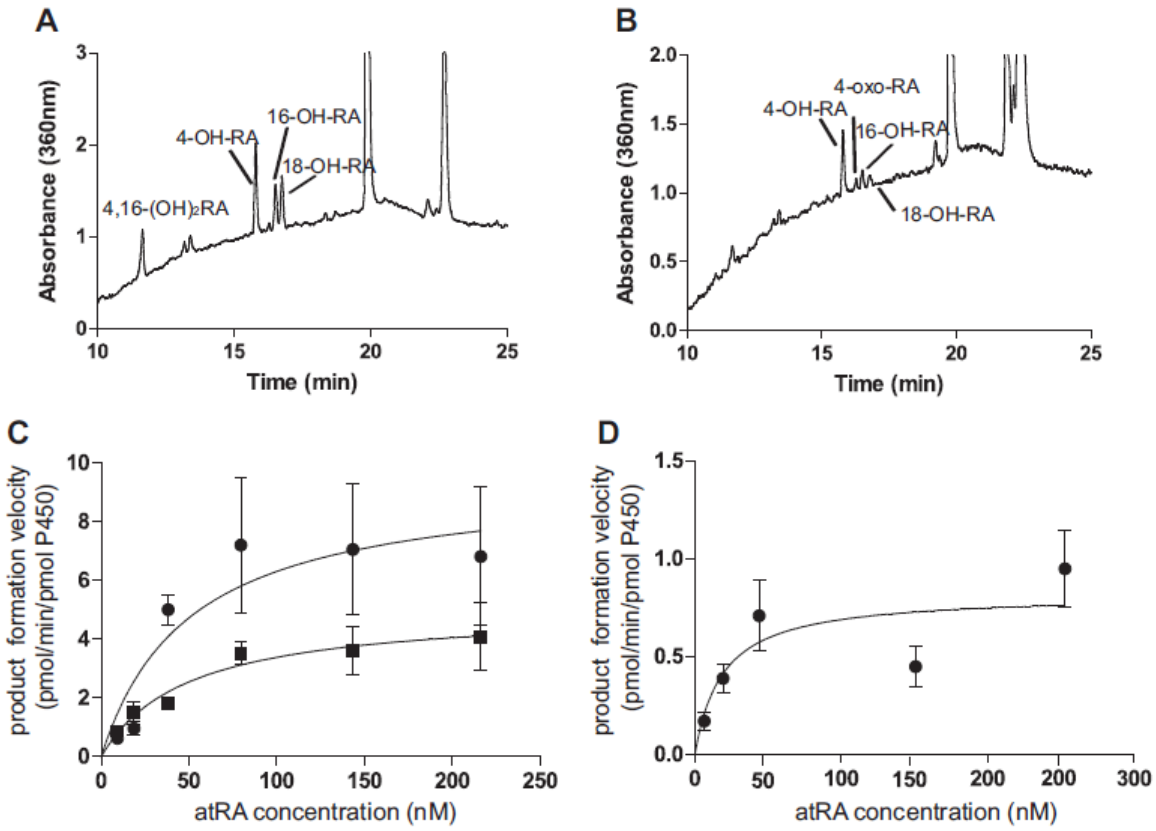

Figure 2.3: Determination of kinetics of formation of 4-OH-RA and 18-OH-RA by CYP26A1 and CYP26B1. The formation of 4-OH-RA and 18-OH-RA was determined using 2 pmol CYP26, 4 pmol reductase and *at*RA concentrations of 10–250 nM incubated for 2 min (CYP26A1) or 5 min (CYP26B1). The Michaelis–Menten equation was fitted to the data. Panels A and B show the representative HPLC–UV chromatograms of 4-OH-RA and 18-OH-RA formation by CYP26A1 and CYP26B1, respectively. The Michaelis–Menten plots are shown for CYP26A1 (C) and CYP26B1 (D) mediated 4-OH-RA (circles) and 18-OH-RA (squares) formation.

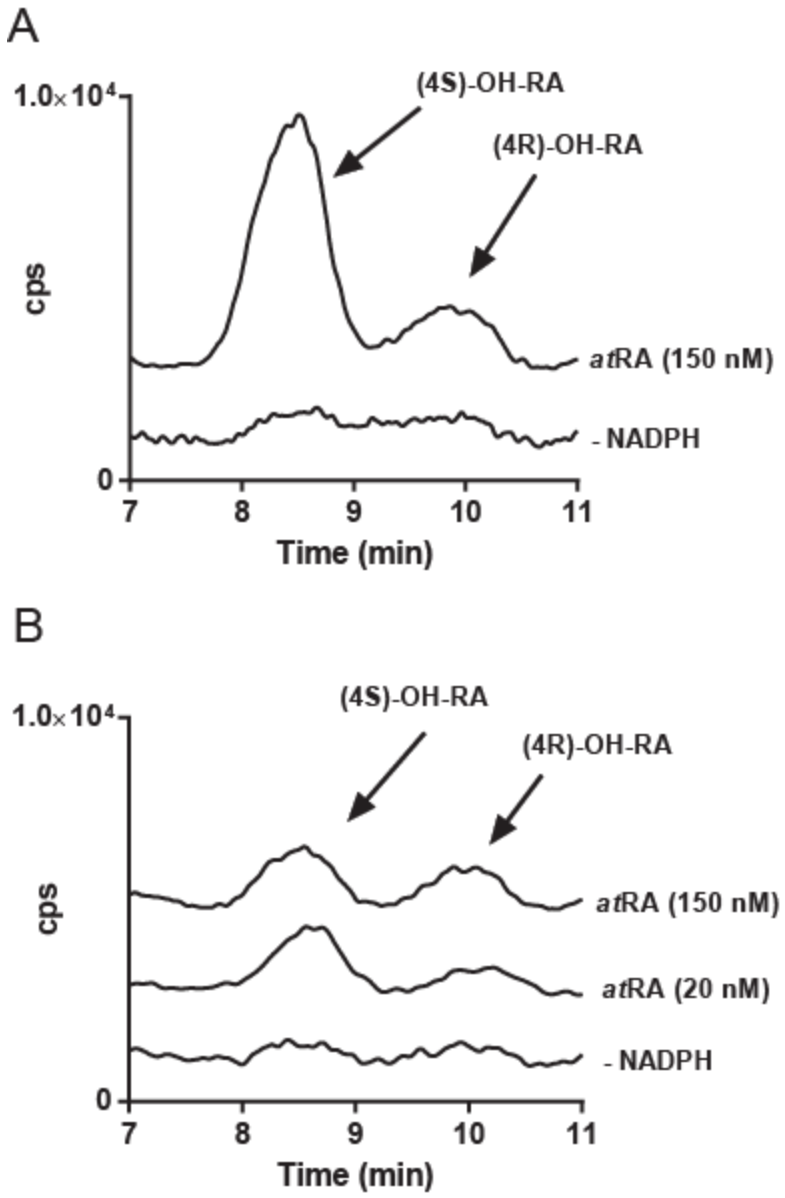

Figure 2.4: Chromatograph of chiral separation of (4S)-OH-RA and (4R)-OH-RA formed by CYP26A1 (A) and CYP26B1 (B) from *at*RA. The relative formation of (4R)-OH-RA to (4S)-OH-RA by CYP26B1 appears to be higher at greater *at*RA concentrations.

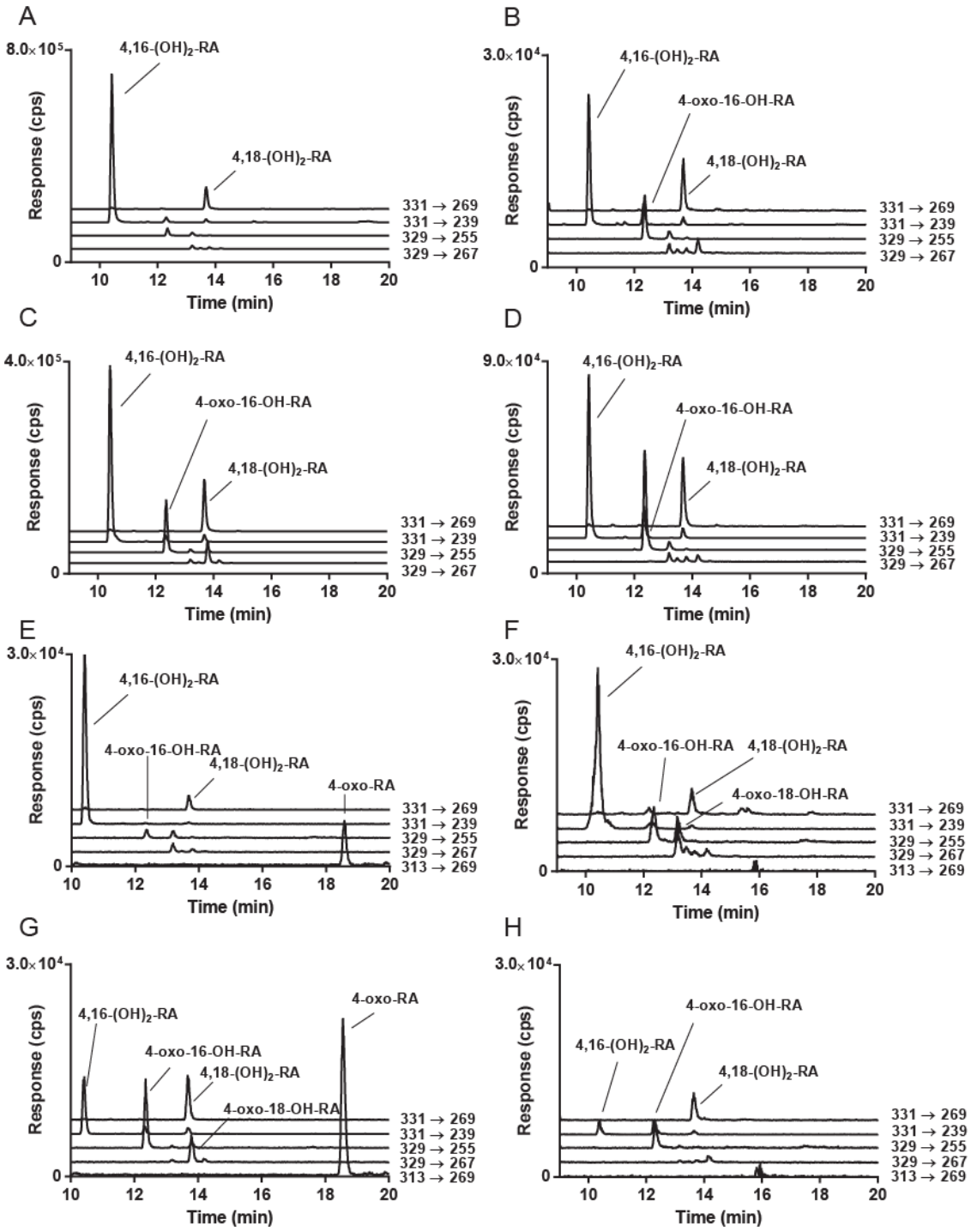

Figure 2.5: Identification of sequential metabolites of *at*RA formed by CYP26A1 and CYP26B1. The traces of the SRM transitions of incubations of *at*RA (A,B), 4-OH-RA (C,D), (4S)-OH-RA (E,F) and (4R)-OH-RA (G,H) with CYP26A1 (left panel) and CYP26B1 (right panel) are shown. The negative ion MS/MS transitions monitored are shown next to each trace and the identified metabolites are indicated for each peak.

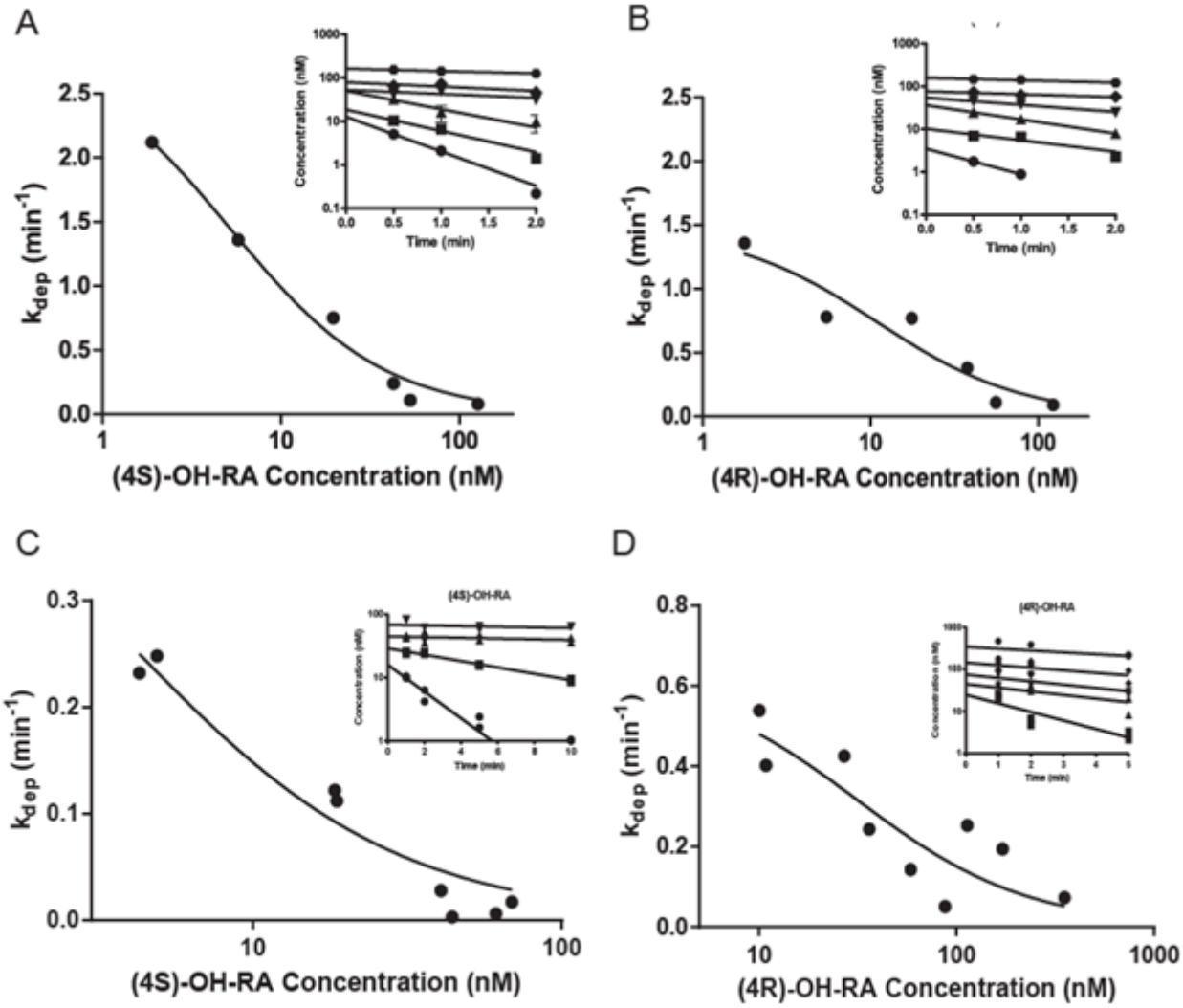

Figure 2.6: Representative determinations of the concentration-dependent depletion of (4S)-OH-RA (left panels) and (4R)-OH-RA (right panels) by CYP26A1 (A, B) and CYP26B1 (C, D) are shown. Depletions were done as described in the methods and depletion rate constants were determined (insets). Equation 2 was fitted to the data of depletion constants as a function of 4-OH-RA concentration to determine the K_ms of (4S)-OH-RA and (4R)-OH-RA depletion by CYP26A1 and CYP26B1. The kinetic values by CYP26A1 were $K_m = 5.2 \pm 1.3$ nM ((4S)-OH-RA) and $K_m = 11.0 \pm 5.2$ nM ((4R)-OH-RA). The kinetic values by CYP26B1 were $K_m = 4.0 \pm 2.5$ nM ((4S)-OH-RA) and $K_m = 31 \pm 19$ nM ((4R)-OH-RA)

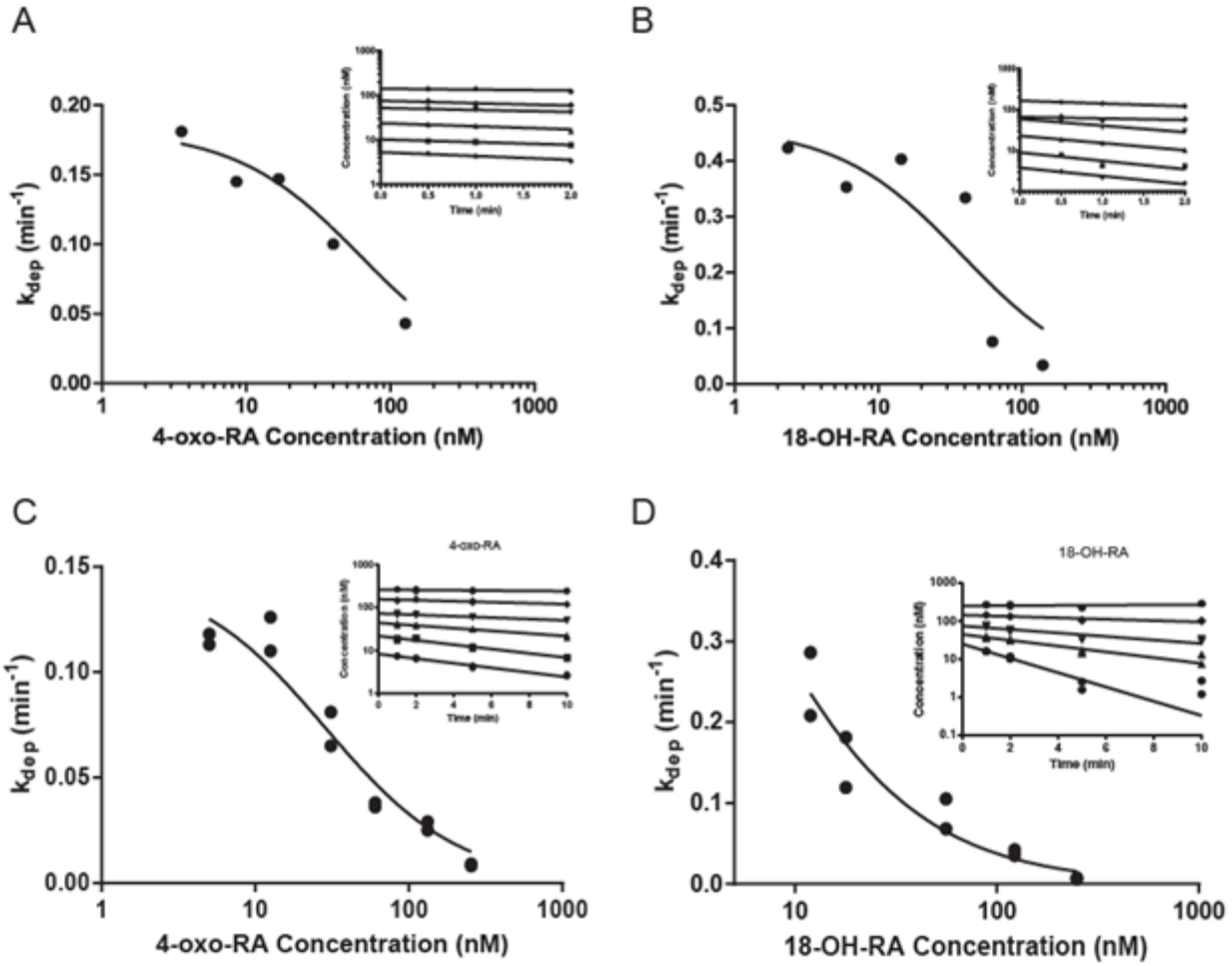

Figure 2.7: Representative determinations of the concentration-dependent depletion of 4-oxo-RA (left panels) and 18-OH-RA (right panels) by CYP26A1 (A, B) and CYP26B1 (C, D) are shown. Depletions were done as described in the methods and the depletion rate constants were determined (insets). Equation 2 was fitted to the data of depletion constants as a function of 4-OH-RA concentration to determine the K_ms of (4S)-OH-RA and (4R)-OH-RA depletion by CYP26A1 and CYP26B1. The kinetic values by CYP26A1 were K_m = 63 ± 24 nM (4-oxo-RA) and K_m = 39 ± 25 nM (18-OH-RA). The kinetic values by CYP26B1 were K_m = 29 ± 6.6 nM (4-oxo-RA) and K_m = 4.8 ± 6.3 nM (18-OH-RA).

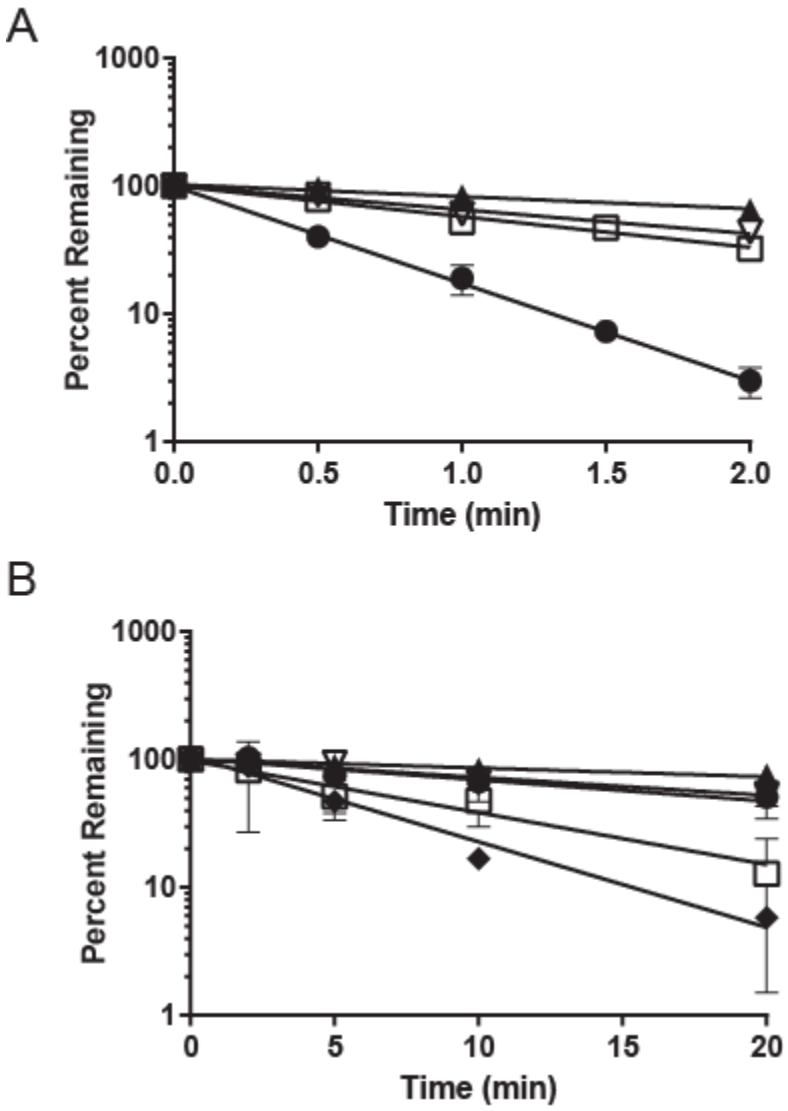

Figure 2.8: Depletion curves of (4S)-OH-RA (closed circles), (4R)-OH-RA (open squares), 4-oxo-RA (closed triangles), 18-OH-RA (open triangles) and *at*RA (closed diamonds) by CYP26A1 (A) and CYP26B1 (B) at a single concentration. Substrates were incubated at concentrations below the K_m (2.5 nM or 5 nM) using 2 pmoles/mL CYP26A1 or 1 pmol/mL CYP26B1. Cl_{int} values of CYP26A1 and CYP26B1-mediated metabolism were calculated from k_{dep} values using equation 3. Metabolism by CYP26A1 was 7 to 31-fold faster than that by CYP26B1 for all substrates.

Table 2-1: Summary of the published NMR chemical shift values in ppm of the all-*trans*-RA and 11-*cis*-RA isomers and selected metabolites of retinoic acid (500 MHz, $CDCl_3$). Olefin proton coupling constants in Hertz of the all-*trans*-RA and 11-*cis*-RA isomers and selected metabolites of retinoic acid are also listed.

δ [ppm]	Olefin Protons					Methyl Groups				Methylene Groups			
	7,8	10	11	12	14	16,17	18	19	20	2	3	4	15
all-*trans*-RA[a]	6.28;6.14	6.13	7.01	6.28	5.78	1.02;1.02	1.71	2.00	2.35	1.50	1.50	2.00	---
11-*cis*-RA[a]	6.29;6.14	6.53	6.59	5.91	5.90	1.03;1.03	1.97	2.36	1.47	1.47	1.62	2.02	---
18-OH-RA	6.20;6.10	6.12	6.96	6.36	5.75	0.97;0.97	4.07	1.94	2.30	1.44	1.60	2.15	---
4-OH-RA[a]	6.20;6.20	6.16	7.04	6.33	5.81	1.04;1.00	1.83	2.01	2.38	----	-----	4.04	----

J (Hz)	H-7/H-8	H-10/H-11	H-11/H-12	MHz/Solvent
all-*trans*-RA[b]	16.0	11.4	15.0	400/HPLC-NMR
11-*cis*-RA[b]	16.4	11.8	12.3	400/HPLC-NMR
18-OH- RA	16.0	11.5	15.0	500/$CDCl_3$
4-OH-RA[c]	16.5	11.5	15.0	500/$CDCl_3$

[a](Schmidt et al., 2002); [b](Strohschein et.al., 1997);[c](Shimshoni et al., 2012)

Table 2-2: Kinetic parameters determined for 4-OH-RA and 18-OH-RA formation by CYP26A1 and CYP26B1.

	4-OH RA (CYP26A1)	18-OH RA (CYP26A1)	4-OH RA (CYP26B1)
K_M (nM)	50.1 ±32.4	48.9 ±13.4	18.8 ±18.7
V_{max}(pmol/min/pmol P450)	9.5 ±2.2	5.0 ±0.5	0.81 ±0.2
Cl'_{int} (µL/min/pmol P450)	190	102	43

Table 2-3: Michaelis-Menten parameter estimates for *at*RA metabolites as substrates of CYP26A1 and CYP26B1. K_m (nM) estimates for both enzymes and Cl_{int} (µL/min/pmoles CYP26A1) for CYP26A1 obtained from full depletion curves (eq. 2) and Cl_{int} for CYP26B1 (µL/min/pmoles CYP26B1) calculated (eq. 3) from single point depletion below the K_m.

	CYP26A1		**CYP26B1**	
Retinoid	**K_m (nM)**	**Cl_{int} (µL/min/pmoles 26A1)**	**K_m (nM)**	**Cl_{int} (µL/min/pmoles 26B1)**
(4S)-OH-RA	5.2 ± 1.3	1450 ± 150	4.0 ± 2.5	46 ± 18
(4R)-OH-RA	11 ± 5.2	740 ± 12	31 ± 19	104 ± 19
18-OH-RA	39 ± 25	290 ± 98	4.8 ± 6.3	33 ± 10
4-oxo-RA	63 ± 24	91 ± 16	29 ± 6.6	15 ± 4.0
*at*RA	9.3[a]	1220[a]	18.8[b]	148 ± 1.0

[a]Values for *at*RA depletion by CYP26A1 were obtained from (Lutz et al., 2009)
[b]Value for K_m of *at*RA metabolism by CYP26B1 obtained from metabolite formation data (**Table 2-2**)

Chapter 3 : Induction of CYP26A1 by Retinoic Acid Metabolites: Clarification of the Role of CYP26A1 as an Enzyme that Eliminates Active Retinoids

3.1 Introduction

Retinoic acid (RA), the active metabolite of vitamin A (retinol), is an essential nutrient during both fetal development and adult life. Disruption of retinoid signaling pathways has been associated with disorders such as fetal malformations, male sterility, and acute promyelocytic leukemia (APL) (Chang et al., 1991; Muindi et al., 1992b; Nau, 1995; Hogarth et al., 2011). All-*trans*-retinoic acid (*at*RA, tretinoin) is used therapeutically to treat APL and emphysema, and is currently being explored as a preventative therapeutic agent for Alzheimer's disease (Ozpolat et al., 2001; Muindi et al., 2008; Lee et al., 2009). The biological activity of *at*RA is believed to be mediated by its binding the retinoic acid receptors (RARs). RARs dimerize with Retinoid X Receptors (RXRs), and the RAR-RXR complex binds to Retinoic Acid Response Elements (RAREs) in the promoter region of target genes. Upon binding of *at*RA to RAR, transcription co-repressors depart and transcription co-activators are recruited to induce mRNA transcription (Marletaz et al., 2006). There are three isoforms of RARs (α, β, and γ) and RXRs (α, β, and γ), and the expression of each is dependent on cell type (Krust et al., 1989; Chambon, 1996). The localization and expression of the RARs and the concentration of *at*RA within a cell regulate cell-specific responses to *at*RA and cell's retinoid signaling (McBurney, 1993; Rhinn and Dolle, 2012).

The concentration of *at*RA is regulated by its synthesis from vitamin A by retinol dehydrogenases (RDH) and retinal dehydrogenases (RALDH) and its elimination via oxidation by P450 enzymes (Napoli, 2012). The enzymes of the cytochrome P450 26 family are primarily responsible for metabolizing *at*RA into hydroxylated metabolites including 4-OH-RA, 18-OH-RA, and 16-OH-RA (White et al., 1997; White et al., 2000; Thatcher et al., 2010; Topletz et al., 2012). CYP26A1 is the predominant *at*RA hydroxylase in the adult human liver (Chithalen et

al., 2002; Thatcher et al., 2010; Thatcher et al., 2011; Topletz et al., 2012). In humans, *at*RA has been shown to induce its own metabolism following multiple doses (Muindi et al., 2008; Tay et al., 2010; Takeuchi et al., 2011) and resistance to *at*RA that frequently occurs in APL patients is hypothesized to be due to hepatic CYP26A1 induction (Muindi et al., 1992b; Ozpolat et al., 2002). Indeed, CYP26A1 mRNA was increased in the rat liver after administration of high doses of *at*RA (Yamamoto et al., 2000) and CYP26A1 mRNA was induced in multiple human cell lines such as MCF-7 and HepG2 cells after *at*RA treatment (White et al., 1997; Tay et al., 2010). The induction of CYP26A1 by *at*RA is likely via the two RAREs present in the CYP26A1 promoter. Similar to CYP26A1, RARβ is also inducible by *at*RA due to the RARE in its promoter (Chambon, 1996; Tay et al., 2010). In HepG2 cells, both CYP26A1 and RARβ mRNAs were induced by the RARα agonist AM580 but not the RARβ agonist AC55649, suggesting that RARα-mediated transcription was responsible for the observed CYP26A1 and RARβ induction.

In addition to *at*RA, the primary hydroxylation products 4-OH-RA and 18-OH-RA as well as the secondary metabolite 4-oxo-RA all bind to RARs including RARα (Idres et al., 2002). Of the metabolites, 4-oxo-RA was the most potent having a three-fold lower EC_{50} than *at*RA (Idres et al., 2002). 4-oxo-RA is also detected in human plasma suggesting it may have biological significance (Muindi et al., 1992b; Arnold et al., 2012). However, the biological role of *at*RA metabolites is largely unknown.

We hypothesized that CYP26A1 is induced by all bioactive retinoids due to their RAR binding affinity but thet CYP26A1 also metabolizes all bioactive retinoids. The aims of this study were to determine if *at*RA metabolites induce their own metabolism using CYP26A1 mRNA induction in HepG2 cells and to establish whether the formation of 4-oxo-RA was

mediated by CYP26A1 in cells. The results show that CYP26A1 is predominantly an enzyme that functions to eliminate bioactive retinoids, and that additional catalytic enzymes are needed to form the other bioactive metabolites such as 4-oxo-RA.

3.2 Materials and Methods

Chemicals and reagents. *at*RA, ketoconazole, fomepizole (4-methylpyrazole), cimetidine, testosterone, and carbenoxolone were purchased from Sigma-Aldrich (St. Louis, MO). 4-oxo-RA-d_3 (3 deuteriums on the C-18 position) and *at*RA-d_5 (2 deuteriums on the C-4 and 3 deuteriums on the C-18 positions) were purchased from Toronto Research Chemicals (North York, Ontario). (4R)-OH-RA, (4S)-OH-RA, 4-oxo-RA, and 18-OH-RA were synthesized as previously described (Samokyszyn et al., 2000; Lutz et al., 2009; Shimshoni et al., 2012; Topletz et al., 2012). Optima-grade water, optima-grade acetonitrile, ethanol and ethyl acetate were purchased from Fisher Scientific (Pittsburgh, PA). Biological DNA/RNA-free water was purchased from Qiagen (Valencia, CA).

Quantitative analysis of retinoids. All extractions of *at*RA, 4-oxo-RA, (4R)-OH-RA, (4S)-OH-RA, or 18-OH-RA were performed under red light in 8 x 13 mm borosilicate glass test tubes as previously described (Thatcher et al., 2010) and after evaporation (nitrogen stream) subsequently reconstituted in 100 µL of acetonitrile for HPLC-MS/MS analysis. Analytes were separated and analyzed using an Agilent Zorbax C18 column (3.5 µm, 2.1 mm x 100 mm) with an AB Sciex API 5500 Q/LIT mass spectrometer equipped with an Agilent 1290 Infinity UHPLC. The analytes were separated with a mobile phase flow of 0.2 mL/min. A linear 30 min gradient with initial mobile phase condition of 10:90 acetonitrile: aqueous 0.1% formic acid increasing to 90:10 acetonitrile: aqueous 0.1% formic acid (held for 2 min) was used followed by a re-equilibration back to initial mobile phase conditions over 3 min. Analytes were detected

using negative ion electrospray mass spectrometry, with declustering potentials of -80 V (4-OH-RA and 18-OH-RA), -90 V (4-oxo-RA-d_3), -140 V (*at*RA), -100 V (*at*RA-d_5) and -95 V (4-oxo-RA and 4-oxo-13-*cis*RA); collision energies of -28 eV (4-OH-RA and 18-OH-RA), -25 eV (4-oxo-RA-d_3), -40 eV (*at*RA-d_5) and -22 eV (*at*RA, 4-oxo-RA and 4-oxo-13-*cis*RA); and collision exit potentials of -7 V (*at*RA, 4-OH-RA and 18-OH-RA), -5 V (4-oxo-RA and 4-oxo-13-*cis*RA), -16 V (*at*RA-d_5) and -10 V (4-oxo-RA-d_3). The parent-fragment MS/MS transitions of *m/z* 299 → 255 Da (*at*RA), 304 → 260 Da (*at*RA-d_5), 315 → 253 Da (4-OH-RA and 18-OH-RA), 313 → 269 Da (4-oxo-RA and 4-oxo-13-*cis*RA), and 316 → 272 Da (4-oxo-RA-d_3) were monitored. The lower limits of quantification were 3.1 nM for 4-OH-RA, 0.3 nM for 4-oxo-RA, and 6.3 nM for 18-OH-RA. Standard curves were reproducible within 15% of each other from three separate extractions on three different days of analysis. Mass spectrometry data was analyzed using Analyst software. Peak heights were used to determine the ratio of substrate to the internal standard (4-oxo-RA-d_3).

Cell culture and mRNA analysis. The HepG2 cells were obtained and cultured in a humidified incubator at 37 °C as previously described (Tay et al., 2010) under a 5% atmosphere of carbon dioxide using ATCC Minimum Essential Media with Earle's balanced salt solution supplemented with 10% FBS and 0.5% penicillin as the growth medium (Tay et al., 2010). For *at*RA and *at*RA metabolite treatments, cells were plated into six well plates (10^6per well) in 2 mL media and allowed to adhere for 24 hours prior to treatments. The cells were treated for 48 hours in 2 mL media, changing media (+ inducer) at 24 hours. The treatments included *at*RA, 4-oxo-RA, (4R)-OH-RA, (4S)-OH-RA, or 18-OH-RA at concentrations of 1 nM to 1 µM or 0.1% EtOH as a vehicle control. All treatments were performed in triplicate. At the completion of each treatment, the media was aspirated and cells were harvested for mRNA extraction. To each well,

1 mL of TRI reagent (Invitrogen, Grand Island, NY) was added and mRNA extracted according to the manufacturer's recommendations. Total RNA was quantified using the Nanodrop 2000c Spectrophotometer (Thermofisher Sci., Waltham, MA) and RNA quality was determined by gel electrophoresis. cDNA was generated from 1µg mRNA using Taqman® Gene expression reagents (Applied Biosystems, Carlsbad, CA). RT-PCR was used to quantify CYP26A1 and RARβ mRNA (StepOnePlus™, Applied Biosystems, Carlsbad, CA) as previously described (Tay et al., 2010). TaqMan real-time Gene Expression Master Mix and PCR primers and fluorescent probes were obtained from Applied Biosystems (Foster City, CA). Probes were labeled with the 5'-reporter dye 5-carboxyfluorescein and a nonfluorescent black hole quencher on the 3'-end. Primer and probe pairs used included: CYP26A1 (Hs00175627_m1, FAM), GAPDH (Hs99999905_m1, VIC), RARα_ (Hs00940446_m1, FAM), RARβ_ (Hs00233407_m1, FAM), and RARγ (Hs00171273_m1, FAM). GAPDH was used as the housekeeping gene and all assays were done as multiplexes. Each sample was analyzed in duplicate. Changes in target mRNA were measured using relative quantification (fold-difference) and the $\Delta\Delta C_T$ method (Tay et al., 2010) using GraphPad Prism v.5 (La Jolla, CA).

Retinoid depletion and subsequent metabolite formation in HepG2 cells. Depletion of *at*RA, 4-oxo-RA, (4R)-OH-RA, (4S)-OH-RA, or 18-OH-RA and formation of subsequent metabolites from these substrates in HepG2 cells was determined using media and cell samples to assess the exposure of the cells to the bioactive retinoids during induction studies. HepG2 cells were plated and incubated as described above. Cells were treated with *at*RA, 4-oxo-RA, (4R)-OH-RA, (4S)-OH-RA, or 18-OH-RA at a concentration of 1 µM (nominal initial concentration in the media) for 48 hours. The media (+ inducer) was changed after 24 hours to mimic the design of the mRNA induction experiments. At 0, 1, 4, 8, 12, 24, and 48 hours, 1 mL

of media was removed, an internal standard (*at*RA-d_5; 20 µL of a 2.5 µM stock solution) was added, and samples were extracted using ethyl acetate as previously described. As a control, 4-oxo-RA, (4R)-OH-RA or (4S)-OH-RA (1 µM) were incubated in 1 mL of media for four hours in a 37 ºC oscillating water bath and media was analyzed for substrate depletion and metabolite formation. Cells were collected at 1, 4, 8, and 12 hours after the beginning of the treatments by addition of 1 mL of acetonitrile to each well. One milliliter of KPi buffer (100 mM, pH 7.4) was added to the acetonitrile phase to facilitate separation of the organic and aqueous layers, an internal standard (4-oxo-RA-d_3; 20 µL of a 2.5 µM stock) was added, and samples were extracted with ethyl acetate as described previously. The amount of the retinoids in the cells was measured and retinoid concentration in cells was calculated using a total intercellular volume of 1 µL/10^6 HepG2 cells (Kewn et al., 2000).

Measurement of CYP26A1 activity in HepG2 cells. The formation of 4-OH-RA-d_4 and 4-oxo-RA-d_3 from *at*RA-d_5 was used to determine CYP26A1 activity and induction during treatment of HepG2 cells with *at*RA. HepG2 cells were treated for 48 hours with *at*RA (1 µM final concentration in media). Media with *at*RA was changed at 24 hours. At each designated time point (0.5, 6, 12, 18, 24, 36, and 48 hours), *at*RA-d_5 (100 nM) was added to each well (3 mL) and formation of 4-OH-RA-d_4 and 4-oxo-RA-d_3 after a 1 hour incubation was measured. Each time point was performed in triplicate in separate wells. An initial aliquot of media (1 mL) was taken 30 seconds after *at*RA-d_5 addition as a control, and after one hour at 37 ºC, a second aliquot of media (1 mL) was removed from each well. No isomerization of 4-oxo-RA to 4-oxo-13-*cis*RA was detected after treatment with *at*RA, deeming 4-oxo-13-*cis*RA appropriate for use as an internal standard. 4-oxo-13-*cis*RA (20 µL of a 2.5 µM stock solution in EtOH) was added to each sample as an internal standard, and samples were extracted using 3 mL ethyl acetate and

analyzed using HPLC-MS/MS as described above. 4-oxo-RA-d_3 was quantified using a reference material. Due to the lack of a standard, relative change in formation of 4-OH-RA-d_4 was measured as analyte to internal standard peak height ratio. Standard curves were constructed for *at*RA-d_5 and 4-oxo-RA-d_3. The rate of 4-oxo-RA-d_3 formation from 4-OH-RA-d_4 was assumed to remain constant during treatment.

Inhibition of 4-oxo-RA and 4-OH-RA formation in HepG2 cells. To determine whether formation of 4-oxo-RA is predominantly P450-mediated in the HepG2 cells, HepG2 cells were incubated with *at*RA or 4-OH-RA (1 µM in media with 0.1% EtOH) for 24 hours in the presence and absence of ketoconazole (10 µM in media with 0.1% EtOH), a potent pan-P450 inhibitor (Thatcher et al., 2011). In addition, HepG2 cells were incubated in the presence of *at*RA and 4-OH-RA with alcohol dehydrogenase inhibitors 4-methylpyrazole (250 µM) and cimetidine (250 µM), the aldo-keto-reductase inhibitor testosterone (25 µM), and the retinol dehydrogenase inhibitor carbenoxolone (25 and 50 µM). All incubations were performed using a triplicate treatment with substrate and no inhibitor as controls. An initial aliquot of media (0.5 mL) was taken before media was added to each well to quantify initial substrate concentrations per well. After 24 hours, a second aliquot of media (0.5 mL) was removed and extracted with ethyl acetate. Standard curves were constructed for *at*RA, 4-oxo-RA and 4-OH-RA and an internal standard of 4-oxo-RA-d_3 (20 µL of a 2.5 µM stock solution) was used. All samples were separated and analyzed using HPLC-MS/MS as described above.

Data analysis. Mass spectrometry data was analyzed using Analyst software. Peak heights were used to determine the ratio of substrate to the internal standard (4-oxo-RA-d_3). The AUCs (0 to 12 hours) of *at*RA, (4R)-OH-RA, (4S)-OH-RA, 4-oxo-RA, and 18-OH-RA were calculated with non-compartmental analysis using Phoenix/WinNonLin 6.3 (Pharsight, Mountain

View, CA). The cell to media ratio was calculated of each inducer and their subsequent metabolites in HepG2 cells using their respective AUCs (0 to 12 hours) in cells or media. One-way analyses of variance coupled with Bonferroni's Multiple Comparison Test were conducted using GraphPad Prism v.5 (La Jolla, CA) to determine significant differences in mRNA treatments. Significant changes in 4-oxo-RA formation from *at*RA or 4-OH-RA in the presence of inhibitors compared to no inhibitor controls were performed using the student's unpaired T-test. A *P*-value of less than 0.05 was considered significant.

3.3 Results

3.3.1 Effects of *at*RA metabolites on CYP26A1 and RARβ mRNA in HepG2 cells.

The mRNA of CYP26A1 and RARβ was significantly ($P < 0.05$) increased after 48 hour treatment with *at*RA, 4-oxo-RA, (4R)-OH-RA, (4S)-OH-RA, and 18-OH-RA (1 μM), with *at*RA resulting in the greatest magnitude of induction (Figure 3.1). The induction of CYP26A1 and RARβ was retinoid concentration dependent (Figure 3.1B and C). The magnitude of CYP26A1 induction following 4-oxo-RA (2980-fold, 1 μM treatments) was ~81 % of that following *at*RA treatment (3700-fold, 1 μM treatments), whereas the induction of CYP26A1 after 4-OH-RA (both enantiomers) and 18-OH-RA treatment was 64 to 91 % less than that observed following *at*RA treatment, respectively (Figure 3.1A, Table 3-1). The magnitude of induction of CYP26A1 mRNA between (4R)-OH-RA and (4S)-OH-RA treatments was similar ($P > 0.05$). *at*RA and its metabolites also induced RARβ mRNA in a concentration-dependent manner, but the magnitude of induction was approximately 82-97% less than that of CYP26A1 (Figure 3.1B, C). The metabolites were significantly less potent than *at*RA (~70 %, $P < 0.05$) in inducing RARβ and were not different from each other. There were no significant changes of RARα or RARγ mRNA upon treatment with *at*RA or any of the *at*RA metabolites (data not shown).

3.3.2 Formation and depletion of (4S)-OH-RA (4R)-OH-RA, 4-oxo-RA and 18-OH-RA in HepG2 cells.

To determine whether the specific metabolites used in the HepG2 cell treatments were responsible for CYP26A1 and RARβ induction, retinoid concentrations both in the media and cellular fractions were quantified following treatment with 1 μM of the metabolites and *at*RA (Figure 3.2). The exposures (AUC) for each retinoid and their metabolites from 0 to 12 hours in the media and cellular fractions are summarized in Table 3-1. In terms of absolute concentrations, *at*RA had the highest intracellular exposure during the treatment ($AUC^{0\text{-}12\ hr}$ of 3750 ± 350 nmoles•hour/mL) whereas (4S)-OH-RA had the lowest exposure ($AUC^{0\text{-}12\ hr}$ of 300 ± 10 nmoles•hour/mL) (Figure 3.2B, Table 3-1). Despite the fact that the exposures to the 4-OH-RA enantiomers were 90% lower than those of *at*RA, the magnitude of CYP26A1 induction by 4-OH-RA enantiomers was nearly 50% of that observed following *at*RA treatment suggesting that 4-OH-RA enantiomers or their metabolites are more potent activators of RAR than is *at*RA. Intracellular exposure to 4-oxo-RA (980 ± 40 nmoles•hour/mL) in the first 12 hours of treatment with 4-oxo-RA was 60% lower than that of *at*RA, but treatment with 4-oxo-RA resulted in similar magnitude of CYP26A1 and RARβ induction as *at*RA, suggesting 4-oxo-RA is a more potent inducer of CYP26A1 and RARβ than *at*RA (Figure 3.2B, Table 3-1). The cell-to-media concentration ratio ranged from 70 for (4S)-OH-RA to 363 for *at*RA demonstrating different partitioning of the retinoids to cells (Table 3-1).

There was no observable depletion of *at*RA and only 23 % of 4-oxo-RA and 34 % of 18-OH-RA was depleted from the media during the first 12 hours of treatment (Figure 3.2C). In contrast, 86 % of (4S)-OH-RA and 65 % of (4R)-OH-RA were depleted from the media during the first 12 hours (Figure 3.2C), and the concentrations of 4-oxo-RA in the cells were similar to those of 4-OH-RA following treatments with the 4-OH-RA enantiomers. After the first 24 hours

of treatment, an increased depletion was observed for *at*RA (61 %), (4R)-OH-RA (89 %), (4S)-OH-RA (87 %) and 18-OH-RA (62 %) but only a small fraction (29%) of 4-oxo-RA was depleted (Figure 3.2C). The depletion of all compounds increased after the first 24 hours and more than 94 % of all inducers were depleted during the 24 to 48 hour treatment. This increased depletion was in agreement with the increased CYP26A1 mRNA after 24 hours of *at*RA treatment. The pronounced decrease in the 4-OH-RA enantiomers observed in the first 12 hours could not be explained by CYP26A1 activity.

The metabolites of *at*RA detected were (4S)-OH-RA, 4-oxo-RA and 18-OH-RA. The major metabolite formed from both 4-OH-RA enantiomers was 4-oxo-RA (Figure 3.3). The cell $AUC^{0\text{-}12hr}$ of 4-oxo-RA as a metabolite of (4S)-OH-RA was 2.1-fold higher than (4S)-OH-RA cell $AUC^{0\text{-}12hr}$ (Table 3-1) while the $AUC^{0\text{-}12hr}$ of 4-oxo-RA was 40 % lower than (4R)-OH-RA in cells treated with (4R)-OH-RA (Table 3-1). In the media, the 4-oxo-RA $AUC^{0\text{-}12hr}$ increased to a concentration 2.3-fold higher than (4R)-OH-RA $AUC^{0\text{-}12hr}$ after 24 hours (data not shown). Based on these data it is likely that following 4-OH-RA treatment, 4-oxo-RA is the predominant retinoid in the cells and responsible for CYP26A1 and RARβ induction. Interestingly, 4-OH-RA was also detected as a metabolite in cells treated with 4-oxo-RA and had an $AUC^{0\text{-}12hr}$ that was 40% of that of 4-oxo-RA in cells (Table 3-1). No degradation of 4-oxo-RA, (4R)-OH-RA, or (4S)-OH-RA in media was observed in the absence of cells (data not shown), indicating that the reversible oxidation/reduction seen in HepG2 cells is cell-mediated. The formation of 4-oxo-RA and 4-OH-RA from *at*RA in the media was not detected in the first 12 hours of *at*RA treatment, and as metabolites of *at*RA 4-oxo-RA and 4-OH-RA had $AUCs^{0\text{-}12hr}$ only 3 % of those calculated for *at*RA in the cellular fractions (Figure 3.3, Table 3-1). Formations of 18-OH-RA, 16-OH-RA

and dihydroxylated products from atRA were detected only after 24 hours of treatment (data not shown), concurrent with increased CYP26A1 activity.

3.3.3 *at*RA increases CYP26A1 activity in HepG2 cells. To determine the time course of CYP26A1 activity induction, the formation of 4-oxo-RA-d_3 and 4-OH-RA-d_4 from *at*RA-d_5 during one-hour incubation was measured at designated time points during a 48 hour treatment with *at*RA (1 μM) in HepG2 cells. Formation of 4-OH-RA-d_4 was constant during the first 12 hours after initial treatment with *at*RA, then increased approximately 7–fold ($P < 0.05$) at 24 hours and 33-fold ($P < 0.05$) at 48 hours after the initial treatment with *at*RA (Figure 3.4A). Formation of 4-oxo-RA-d_3 increased approximately 7-fold ($P < 0.05$) at 24 hours and 22-fold ($P < 0.05$) at 48 hours after the initial treatment with *at*RA (Figure 3.4B). The ratio of 4-OH-RA-d_4 to 4-oxo-RA-d_3 formation did not change with treatment time, indicating that 4-oxo-RA formation from 4-OH-RA is constant after *at*RA treatment.

3.3.4 4-oxo-RA formation from *at*RA and 4-OH-RA in HepG2 cells: To determine whether 4-oxo-RA formation from 4-OH-RA is P450 mediated, HepG2 cells were co-incubated with ketoconazole and *at*RA, 4-OH-RA, or 4-oxo-RA. As 4-oxo-RA is formed from 4-OH-RA, and formation of 4-OH-RA from *at*RA is predominantly CYP26-mediated, inhibition of 4-OH-RA formation from *at*RA by ketoconazole was used as a positive control for CYP26A1 inhibition. Ketoconazole decreased 4-OH-RA formation by 84 % ($P < 0.05$) and 4-oxo-RA formation by 80 % ($P < 0.05$) in cells treated with *at*RA in the absence of ketoconazole (Table 3-2). When 4-OH-RA and HepG2 cells were co-incubated with ketoconazole, the depletion of 4-OH-RA was decreased by 25% ($P < 0.05$) but 4-oxo-RA formation from 4-OH-RA was not affected (Table 3-2). None of the other inhibitors decreased 4-oxo-RA formation from 4-OH-RA or *at*RA (Table 3-2).

3.4 Discussion

*at*RA is considered to be the active metabolite of vitamin A but existing evidence suggests that *at*RA metabolites may also play biological roles. Loss of differentiation was observed in CYP26A1$^{-/-}$ P19 EC cells compared to the wild type when treated with *at*RA, suggesting that *at*RA metabolites formed by CYP26A1 may be necessary in regulating cell differentiation into various cell types (Langton and Gudas, 2008). However, *at*RA concentrations in the CYP26A1$^{-/-}$ were also increased potentially explaining the activation of apoptosis pathways. Despite this, there is evidence of biological effects of *at*RA metabolites, such as binding to RARs and inducing cell-cycle arrest and differentiation of NB4 cells, This supports the hypothesis that some metabolites may have specific roles in cellular homeostasis and differentiation (Idres et al., 2001; Idres et al., 2002). In contrast, partial disruption of *at*RA synthesis (Aldh1a2$^{+/-}$) during development in Cyp26a1$^{-/-}$ mice rescued the lethal genotype of Cyp26a1$^{-/-}$ mice (Niederreither et al., 2002). This result suggests that the decreased *at*RA exposure, not the recovery of Cyp26a1-mediated formation of *at*RA hydroxylated metabolites, rescued an otherwise lethal phenotype. However some non-lethal malformations remained, which the authors attributed to the lack of 4-oxo-RA formation. 4-oxo-RA has also been shown to have teratogenic effects in *Xenopus laevis*, and to induce Hox4 and Hox9 genes at higher concentrations than *at*RA (Pijnappel et al., 1993).

Consistent with RAR binding and a biological activity of the metabolites, *at*RA and its metabolites, (4R)-OH-RA, (4S)-OH-RA, 4-oxo-RA and 18-OH-RA all induced CYP26A1 and RARβ mRNA. The large induction of CYP26A1 mRNA observed in the HepG2 cells after *at*RA treatment (3700-fold after 1 μM treatment in media) is consistent with previous studies in various cell lines that have shown that CYP26A1 is induced by *at*RA (Tay et al., 2010; Zhang et

al., 2010). Perhaps because the CYP26A1 promoter has two RAREs and RARβ has one, RARβ mRNA was increased 90% less in magnitude (250-fold after a 1 μM treatment with *at*RA, Figure 3.1A) than was CYP26A1 mRNA, similar to previous results (Chambon, 1996; Tay et al., 2010).

Induction of CYP26A1 and RARβ mRNA has been shown to be RARα-mediated in HepG2 cells (Tay et al., 2010) and 4-oxo-RA, 4-OH-RA, and 18-OH-RA activate RARα (Idres et al., 2002). These compounds also resulted in increased CYP26A1 and RARβ mRNA in HepG2 cells. However, the reported EC_{50}s of RARα-mediated activation by *at*RA, 4-oxo-RA, 4-OH-RA, and 18-OH-RA were not in agreement with the extent of CYP26A1 mRNA induction in this study, potentially due to differences in cellular exposures to each inducer. In transfected COS-7 cells, RARα activation was similar between *at*RA (EC_{50} = 169 nM) and 18-OH-RA (EC_{50} = 162 nM), five-fold less potent by racemic 4-OH-RA (EC_{50} = 791 nM) (Idres et al., 2002). 4-oxo-RA-mediated RARα activation (EC_{50} = 33 nM) was three-fold more potent than that for *at*RA (Idres et al., 2002). However, 4-oxo-RA induced CYP26A1 to a similar extent to *at*RA at each concentration tested in HepG2 cells (Figure 3.1A). 4-OH-RA and 18-OH-RA induced CYP26A1 3 to 10-fold less potently than *at*RA after a 1 μM (in media) treatment. Since the extent of CYP26A1 induction by *at*RA, 4-oxo-RA, (4R)-OH-RA and (4S)-OH-RA and 18-OH-RA were not reflective of their respective RARα-mediated activities, we compared the cellular exposures ($AUC^{0\text{-}12\ hr}$) of each inducer to CYP26A1 mRNA induction to determine their relative potencies to each other. Interestingly, 4-oxo-RA was the most potent retinoid tested. The cellular concentration of 4-oxo-RA (980 ± 40 nmoles•hour/mL) in the first 12 hours was 60% lower than *at*RA, but the extent of CYP26A1 and RARβ mRNA induction was similar to *at*RA (Figure 3.1, Table 3-1). This result agrees with previous data that showed 4-oxo-RA to have a much greater affinity to RARα-mediated transcription than *at*RA in transfected COS-7 cells

(Idres et al., 2002). The least potent retinoid tested was 18-OH-RA. The intracellular exposure of 18-OH-RA (1740 ± 70 nmoles•hour/mL) in the first 12 hours was 1.7-fold greater than 4-oxo-RA, but CYP26A1 mRNA was induced 90 % less after a 1 μM treatment (300 ± 90-fold, Table 3-1). Induction of CYP26A1 mRNA was similar between (4R)-OH-RA (1350 ± 230-fold) and (4S)-OH-RA (1360 ± 240-fold) after a 1 μM (in the media) treatment, indicating that there was no enantiomer-specific effect on RAR-mediated transcription (Table 3-1). This result is not surprising as over 60% of both enantiomers were depleted within the first 12-hours to form 4-oxo-RA, thus 4-oxo-RA may be the active moiety after treatment with (4S)-OH-RA and (4R)-OH-RA (Figure 3.3, Table 3-1). The $AUC^{0\text{-}12\ hr}$ for all retinoids tested was higher in media than in cells, and the ratio differed between each inducer. The concentration after one hour between the media and cellular fractions also differed, indicating that there was a difference in cellular exposure independent of subsequent metabolism.

Induction of CYP26A1 is believed to be responsible for emergence of *at*RA resistance during therapy, and patients are often removed periodically from *at*RA treatment due to increased clearance and decreased efficacy (Muindi et al., 1992a; Ozpolat et al., 2002). In support of increased oxidative clearance of *at*RA, the plasma AUC of *at*RA was shown to decrease by two-thirds; however, plasma AUC of 4-oxo-RA did not significantly change after an eight day treatment with *at*RA (1 or 2 mg/kg/day) in emphysema patients (Muindi et al., 2008). Formation of 4-oxo-RA depends on the AUC of 4-OH-RA which in turn is dependent on the formation of 4-OH-RA by CYP26A1 from *at*RA and the elimination of 4-OH-RA. An increase in CYP26A1 activity will result in an increased AUC of 4-OH-RA and a subsequent increase in 4-oxo-RA if 4-oxo-RA elimination remained constant. However, 4-oxo-RA is metabolized by CYP26A1 (Topletz et al., 2012). As the AUC of a metabolite depends on both its formation and

elimination clearances, the observed lack of change in 4-oxo-RA AUC after *at*RA treatment is in agreement with both induced formation of 4-OH-RA leading to increased formation of 4-oxo-RA and increased elimination of 4-oxo-RA. In this study, we have shown that CYP26A1-mediated metabolism of *at*RA increases after *at*RA treatment in HepG2 cells (Figure 3.4), and that the increase in CYP26A1 activity corresponded with the observed increase in CYP26A1 mRNA. Thus, it can be inferred that *at*RA metabolites also induced CYP26A1 activity in HepG2 cells. Together, these data support the hypothesis that hepatic CYP26A1 is increased upon *at*RA treatment and that the *at*RA metabolites may also contribute to an increase in CYP26A1, thus inducing their own metabolism *in vivo*.

CYP26 is the predominant P450 enzyme family involved in *at*RA metabolism. However, the non-CYP26-mediated metabolite 4-oxo-RA, is the only non-glucuronidated *at*RA metabolite currently detected in human plasma both endogenously and after *at*RA treatment. 4-oxo-RA accounts for 10-20 % of the *at*RA dose in vivo, both in plasma and as 4-oxo-RA-glucuronide in the urine (Muindi et al., 1992b; Muindi et al., 2008; Arnold et al., 2012). We have also shown 4-oxo-RA to be a more potent CYP26A1 inducer that *at*RA in HepG2 cells. Together, these data suggest that 4-oxo-RA formation may contribute to some of the observed retinoid effects in vivo. There was no change in 4-oxo-RA formation from 4-OH-RA in the presence of the P450-inhibitor ketoconazole and thus conclude that 4-oxo-RA formation in HepG2 cells is not CYP26A1-mediated (Table 3-2). We have also shown that formation of 4-oxo-RA from 4-OH-RA was not decreased in the presence of chemical inhibitors of alcohol dehydrogenase, aldo-ketoreductase, or membrane-bound retinol dehydrogenase enzymes in HepG2 cells (Table 3-2). Further studies are needed to identify the enzyme responsible for 4-oxo-RA formation.

In conclusion, all our data supports the notion that CYP26A1 functions primarily as an enzyme that metabolizes *at*RA, 4-OH-RA, 18-OH-RA, and 4-oxo-RA into biologically inactive retinoids. The results demonstrate that 4-oxo-RA, (4S)-OH-RA, (4R)-OH-RA, and 18-OH-RA all induce CYP26A1, although to different extents. In this study we also showed that 4-oxo-RA formation from 4-OH-RA is depend on an enzyme other than CYP26A1 and that 4-oxo-RA induced CYP26A1 more potently than the other retinoids tested. Together, these data support the hypothesis that 4-oxo-RA has a biological role independent of *at*RA.

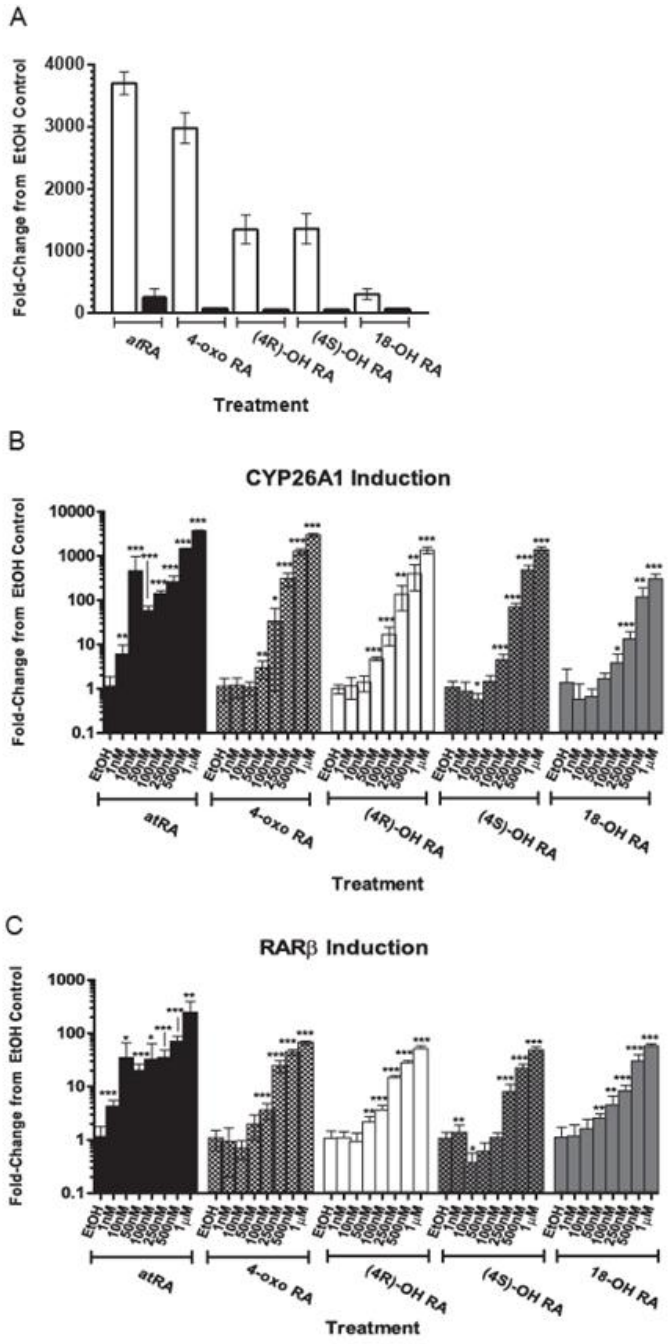

Figure 3.1: Induction of CYP26A1, and RARβ in HepG2 cells treated with *at*RA and its metabolites. (A) Comparative induction of CYP26A1 (white bars) and RARβ (black bars) mRNA by *at*RA, 4-oxo-RA, (4R)-OH-RA, (4S)-OH-RA, and 18-OH-RA after a 1 μM treatment for 48 hours in HepG2 cells. Induction of (B) CYP26A1 and (C) RARβ mRNA by *at*RA, 4-oxo-RA, (4R)-OH-RA, (4S)-OH-RA, and 18-OH-RA in HepG2 cells. Cells were treated for 48 hours at seven concentrations (ranging from 1 nM to 1 μM) of each substrate, changing media after 24 hours. A vehicle control was EtOH-treated cells and GAPDH was used as a housekeeping gene for RT-PCR analysis.

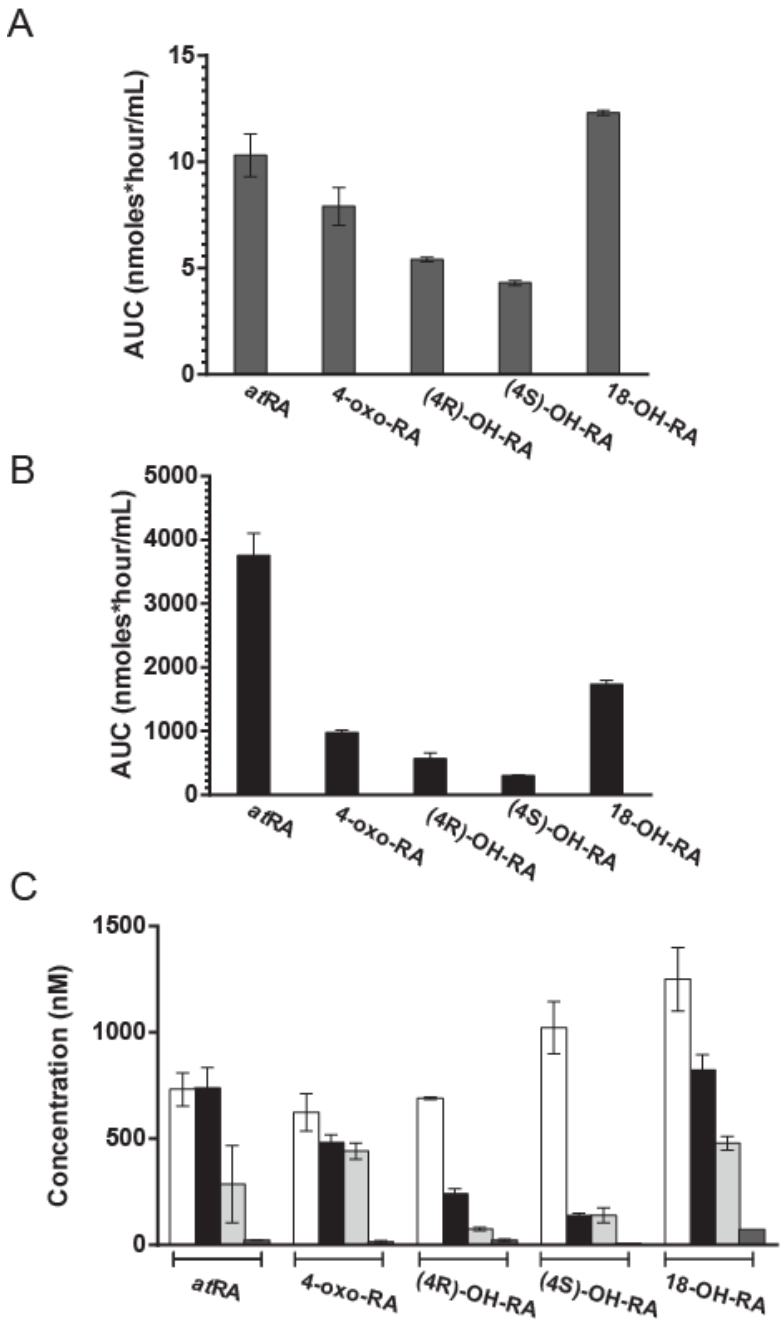

Figure 3.2: Exposure of inducers in cell and media fractions. AUCs$^{0\text{-}12hr}$ of *at*RA, (4R)-OH-RA, (4S)-OH-RA, 4-oxo-RA and 18-OH-RA in media (A) and cellular (B) fractions after 1 µM treatment with each compound.. Panel (C) shows *at*RA, (4R)-OH-RA, (4S)-OH-RA, 4-oxo-RA and 18-OH-RA concentrations at 0 (white bars), 12 (black bars), 24 (light grey bars), and 48 (dark grey bars) hours after 1 µM treatments with each of the compounds in HepG2 cells. Media containing the inducer was changed at 24 hours after a 1 mL media aliquot was taken for analysis.

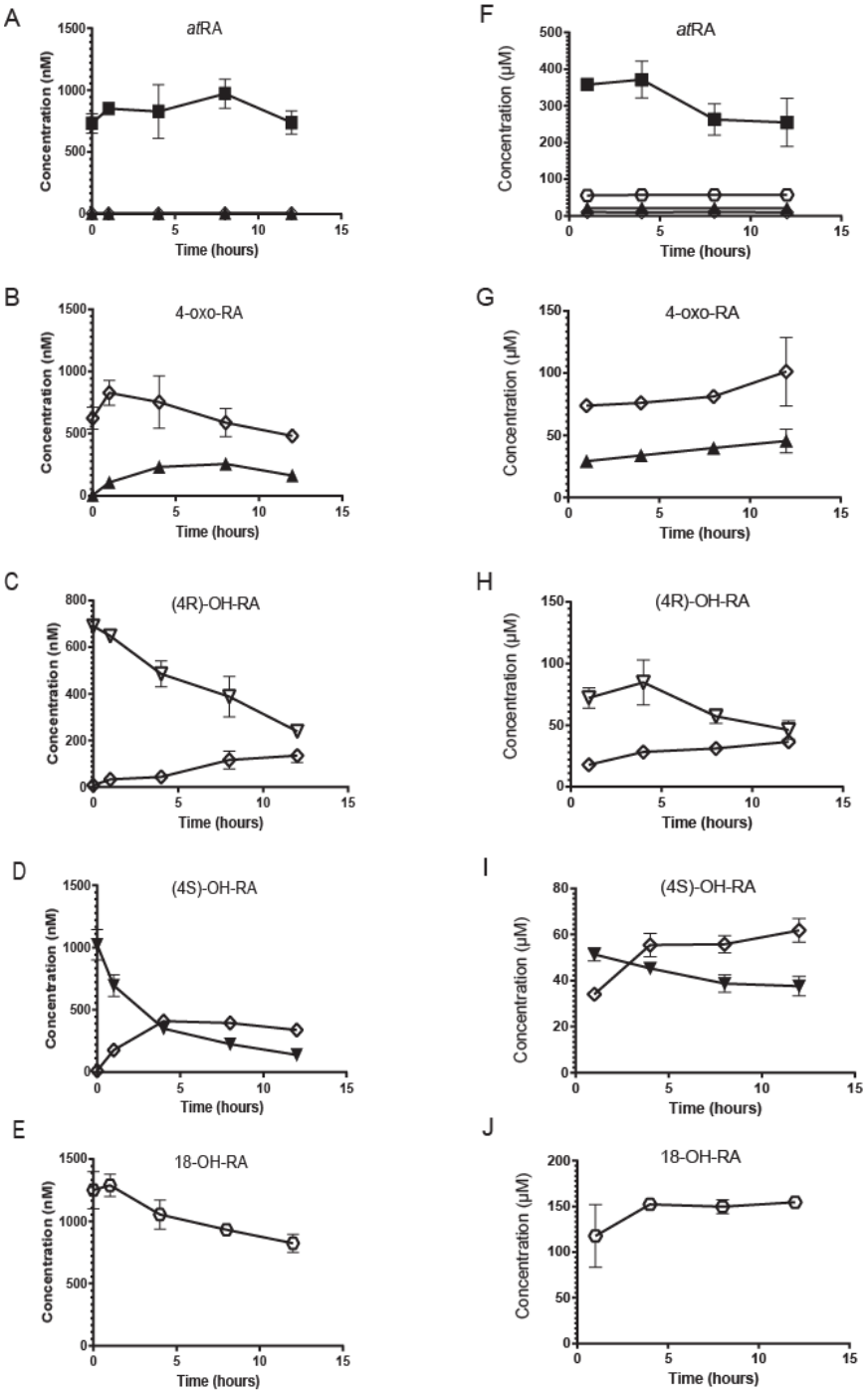

Figure 3.3: Inducer and subsequent metabolite concentration versus time profiles in HepG2 cells treated with *at*RA and its metabolites. HepG2 cells were treated with each inducer (1 μM) for 48 hours. Aliquots were taken from the media (A-E) at 0, 1, 4, 8 and 12 hours. Cells (F-J) were collected for analysis at 1, 4, 8, and 12 hours. Aliquots were extracted and analyzed for inducer (*at*RA, solid squares, A/E; 4-oxo-RA, open diamonds, B/G; (4R)-OH-RA, open triangles, C/H; (4S)-OH-RA, solid triangles, D/I; and 18-OH-RA, open hexagons, E/J) and subsequent metabolite concentrations at each time point.

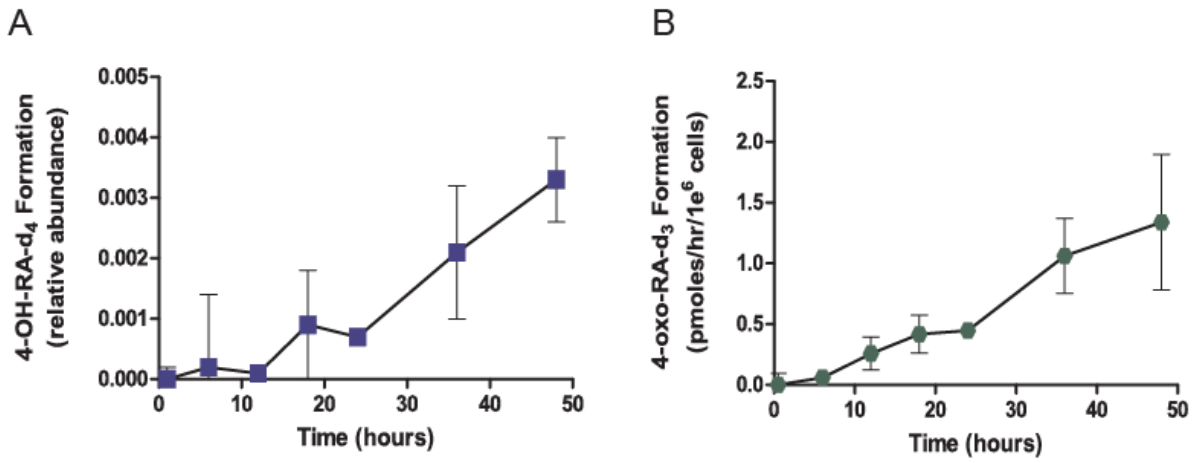

Figure 3.4: Induction of CYP26A1 activity in HepG2 cells treated with *at*RA. (A) 4-oxo-RA-d_3 and (B) 4-OH-RA-d_4 formation after one-hour treatments of *at*RA-d_5 (100 nM) taken during a 48 hour *at*RA (1 μM) treatment in HepG2 cells. Co-incubations with *at*RA-d_5 (1 hour incubations per time point) were performed every 6 to 12 hours (ranging from 0.5 to 48 hours) to accurately estimate increased CYP26A1 activity over time.

Table 3-1: The comparison of the exposures (AUCs) of each substrate and its metabolites in cells (0-12 hours), and the observed CYP26A1 mRNA after a 1 μM treatment with the test compound.

Treatment	$AUC^{0\text{-}12hr}$ of Inducer in Cells (nmoles•hour/mL)	$AUC^{0\text{-}12hr}$ of Subsequent Metabolites in Cells (nmoles•hour/mL)	$AUC^{0\text{-}12hr}$ Cell-to-Media Ratio	CYP26A1 mRNA (fold-↑, 1 μM)
*at*RA	3750 ± 350	130 ± 6 (4-oxo-RA) 120 ± 2 (4-OH-RA)	363	3700 ± 180
4-oxo-RA	980 ± 40	270 ± 10 (4-OH-RA)	123	2980 ± 250
(4R)-OH-RA	570 ± 90	340 ± 30 (4-oxo-RA)	106	1350 ± 230
(4S)-OH-RA	300 ± 10	630 ± 7 (4-oxo-RA)	70	1360 ± 240
18-OH-RA	1740 ± 70	------	141	300 ± 90

Table 3-2: The effect of selective P450 and inhibitors on 4-oxo-RA or 4OH-RA formation from *at*RA and formation of 4-OH-RA from 4-oxo-RA in HepG2 cells. The inhibitors used were 4-methylpyrazole (250 µM, alcohol dehydrogenases), cimetidine (250 µM, alcohol dehydrogenases), ketoconazole (10µM, P450s), testosterone (25 µM, aldo-ketoreductases), or carbenoxolone (25 µM and 50µM, retinol dehydrogenases). Significant changes in comparison to no inhibitor controls were performed using the student's unpaired T-test and are indicated as $*P < 0.05$.

Treatment	4-oxo-RA Formation (% of Control)	4-OH-RA Formation (% of Control)
*at*RA (control)	100 ± 3	100 ± 7
*at*RA + 4-methylpyrazole	109 ± 8	122 ± 11
*at*RA+cimetidine	130 ± 6*	149 ± 5*
*at*RA+ketoconazole	20 ± 1*	16 ± 6*
*at*RA+testosterone	109 ± 6	133 ± 4*
*at*RA + carbenoxolone (25 µM)	74 ± 3*	92 ± 22
*at*RA + carbenoxolone (50 µM)	80 ± 8*	99 ± 25
Treatment	**4-oxo-RA Formation (% of Control)**	**4-OH-RA Depletion (% of Control)**
4-OH-RA (Control)	100 ± 6	100 ± 6
4-OH-RA + 4-methylpyrazole	121 ± 12	96 ± 3
4-OH-RA + cimetidine	121 ± 3*	99 ± 2
4-OH-RA + ketoconazole	110 ± 0	75 ± 0*
4-OH-RA + testosterone	107 ± 1	107 ± 0
4-OH-RA + carbenoxolone (25 µM)	115 ± 9	80 ± 9*
4-OH-RA + carbenoxolone (50 µM)	117 ± 6*	96 ± 3

Chapter 4 : Hepatic Cyp2d and Cyp26 mRNA and Activities are Increased During Mouse Pregnancy

This chapter has been Published In:

Drug Metabolism and Disposition (2013) Vol. 41: 312-319

4.1 Introduction

Altered drug disposition during human pregnancy could compromise the therapy to the mother or affect the risk of medications to the fetus. Chronic or pregnancy-related conditions such as epilepsy, depression, asthma, preeclampsia or gestational diabetes often require medical treatment during pregnancy, and as a consequence the use of prescription and over-the-counter medications during pregnancy is common (Andrade et al., 2004). For example, 95.8% of pregnant women in rural West Virginia were administered prescription medications, 92.6% took over-the-counter medications, and 45.2% used herbal medicines (Glover et al., 2003). However, little is known about whether the same dosing regimens of drugs used in non-pregnant women and in men can be used during pregnancy. In fact, there is accumulating evidence that pregnancy alters the disposition of drugs significantly and hence drug doses need to be adjusted during pregnancy (Anderson, 2005).

Pharmacokinetic studies using probe drugs have shown that the activity of liver cytochrome P450 enzymes (P450s) changes during pregnancy in an enzyme specific fashion (Anderson, 2005). The activity of CYP3A4 is increased approximately 2-fold during human pregnancy based on midazolam clearance (Hebert et al., 2008). The 6-fold increase in metoprolol oral clearance (Hogstedt et al., 1983) and decrease in dextromethorphan urinary ratio (Tracy et al., 2005) during pregnancy indicate up to 6-fold increase in CYP2D6 activity during pregnancy. In contrast, CYP1A2-mediated metabolism of caffeine and theophylline is decreased approximately 50% during human pregnancy, and CYP2C19 activity appears to be decreased based on proguanil metabolism (Wadelius et al., 1997; Anderson, 2005; Tracy et al., 2005). Together these studies show a complicated network of pregnancy mediated pharmacokinetic changes. However, the mechanisms causing these changes during pregnancy are still largely

unknown. Due to the lack of mechanistic understanding, extrapolation of the findings from one gestational age to another cannot be done for specific P450s.

Animal models have been used to identify specific mechanisms by which pregnancy alters drug disposition. For example, in the mouse an increase was detected in liver Cyp3a16, Cyp3a41, and Cyp3a44 mRNA, in liver Cyp3a activity and in the activity of the human CYP3A4 promoter during pregnancy (Mathias et al., 2006; Zhang et al., 2008; Dai et al., 2011). This increase in CYP3A mRNA, activity and transcription is in agreement with the observed increase in CYP3A4 activity during human pregnancy. In addition, similar to what is observed during human pregnancy, the clearance of nelfinavir increased during mouse pregnancy (Mathias et al., 2006). Together these data suggest that the mouse is a good model for investigating the mechanisms responsible for changes in CYP3A4 activity during human pregnancy. Similarly, the observed 50% decrease in caffeine clearance during human pregnancy was replicated in the pregnant rat with CYP1A2 activity, expression and mRNA decreasing during rat pregnancy (Walker et al., 2011). However, Cyp2d mRNA and activity were also decreased during rat pregnancy, contradictory to the apparent increase in CYP2D6 activity in pregnant humans (Dickmann et al., 2008), suggesting that the rat does not replicate some aspects of human pregnancy. Nevertheless, the study demonstrated that Cyp2d mRNA and activity were altered during pregnancy. This is important since there are no known xenobiotic inducers of CYP2D6 expression and classic inducers of P450 enzymes do not affect CYP2D6 activity. Interestingly, in the rat, a correlation between the Cyp2d isoform mRNA and retinoic acid receptor (RAR) α and hepatocyte nuclear factor (HNF) 3β mRNA was found, and retinoic acid (RA) signaling was suggested as potential mechanism of Cyp2d regulation (Dickmann et al., 2008).

The first aim of this study was to determine whether Cyp2d mRNA and activity increases during mouse pregnancy. The second aim was to explore whether RA signaling is also increased during mouse pregnancy and correlates with Cyp2d mRNA similar to what was observed in the rat. The overall hypothesis of the study was that according to the changes observed during human pregnancy, the mRNA and activity of Cyp2d enzymes is increased during pregnancy and as suggested by the rat data this increase will correlate with RA signaling in the mouse liver.

4.2 Materials and Methods

Chemicals and Reagents. *at*RA, dextromethorphan, and dextrorphan were purchased from Sigma Aldrich (St. Louis, MO). 4-OH-RA and 4-oxo-RA were synthesized as previously described (Samokyszyn et al., 2000; Topletz et al., 2012). Optima-grade water, optima-grade acetonitrile, and ethyl acetate used for chemical analyses were purchased from Thermo Fisher Scientific. Water used for mRNA analysis was purchased from Qiagen (Valencia, CA). Potassium phosphate (KPi) buffers used were prepared in house and included a tissue homogenization buffer (50 mMKPi, 0.25 M sucrose, 1 mM EDTA, 1 mM PMSF) and a 100 mMKPi buffer (pH 7.4) for incubations.

Breeding and Tissue Preparation. Wild-type FVB mice (Taconic) were cared for and housed in the specific pathogen free facility at the University of Washington. The studies were approved by the Institutional Animal Care and Use committee of the University of Washington. Wild type female mice 8-10 weeks of age were mated and pregnancy was determined by the detection of a vaginal plug. The mice were then divided in random order into two groups. The mice in group one (n = 9) were sacrificed at gestational day (GD) 15 and the mice in group 2 (n = 9) were sacrificed at GD 19. The mice were sacrificed using CO_2, and the livers were collected. In addition, virgin, age matched females (n = 9), from the same cohort of animals,

were sacrificed as non-pregnant controls. The tissues were flash-frozen in liquid N_2 and stored at -80°C until use.

All tissue processing and preparation was performed on ice. For activity assays, 0.1-0.2 g of liver tissue of non-pregnant (*n* = 5), GD 15 (*n* = 3), and GD 19 (*n* = 3) mice were homogenized in 2 mL Omni Hard Tissue Homogenizing tubes containing 1.4 mm ceramic beads, 0.3 mL homogenization buffer (50 mMKPi, 0.25 M Sucrose, 1 mM EDTA, 1 mM PMSF), and the tissue using an Omni Bead Ruptor 24 containing dry ice in acetone (Omni International, Kennesaw, GA). The mixture was homogenized for 2 x 20 s. The homogenates were aliquoted and stored at -80°C until further use. Protein content was determined using a Pierce BCA Protein Assay (Thermo Fisher Scientific) according to manufacturer's instructions with albumin as the standard.

mRNA Extraction and Real-Time PCR Assay. Total RNA was extracted from livers of non-pregnant (*n* = 4), GD 15 (*n* = 6), and GD 19 (*n* = 6) mice. To 0.1-0.2 g tissue, 1 mL of TRIzol reagent (Invitrogen, Grand Island, NY) was added, and mRNA extracted according to manufacturer's recommendations. Total RNA content was quantified using the Nanodrop 2000c Spetrophotometer (Thermofisher Sci., Waltham, MA) and RNA quality was confirmed by gel electrophoresis. cDNA was generated from 1µg of mRNA using the TaqMan Gene expression reagents (Applied Biosystems, Carlsbad, CA) as previously described (Tay et al., 2010). Taqman Real-Time Universal polymerase chain reaction (PCR) master mix and PCR fluorescent primers and probes were purchased from Applied Biosystems (Foster City, CA). Probes used were as follows: Cyp2d9 (Mm00651731), Cyp2d10 (Mm00731648), Cyp2d11 (Mm04205381), Cyp2d22 (Mm01306302), Cyp2d26 (Mm00472520), Cyp2d40 (Mm01303815_m1), Cyp26a1 (Mm00514486), Rarα (Mm01296312_m1), Rarβ (Mm01319677) and β-actin

(Mm00607939_s1). β-actin was used as the endogenous control (housekeeping gene). RT-PCR reactions were conducted using a StepOnePlus Real-Time PCR instrument (Applied Biosystems) according to manufacturer's recommendations. The fold-changes in Cyp2d9, Cyp2d10, Cyp2d11, Cyp2d22, Cyp2d26, and Cyp2d40 mRNA as well as Cyp26a1 and Rarβ mRNA during pregnancy in comparison to non-pregnant mice were quantified using RT-PCR.

Dextromethorphan Metabolism in Mouse Liver Homogenates. To quantify Cyp2d activity, the formation of dextrorphan from dextromethorphan by mouse liver homogenates (MLH) was determined. A total of eleven MLHs were used from non-pregnant (n = 5), GD 15 (n = 3) and GD 19 (n = 3) mice. All incubations were conducted at the protein and time linear range of dextromethorphan metabolism. MLHs (0.4 mg/mL) were incubated individually with two concentrations (1 and 50 µM) of dextromethorphan. These concentrations were chosen based on prior data of dextromethorphan metabolism in rat liver microsomes (Dickmann et al., 2008) and the known K_m for CYP2D6-mediated formation of dextrorphan (Lutz and Isoherranen, 2012). The 1 µM concentration is below the K_m of dextromethorphan in rat liver microsomes and for CYP2D6 allowing evaluation of intrinsic clearance changes as reported previously (Dickmann et al., 2008), whereas 50 µM is much greater than the K_m and allows determination of V_{max} in rat liver microsomes and for human CYP2D6. Michaelis-Menten kinetic constants for dextrorphan formation were determined using MLH from 7 mice (3 non-pregnant, 2 GD 15 and 2 GD 19). The MLHs (0.4 mg/mL) were incubated with six concentrations of dextromethorphan (0.5, 1, 5, 10, 25, 50 µM). All incubations were performed using 96-well plates in 100 mMKPi buffer (pH 7.4) in a total volume of 0.2 mL per well. Samples were preincubated for 5 min before initiation with NADPH (1 mM final concentration). After an incubation period of 10 min, 0.125 mL of each sample was removed and quenched into cold acetonitrile (0.125 mL) in a fresh

96-well plate. Plates were then centrifuged for 20 min at 612g, 4ºC and 0.125 mL supernatant was removed and transferred into a fresh 96-well plate for UFLC-MS/MS (ultra fast liquid chromatography-tandem mass spectrometry) analysis.

Dextrorphan was separated using a Thermo Scientific Hypersil gold column (1.9 µm, 2.1mm x 100 mm, Thermo Fisher Scientific) with a Shimadzu UFLC XR DGU-20A5 (Shimadzu Scientific Instruments, Columbia, MD) coupled to an AB Sciex 3200 Mass Spectrometer (AB Sciex, Framingham, MA). The analytes were separated using a linear seven minute gradient from an initial mobile phase of 10% acetonitrile 90% aqueous with 0.1% formic acid to a final condition of 90% acetonitrile 10% aqueous with 0.1% formic acid. Dextrorphan was detected using positive ion electrospray mass spectrometry, with a declustering potential of 61, a collision energy of 49, and a collision exit potential of 4.5 (Lutz and Isoherranen, 2012). The parent-fragment MS/MS transition of *m/z* 258.2 → 157.2 Da was monitored. The injection volume was 10 µL. A six point standard curve for dextrorphan was constructed using concentrations between 5 and 500 nM and dextrorphan concentrations were quantified based on dextrorphan peak height.

atRA Metabolism in Mouse Liver Homogenates. Changes in hepatic *at*RA metabolism were determined by quantifying the formation of 4-OH-RA, 4-oxo-RA and 16-OH-RA from *at*RA by MLHs. All *at*RA incubations were conducted under red light. MLHs (0.4 mg/mL) were incubated with *at*RA (1 µM) in borosilicate glass tubes (8 x 13 cm). A total incubation volume of 0.5 mL in 100 mMKPi buffer (pH 7.4) was used. Samples were preincubated for 5 minutes before reactions were initiated with NADPH. Following a 25-min incubation, reactions were quenched by adding 3 mL of ethyl acetate to each incubation together with an internal standard (20 µL of 2.5 µM 4-oxo-RA-d_3). Samples were then centrifuged, and the organic layer extracted and evaporated under a stream of N_2 and then reconstituted in 100 µL of optima grade

acetonitrile for MS/MS analysis. Analytes were separated and analyzed using an Agilent Zorbax C18 column (3.5µm, 2.1 mm x 100 mm) with an AB Sciex API 5500 Q/LIT mass spectrometer (AB Sciex) equipped with an Agilent 1290 Infinity UHPLC. The analytes were separated over a linear 35-min gradient using an initial mobile phase of 5% acetonitrile 95% aqueous with 0.1% formic acid to a final condition of 95% acetonitrile 5% aqueous with 0.1% formic acid. Analytes were detected using negative ion electrospray mass spectrometry, with declustering potentials of -80 (4-OH-RA), -90 (16-OH-RA and 4-oxo-RA-d_3), and -95 (4-oxo-RA); collision energies of -28 (4-OH-RA), -25 (16-OH-RA and 4-oxo-RA-d_3) and -22 (4-oxo-RA); and collision exit potentials of -7 (4-OH-RA), -16 (16-OH-RA), -5 (4-oxo-RA) and -10 (4-oxo-RA-d_3). The parent-fragment MS/MS transitions of *m/z* 315 → 253 Da (4-OH-RA), 315 → 241 Da (16-OH-RA), 313 → 269 Da (4-oxo-RA), and 316 → 272 Da (4-oxo-RA-d_3) were monitored. Standard curves were constructed at concentrations between 2.5 and 100 nM for 4-OH-RA and 4-oxo-RA. Due to the lack of a synthetic standard for the 16-OH-RA, the relative changes in 16-OH-RA formation were measured from analyte to internal standard peak height ratio. As 4-oxo-RA is formed from 4-OH-RA sequentially, the sum of 4-OH-RA and 4-oxo-RA formation rates was used to determine total 4-OH-RA formed by MLHs.

RARE Identification within Promoter Regions of Cyp2d, Cyp26a1 and Rarβ. The DNA sequences of the mouse *Cyp2d* genes, *Cyp26a1* and*Rarβ* were scanned to determine if any retinoic acid response elements (RAREs) existed within the respective promoter regions. In-house Perl scripts were written to collect and parse stretches of genomic information for potential RARE promoter sequences in a two-step process. The first step uses the BioMart API (http://www.biomart.org) to access Ensembl (http://www.ensemble.org) and record the user-defined gene information to a text file in FASTA format. Genes of interest are listed in FASTA

format and are accessed by the Perl script. For each gene in the input file, 10,000 DNA base pairs are captured directly upstream of the gene and amended to an output file. The second step uses an independent Perl script to parse the aforementioned collection of gene information for RARE sequences. Perl string matching is employed to match sequences with the following requirement: (A|G)G(G|T)T(C|G)A(A|G|T|C)^{n}(A|G)G(G|T)T(C|G)A, where n is one, two or five bases as defined by DR1, DR2 and DR5 RARE sequences, respectively. As defined by Perl, bases listed within parentheses and separated by the character '|' allow the string matching algorithm to match only one of the listed bases. If a series of base pairs in a gene match the string representing a potential RARE sequence based on the above rule, the gene name and the actual RARE sequence found are listed in a FASTA format output file.

Data and Statistical Analysis. Changes in mRNA were quantified as fold-difference from control using the comparative C_T method ($\Delta\Delta C_T$) with β-actin as the housekeeping gene. All data were fitted via linear and nonlinear regression using Prism v.5 (GraphPad Software, Inc., La Jolla, CA) and all statistical analyses were performed using Prism v.5 (GraphPad). One-way analyses of variance were performed to determine statistical significance of differences in mRNA expression and Cyp2d and Cyp26a1 activity between non-pregnant mice and pregnant mice at GD 15 and GD 19. A P value < 0.05 was considered significant. Significant differences between non-pregnant, GD 15 and GD 19 mice were then determined using Bonferroni's Multiple Comparison Test. All correlations between mRNA of Cyp2d isoforms, Cyp26a1 and Rarβ across the gestational ages were tested using linear regression. Regressions with P values < 0.05 were considered significant.

All enzyme kinetic data were fitted using nonlinear regression. All parameter estimates are given as means ± S.D. Michaelis-Menten parameters for dextrorphan formation were estimated

using Eq. 4.1 , where *v* is the formation velocity of the metabolite and [*S*] is the initial substrate concentration (dextromethorphan).

$$v = \frac{V_{\max} \cdot [S]}{K_m + [S]} \qquad \text{equation 4.1}$$

Intrinsic clearance (CL_{int}) of dextrorphan formation was calculated using Eq.4.2.

$$CL_{\text{int}} = \frac{V_{\max}}{K_m} \qquad \text{equation 4.2}$$

Formation velocity of 4-OH-RA + 4-oxo-RA from *at*RA was used as a measure of *at*RA metabolism due to the sequential oxidation of 4-OH-RA to 4-oxo-RA (Lutz et al., 2009).

The changes in the in vivo intrinsic clearance of dextromethorphan and *at*RA were predicted using in vitro-to-in vivo extrapolation. The intrinsic clearances were scaled up to in vivo CL_{int} at different gestational stages and in non-pregnant controls according to Eq. 4.3 using total milligrams of protein per gram of liver measured in each animal (Table 4-3) and the average maternal mouse liver weight for each gestational time point. Values for the average liver weight at each gestational age were used as previously reported: 1.35 ± 0.25 g (non-pregnant), 2.48 ± 0.39 g (GD 15), and 2.62 ± 0.49 g (GD 19) (Dai et al., 2011). The values of mg protein per gram of liver were calculated for each animal and used to scale up to total $CL_{int,\ liver}$ before each gestational time point was averaged.

$$CL_{\text{int},liver} = CL_{\text{int}\,per\,mg\,protein} \times (mg\,protein\,per\,g\,liver) \times (total\,g\,liver) \qquad \text{equation 4.3}$$

4.3 Results

4.3.1 Changes in Cyp2d mRNA during Mouse Pregnancy. Cyp2d10, Cyp2d11, Cyp2d22, Cyp2d26, and Cyp2d40 are all found in both murine genders (Renaud et al., 2011). The mRNA of Cyp2d11, Cyp2d22, Cyp2d26, and Cyp2d40 was increased significantly ($P < 0.01$) on GD 15 and GD 19 when compared to the non-pregnant control mice (Figure 4.1A), with

Cyp2d40 showing the greatest increase in mRNA (6-fold) during gestation. The mRNA of Cyp2d10 at GD 15 and GD 19 was not different from the non-pregnant controls ($P > 0.05$). The mRNA of the male-specific enzyme Cyp2d9 was also unchanged during pregnancy ($p > 0.05$). No differences ($P > 0.05$) were found between GD 15 and GD 19 for any of the Cyp2d enzymes. Baseline (non-pregnant) C_T values indicated that average mRNA levels were highest for Cyp2d26 ($C_{T,Ave\ NP} = 23.3$), Cyp2d22 ($C_{T,Ave\ NP} = 25.8$), and Cyp2d10 ($C_{T,Ave\ NP} = 24.7$), with lower mRNA baseline quantification for Cyp2d40 ($C_{T,Ave\ NP} = 32.6$), Cyp2d9 ($C_{T,Ave\ NP} = 32.9$) and Cyp2d11 ($C_T = 36.8$).

4.3.2 Changes in Dextromethorphan Metabolism during Mouse Pregnancy. To determine whether increased Cyp2d mRNA levels translated to increased Cyp2d activity, dextrorphan formation from dextromethorphan was evaluated in MLHs (non-pregnant, $n = 5$; GD 15, $n = 3$; and GD 19, $n = 3$) at two concentrations: 1 µM (below apparent K_m in rat liver microsomes) and 50 µM (~10*K_m in rat liver microsomes providing estimate of V_{max}). A 2.7-fold increase in dextrorphan formation was observed between non-pregnant (20.8 ± 11.2 pmoles/min/mg protein) and GD 19 (56.8 ± 39.4 pmoles/min/mg protein) MLHs at 50 µM dextromethorphan ($P < 0.05$), but the 1.7-fold increase in dextrorphan formation between non-pregnant and GD 15 (36.3 ± 8.4 pmoles/min/mg protein) MLHs was not significant ($P > 0.05$) (Figure 4.1B). Formation of dextrorphan at 1 µM was comparable ($P > 0.05$) between all three gestational ages (Figure 4.1C).

To evaluate the reasons for the increased dextrorphan formation at 50 µM dextromethorphan, Michaelis-Menten constants were determined in MLHs from seven mice; three non-pregnant, two GD 15, and two GD 19. A 1.3-fold increase in the V_{max} of dextrorphan formation was observed at GD 19 when compared to non-pregnant controls (Figure 4.1D,Table

4-1), suggesting increased Cyp2d protein expression. The average V_{max} on GD 15 was not different from non-pregnant mice (Table 4-1). The increase in the apparent K_m for dextrorphan formation during gestation was also not significant (Table 4-1). The Eadie-Hofstee plots of dextrorphan formation in the three gestational ages were linear (Figure 4.4). The average intrinsic clearance of dextrorphan formation from dextromethorphan in MLHs did not change on GD 15 and GD 19 when compared to that of non-pregnant mice (Table 4-1). However, the in vivo intrinsic clearance of dextromethorphan was predicted to increase 1.5 to 1.8- fold during mouse pregnancy (GD 15 and GD 19) in comparison to the non-pregnant controls. The predicted in vivo CL_{int} values were 2041 ± 590 µL/min (non-pregnant), 2969 ± 1267 µL/min (GD15) and 3773 ± 772 µL/min (GD 19).

4.3.3 Changes in Cyp26a1, Rarα, and Rarβ mRNA during Mouse Pregnancy. The mRNA of Cyp26a1 was increased ($P < 0.05$) on both GD 15 (10-fold) and GD 19 (9.7-fold) compared to non-pregnant controls (Figure 4.2A). Rarβ mRNA also increased on GD 15 (2.8-fold, $P < 0.01$) but the increase on GD 19 (2.0-fold) was not significant ($P > 0.05$). There was no significant change in Rarα mRNA at GD 15 and GD 19 when compared to non-pregnant controls. No differences in mRNA expression were observed between GD 15 and GD 19 for Cyp26a1, Rarα, or Rarβ ($P > 0.05$).

4.3.4 Changes in 4-OH-RA, 4-oxo-RA, and 16-OH-RA Formation during Mouse Pregnancy. Since Cyp26a1 mRNA was increased during pregnancy, *at*RA metabolism by MLHs was quantified using the additive formation rates of 4-OH-RA and 4-oxo-RA. While 4-OH-RA is formed by multiple P450 enzymes, 16-OH-RA appears to be a specific metabolite for CYP26A1 (Thatcher et al., 2011). Hence, the relative formation of 16-OH-RA was measured as a specific Cyp26a1 probe. Formation of 4-OH-RA, 4-oxo-RA and 16-OH-RA from *at*RA was

detected in all livers, regardless of gestational age. The combined formation rate of 4-oxo-RA and 4-OH-RA (Figure 4.2B) was not significantly between the different gestational days: 2.05 ± 0.57 pmol/min/mg protein (non-pregnant), 2.11 ± 0.55 pmol/min/mg protein (GD 15), and 2.21 ± 0.20 pmol/min/mg protein (GD 19). The relative formation of 16-OH-RA (Figure 4.2C), increased 1.8-fold ($P< 0.05$) on GD 15 compared with the non-pregnant animals. The in vivo CL_{int} for 4-OH-RA and 4-oxo-RA formation was predicted to increase 1.7 and 2.2-fold on gestational days 15 and 19, respectively, when compared to the non-pregnant controls. The predicted CL_{int}, values were 391.0 ± 105.6 µL/min (non-pregnant), 673.4 ± 314.8 µL/min (GD15) and 873.4 ± 358.0 µL/min (GD19) suggesting that *at*RA clearance is increased during mouse pregnancy.

4.3.5 Correlations between Cyp2d isoforms, Cyp26a1 and Rarβ mRNA. To explore the role of*at*RA in regulating Cyp2d expression, correlation between Cyp2d mRNA and the mRNA of marker genes of Rar activation was evaluated. The mRNA of Cyp2d11, Cyp2d22, Cyp2d26, and Cyp2d40 positively correlated ($P < 0.05$) with Cyp26a1 mRNA (Table 4-2). There was no correlation ($P > 0.05$) between Cyp26a1 mRNA and the mRNA of Cyp2d9 and Cyp2d10 (Table 4-2). Similar to the correlation between Cyp2d enzymes and Cyp26a1, a correlation ($P < 0.05$) was observed between Rarβ mRNA and Cyp2d22, Cyp2d26, and Cyp2d40 mRNA. There was no correlation between Rarβ mRNA and Cyp2d11, Cyp2d9 and Cyp2d10 mRNA ($P> 0.05$) (Table 4-2). In addition, of the Cyp2d enzymes, Cyp2d22 and Cyp2d40 mRNA correlated ($P < 0.05$) with Cyp2d11, the mRNA of Cyp2d26 and Cyp2d40 correlated with Cyp2d22 mRNA, and the mRNA of Cyp2d40 correlated with Cyp2d26 mRNA. A positive and correlation was also detected between Cyp26a1 and Rarβ mRNA ($P < 0.05$) (Table 4-2).

4.3.6 Identification of an RARE in within Mouse *Cyp2d40, Cyp26a1* and *Rarβ*

Promoter Regions. The location of the *Cyp2d11, Cyp2d22, Cyp2d10, Cyp2d40* and *Cyp2d26* genes in the *Cyp2d* gene locus is shown in Figure 4.3A. An RARE-DR2 promoter sequence was found within the *Cyp2d40* promoter (Figure 4.3, B and E) but due to the location of the Cyp2d genes it is possible that this RARE also contributes to the regulation of the other Cyp2d genes in this locus. No additional RARE sequences were found in the *Cyp2d* gene locus. *Cyp26a1* and *Rarβ* have previously been shown to contain identical RARE-DR5 promoter regions (Loudig et al., 2000; Loudig et al., 2005), and these RAREs were identified in the current study as well (Figure 4.3, C, D, and E).

4.4 Discussion

Based on probe studies, one of the largest effects of pregnancy on specific P450 activity is observed with CYP2D6. The increased activity of CYP2D6 is clinically important as approximately 30% of drugs on the market are metabolized by CYP2D6 (Shimada et al., 1994), including many drugs administered to pregnant women such as antidepressants, antipsychotics, and β-blockers (Wadelius et al., 1997). The oral clearance of metoprolol, a CYP2D6 probe, increased 6-fold and the bioavailability decreased to half at 26-30 weeks of gestation compared to postpartum (Hogstedt et al., 1985). A decrease in the urinary dextromethorphan-dextrorphan metabolic ratio was also observed at all trimesters (Tracy et al., 2005). In CYP2D6 extensive metabolizers, at 36 weeks of gestation a 50% decrease in the plasma dextromethorphan-dextrorphan metabolic ratio was detected when compared to post-partum, suggesting CYP2D6 induction (Wadelius et al., 1997). In individuals lacking functional CYP2D6, a 50% increase in parent/metabolite ratio was detected (Wadelius et al., 1997). Together these data provide evidence that CYP2D6 activity is increased during human pregnancy.

The apparent induction of CYP2D6 during pregnancy is puzzling since CYP2D6 is not considered to be inducible by xenobiotics. It has been shown that classic xenobiotic inducers that activate PXR, AhR and CAR, do not induce CYP2D6 (Niemi et al., 2003; Dixit et al., 2007; Hewitt et al., 2007; Westerink and Schoonen, 2007). There does, however, appear to be transcriptional regulation of CYP2D6. The variation of CYP2D6 activity correlates well with CYP2D6 mRNA in humans (Carcillo et al., 2003) and previous studies have shown that the orphan nuclear receptor HNF4α regulates CYP2D6 transcription via binding to a direct repeat site (DR1) on the CYP2D6 promoter (Cairns et al., 1996).In addition, in human hepatocytes, analysis of P450 gene expression after adenoviral HNF4α antisense RNA transfection resulted in a 45% decrease in CYP2D6 gene expression (Jover et al., 2001). In CYP2D6 humanized mice lacking HNF4α in the liver, a 50% decrease in CYP2D6 mRNA and activity was observed (Corchero et al., 2001). However, HNF4□ is a common regulator of many liver P450 enzymes, which all change in different manner during pregnancy, and as such it is unlikely that changes in CYP2D6 activity during human pregnancy can be completely explained by changes in HNF4α-mediated transcriptional activity.

Studies in pregnant rats have shown that both Cyp2d mRNA and activity change significantly during pregnancy, but a decrease instead of an increase in Cyp2d mRNA and activity was observed during rat pregnancy (Dickmann et al., 2008). In contrast to the findings in the rat, this study shows that during mouse pregnancy the mRNA of Cyp2d40 was increased up to 6-fold and Cyp2d11, Cyp2d22 and Cyp2d26 were increased approximately 2-fold. This increase in Cyp2d mRNA is in agreement with the observed increase in CYP2D6 activity in the human, and suggests that the mouse can replicate changes in Cyp2d activity and may be an appropriate model to study the mechanisms underlying CYP2D regulation during pregnancy.

Indeed, when the in vitro intrinsic clearance of dextrorphan during mouse pregnancy was extrapolated to in vivo, a 2.2 to 3.7-fold increase in dextromethorphan intrinsic clearance was predicted on GD15 and GD19, respectively. This predicted increase is in agreement with the 2-fold increase in dextromethorphan clearance observed in humans (Wadelius et al., 1997). The increase in predicted Cyp2d activity and dextromethorphan intrinsic clearance is most likely due to increased apparent V_{max} for dextrorphan formation. The apparent V_{max} value was increased by 30% at GD 19, and the dextrorphan formation velocity in a different set of mice was increased by 2.8-fold at GD 19 at a dextromethorphan concentration of 50 µM.

The increased V_{max} value for dextrorphan formation is in agreement with the increase in Cyp2d40, Cyp2d11, Cyp2d22 and Cyp2d26 mRNA. Nevertheless, it is not possible to differentiate the relative contributions of individual Cyp2d enzymes to dextrorphan formation. Using Cyp2d knock-out mice it has been shown that Cyp2d enzymes mediate the overall elimination of dextromethorphan in mice (Scheer et al., 2012), but dextromethorphan metabolism has been kinetically characterized only for Cyp2d22 (K_m = 250 µM) (Yu and Haining, 2006). The observed K_m values for dextrorphan formation in the mouse liver homogenates (2.5 to 3.5 µM), were ~40-fold lower than that shown for Cyp2d22, suggesting that multiple enzymes contribute to dextrorphan formation in mouse liver. However, the Eadie-Hofstee plots were linear preventing identification of multiple contributing enzymes. The observed K_m values in MLHs were similar to those previously determined in rat liver microsomes (2.5-10 µM) from pregnant and non-pregnant animals (Dickmann et al., 2008) and in agreement with the K_m values of dextrorphan formation determined for all four recombinant rat Cyp2d enzymes (K_m values 0.3-49 µM) (Narimatsu et al., 2009). The trend towards higher K_m during pregnancy is similar to that observed in rats, and could be entirely a result of

increased contribution of a low affinity Cyp2d enzyme to dextrorphan formation in relation to a high affinity Cyp2d enzyme. Assuming similar PCR amplification efficiencies and the obtained absolute C_T values for the Cyp2d enzymes, Cyp2d26, Cyp2d22 and Cyp2d10 are the predominant Cyp2d enzymes in female mouse liver. Therefore, it is likely that the obtained K_m is a combination of the activities of these three enzymes together with increased contribution of Cyp2d40 to dextromethorphan metabolism during pregnancy. It is also likely that at low dextromethorphan concentrations (< 5 µM) dextrorphan formation is mainly catalyzed by a high affinity Cyp2d enzyme which does not change during pregnancy. This high affinity Cyp2d enzyme could be Cyp2d10. The metabolism at 50 µM is likely to be catalyzed by low affinity enzymes, possibly Cyp2d22 and Cyp2d40, which are significantly increased during pregnancy. It is also possible that the recombinant enzyme system used for Cyp2d22 characterization is different in the lipid content and protein-protein interactions than MLHs, resulting in possible differences in measured enzyme kinetic values. Together these data suggest that the increased dextrorphan formation on GD19 is due to increased expression of Cyp2d proteins. However, due to the likely contribution of multiple mouse P450 enzymes to dextromethorphan metabolism, a humanized CYP2D6 mouse model may be a better option for studying changes in CYP2D6 activity during pregnancy.

It has been proposed that RA signaling contributes to CYP2D regulation during pregnancy and RA was shown to alter CYP2D6 mRNA in HepG2 cells (Dickmann et al., 2008). To further evaluate this relationship, the changes in the mRNA of two classic model *at*RA responsive genes, *Cyp26a1* and *Rarβ*, were measured during mouse pregnancy. The mRNA of both of these genes was significantly increased during pregnancy in agreement with activation of Rars and *at*RA signaling. The promoter regions of *Cyp26a1* and *Rarβ* have characteristic

RAREs with direct repeats separated by 5 bases (DR5) (Figure 4.3C, D, and E) that are typically associated with increased transcription (Chambon, 1996). The increase in Cyp26a1 mRNA was greater than Rarβ during pregnancy, similarly to what has been previously observed following RA treatment in HepG2 cells (Tay et al., 2010). The increase in Cyp26a1 mRNA was coupled with increase in 16-OH-RA formation, a reaction indicative of increased Cyp26a1 activity. The increased Cyp26a1 and Rarβ mRNA during pregnancy suggest that *at*RA signaling is also increased in the maternal liver. *at*RA is a critical signaling molecule during mammalian development (Clagett-Dame and DeLuca, 2002; Maden, 2007; Duester, 2008) and plays a role in fetal organogenesis. Positive correlations between activation of Rars (using Cyp26a1 and Rarβ mRNA as markers), and Cyp2d mRNA were observed in this study. On the basis of these correlations and previous data, it was speculated that RA signaling may contribute to Cyp2d regulation. A DR2 RARE was identified in the *Cyp2d40* promoter (Figure 4.3B and E). The DR2 RARE has been shown to be associated with an RA mediated increase in transcription of the *CRABPII* gene (Lefebvre et al., 1995; Chambon, 1996). The DR2 element may be responsible for the correlation between Cyp2d40 mRNA and Cyp26a1 mRNA, the increased mRNA of Cyp2d22, Cyp2d11, Cyp2d40, and Cyp2d26 and the correlation of the mRNA of these four genes due to the orientation of these genes and a co-regulation of the linked genes. However, further detailed biochemical studies are needed to demonstrate that the identified RARE is a functional promoter element and to determine whether RA signaling contributes to the increased Cyp2d mRNA during pregnancy.

In conclusion, this study shows that Cyp2d mRNA and activity together with Cyp26a1 and Rarβ are increased during mouse pregnancy. As hypothesized, the increased Cyp2d mRNA correlated with increased RA signaling in the mouse liver during pregnancy. This is the first

study to demonstrate that Cyp2d mRNA is increased during pregnancy and hence the data presented provides important evidence toward potential transcriptional regulation of CYP2D6 and Cyp2d enzymes during human and mouse pregnancy. Further mechanistic characterization of the possible involvement of RA signaling in CYP2D6 regulation is needed.

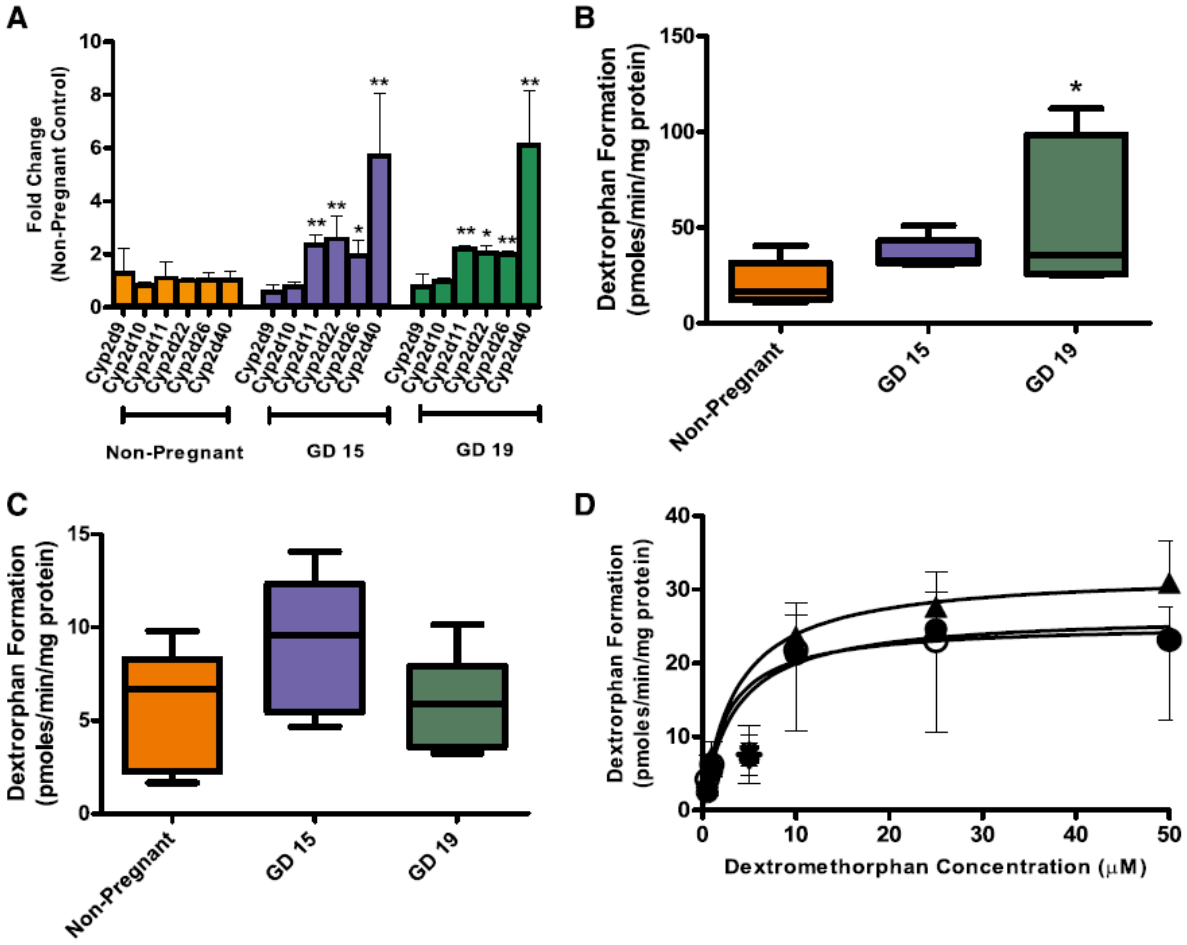

Figure 4.1: (A) The fold change in Cyp2d mRNA on GD 15 (n = 6, blue bars), and GD 19 (n = 6, green bars) in comparison with non-pregnant mice (n = 4, yellow bars). The measured dextrorphan formation velocity at 50 mM (B) and 1 mM (C) concentration of dextromethorphan is shown at two gestational ages and in non-pregnant controls using MLH from a separate group of animals. The panels show box and whiskers plots of dextrorphan formation velocity in non-pregnant (n = 5), GD 15 (n = 3) and GD 19 (n = 3) mice. The line shows the median, the box the 75th and 25th percentile and the error bar the range of the measurements in each group. The Michaelis-Menten parameters of dextrorphan formation from dextromethorphan were measured in MLHs from individual animals (D) using three control (open circles), two GD15 (closed circles) and two GD19 (closed triangles) MLHs. The lines indicate the fit of Michaelis-Menten equation to the average data from all animals on that gestational age and the error bars show the range of formation velocities observed at a given concentration of dextromethorphan in the different animals. The Eadie-Hofstee plots for each GD are shown in Figure 4.4. The Km and Vmax values are listed in Table 4-1. Significant changes in comparison with nonpregnant controls are indicated as $^{**}P < 0.01$ and $^{*}P < 0.05$.

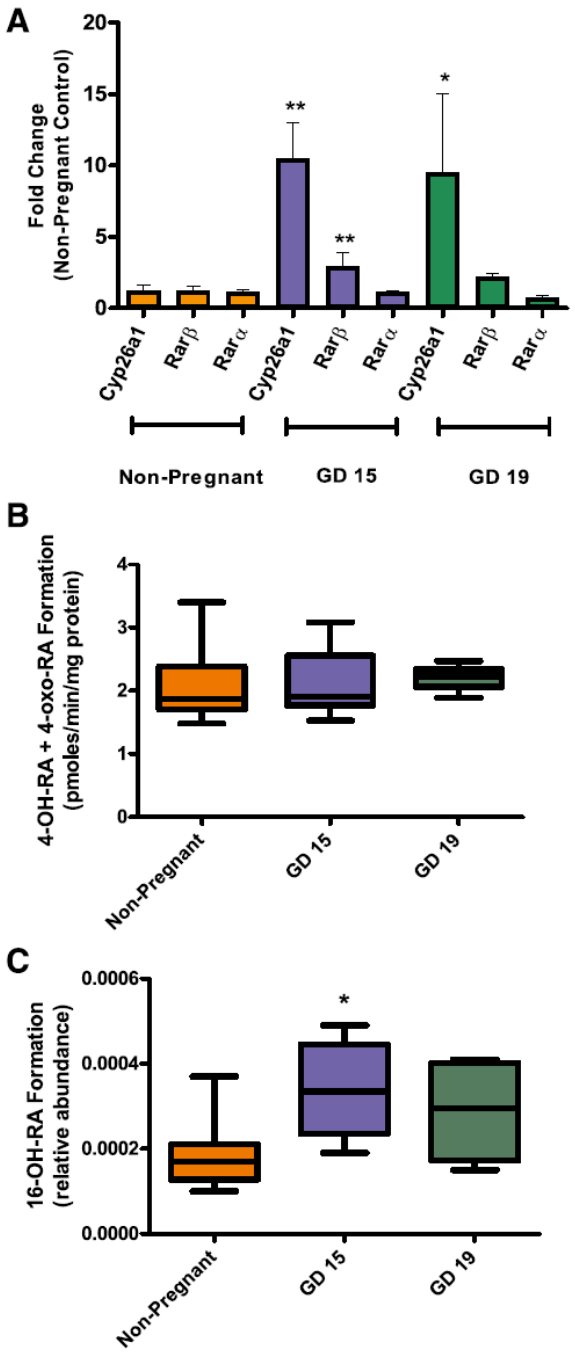

Figure 4.2: (A) The fold change in Cyp26a1, Rara and Rarb mRNA in GD 15 (n = 6, blue bars) and GD 19 (n = 6, green bars) mice in comparison to non-pregnant (n = 4, yellow bars) mice. The fold differences were calculated relative to non-pregnant values. (B) A box and whiskers plot of 4-OH-RA + 4-oxo-RA formation from atRA (1 mM) in MLHs in non-pregnant (n = 5), GD 15 (n = 3) and GD 19 (n = 3) mice. (C) The relative quantification of 16-OH-RA formation from atRA in MLHs from non-pregnant (n = 5), GD 15 (n = 3) and GD 19 (n = 3) mice. Significant changes in comparison with non-pregnant controls are indicated as $^{**}P < 0.01$ and $^{*}P < 0.05$.

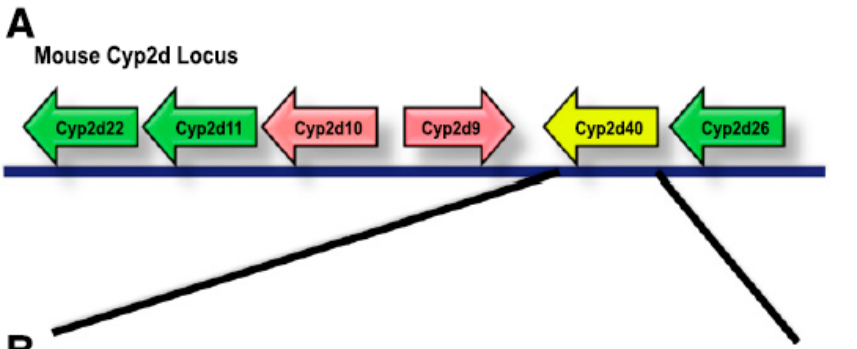

E

Type	Gene	RARE Sequence
RARE-DR2	Cyp2d40	AGGTCA GG AGTTCA
RARE-DR5 (1)	Cyp26a1	TGAACT TTGGG TGAACT
RARE-DR5 (2)	Cyp26a1	GGGTCA CAGGC GGGTCA
RARE-DR5	Rarβ	GGTTCA CCGAA AGTTCA

Figure 4.3: (A) The orientation of the Cyp2d genes in the Cyp2d gene locus. The promoter region of Cyp2d40 gene is enlarged in (B) and the identified RARE is shown. The promoters of Cyp26a1 and Rarb with the RAREs identified are shown in (C and D). Panel (E) shows sequences of the identified RAREs in the respective genes.

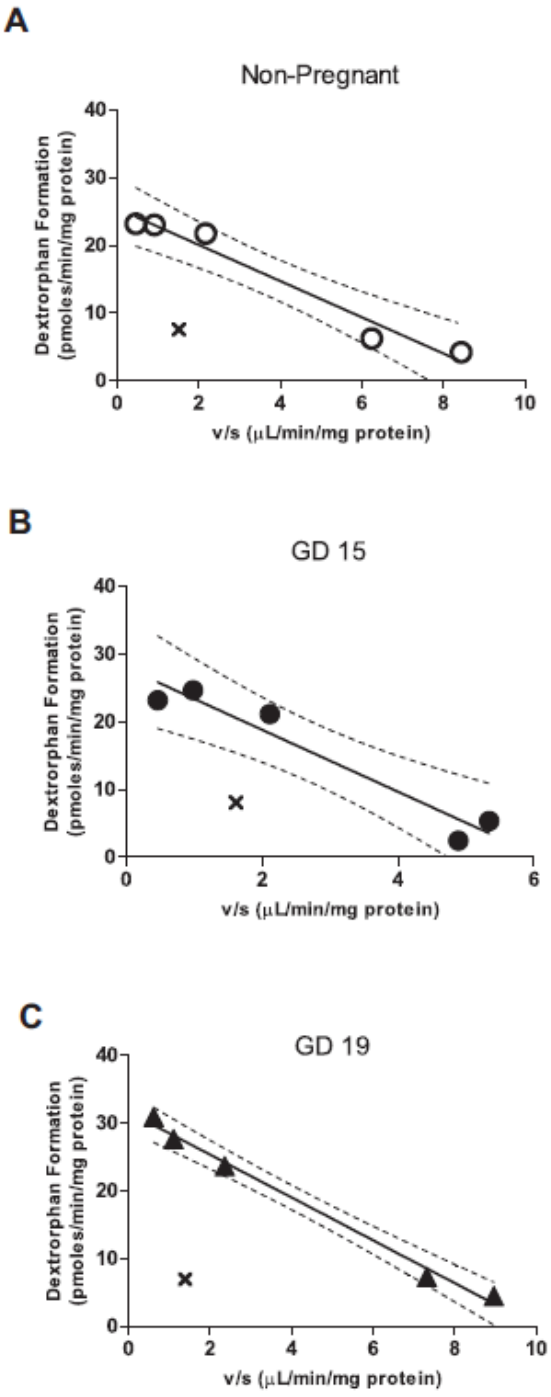

Figure 4.4: EadieHofstee plots of dextrorphan formation in mouse liver homogenates prepared from nonpregnant (top, open circles), Gestational day 15 (GD15, closed circles) and gestational day 19 (GD19, closed triangles). X indicates a datapoint that was omitted as an outlier. Experimental conditions were as described in materials and methods.

Table 4-1: Characterization of changes in dextromethorphan metabolism in mouse liver during gestation. Michaelis-Menten Parameters for Dextromethorphan in MLH from Pregnant and Nonpregnant Mice

Gestational Age	**V_{max}**	**K_m**	**Cl_{int}**
	pmol/min/mg protein	*μM*	*μL/min/mg protein*
Nonpregnant (*n* = 3)	25.4 ± 1.0	2.5 ± 0.5	10.1 ± 2.1
15 days (*n* = 2)	26.6 ± 1.6	3.4 ± 1.0	7.9 ± 2.3
19 days (*n* = 2)	32.3 ± 0.7*	3.5 ± 0.4	9.2 ± 1.0

*Indicates statistical significance at $P < 0.05$ compared with nonpregnant and GD15 mice.

Table 4-2: Statistical analyses of mRNA correlations between Cyp2d isoforms and the retinoic acid responsive genes Cyp26a1 and Rarβ.

	Correlation with Cyp26a1		
	R^2	*P* Value	Significant
Cyp2d9	0.0002	0.95	No
Cyp2d10	0.09	0.27	No
Cyp2d11	0.62	< 0.001	Yes
Cyp2d22	0.65	0.008	Yes
Cyp2d26	0.38	0.01	Yes
Cyp2d40	0.62	0.005	Yes
	Correlation with Rarβ		
	R^2	*P* Value	Significant
Cyp2d9	0.14	0.15	No
Cyp2d10	0.001	0.92	No
Cyp2d11	0.19	0.09	No
Cyp2d22	0.72	< 0.001	Yes
Cyp2d26	0.31	0.03	Yes
Cyp2d40	0.49	0.03	Yes
Cyp26a1	0.34	0.02	Yes

Table 4-3: Miligram protein obtained per gram of liver for the mouse liver homogenates.

Mouse Liver Homogenate	Gestational Age (days)	Miligram protein per gram of liver homogenate
MLH 1	Non-Pregnant	155.40
MLH 2	Non-Pregnant	135.60
MLH 3	Non-Pregnant	147.23
MLH 4	GD 15	135.00
MLH 5	GD 15	164.60
MLH 6	GD 19	241.85
MLH 7	GD 19	102.99
MLH 8	Non-Pregnant	145.91
MLH 9	Non-Pregnant	119.45
MLH 10	GD 15	80.91
MLH 11	GD 19	119.10

Chapter 5 : Role of the Human Fetal Liver in Limiting Fetal Exposure to *at*RA

5.1 Introduction

all-*trans*-retinoic acid (*at*RA), the active metabolite of retinol (vitamin A), is a critical signaling molecule during organogenesis and fetal development (Duester, 2008), and tight regulation of fetal exposure to *at*RA is critical for ensuring normal development. The overall concentrations of *at*RA are regulated by synthesis and metabolism of *at*RA. Over-exposure to *at*RA or its isomer 13-*cis*RA (Nau, 2001) has been associated with fetal malformations such as cleft palate, cerebellar hypoplasia, and spina bifida while RA deficiency is also associated with malformations (Creech Kraft et al., 1989; Niederreither et al., 2002; Scott and Goez, 2011). The balance between maternal supply of *at*RA to the fetus and synthesis of *at*RA within the fetal tissues remains unclear, although teratogenicity of retinoids demonstrates that maternal *at*RA can, at high concentrations, reach the fetus (Creech Kraft et al., 1989). Whether at endogenous concentrations maternal *at*RA crosses the placenta and escapes metabolism by the fetal liver is not well characterized.

Based on the expression patterns of *at*RA synthesizing enzymes in the fetus and the studies of retinol uptake to the fetus, at endogenous concentrations the fetus synthesizes *at*RA in situ and depends on maternal retinol as its vitamin A source. Enzymes that synthesize *at*RA have been detected in the placenta and in multiple human fetal tissues, including fetal liver and brain (Xi and Yang, 2008). In maternal plasma, retinol is highly bound to retinol binding protein (RBP) with essentially no free retinol in circulation. Stra6, the uptake transporter for retinol, is expressed in the placenta and takes up retinol directly from holo-RBP (Kawaguchi et al., 2007). Mutations in Stra6 have been found to reduce retinol uptake and cause severe birth defects or even fetal lethality, consistent with a lack of *at*RA in the fetus and limiting uptake of maternal

retinol by Stra6 (Kawaguchi et al., 2007). Whether the lack of maternal *at*RA supply to the fetus is due to *at*RA metabolism in the placenta and fetal liver is not known.

Metabolism of *at*RA is mediated primarily by P450 enzymes and the main metabolites formed include 4-hydroxy-RA (4-OH-RA) by CYP26, CYP3A and CYP2C enzymes and 16- and 18-hydroxy-RA by CYP26A1 and CYP26B1 enzymes (Thatcher et al., 2010); (Topletz et al., 2012). The main P450 enzymes responsible for *at*RA clearance in adult human liver and during mouse development appear to be the CYP26 enzymes (Abu-Abed et al., 1998; Yashiro et al., 2004; White and Schilling, 2008; Thatcher et al., 2010) and CYP26 mRNA was also previously detected in human fetal liver tissues (Trofimova-Griffin and Juchau, 1998; Xi and Yang, 2008). However, the importance of CYP26 enzymes in mediating fetal *at*RA exposure and the role of CYP26 enzymes as a first pass barrier for fetal *at*RA exposure is uncertain. CYP3A7 has been shown to metabolize *at*RA and suggested to be responsible for *at*RA metabolism in the fetal liver (Chen et al., 2000); (Thatcher et al., 2010) but the quantitative importance of CYP3A7 to *at*RA metabolism in the human fetal liver is not known. CYP3A7 constitutes approximately 32% of the fetal liver P450 enzymes (Schuetz et al., 1993; Thatcher et al., 2010) and its expression is fairly constant across different gestational ages (Chen et al., 2000; Leeder et al., 2005). Similarly, testosterone metabolism in the human fetal liver does not change with gestational age suggesting CYP3A7 activity is unchanged with gestational age (Leeder et al., 2005). In contrast, previous studies with human fetal liver showed that the formation of 4-OH-RA from *at*RA increased approximately 30-fold between the first and second trimesters (Chen et al., 2000). The different gestational age dependency in *at*RA hydroxylation and CYP3A7 expression suggests that other enzymes except CYP3A7 contribute to *at*RA hydroxylation in the fetal liver. The aim of this study was to determine the relative importance of CYP26 and

CYP3A7 to *at*RA metabolism in the fetal liver and to establish the extraction ratio of the fetal liver towards *at*RA to quantify what fraction of maternally available *at*RA would escape metabolism by fetal liver upon exposure.

5.2 Materials and Methods

Chemicals and Reagents: *at*RA, ketoconazole, fluconazole, and talarazole were purchased from Sigma-Aldrich (St. Louis, MO). 4-oxo-RA-d_3 and *at*RA-d_5 were purchased from Toronto Research Chemicals (North York, Ontario). 4-OH-RA, 4-oxo-RA, and 18-OH-RA were synthesized as previously described (Samokyszyn et al., 2000; Topletz et al., 2012). Optima-grade water, optima-grade acetonitrile, ethanol and ethyl acetate were purchased from Fisher Scientific (Pittsburg, PA). Potassium phosphate (KPi) buffers used were prepared in house and included a tissue homogenization buffer (50nM KPi, 0.25M sucrose, 1mM EDTA, 1mM PMSF) and a 100 mM KPi buffer (pH 7.4) for incubations.

Collection and Preparation of Human Fetal Liver (hFL) S9 Fractions: The study was approved by the Institutional Review Board (IRB) at the University of Washington. Human fetal liver tissues (n = 27) ranging from gestational days 67 to 137 were collected by the Birth Defects Laboratory at the University of Washington and flash frozen upon collection using liquid nitrogen and stored at -80ºC until ready for use. Donated tissues were from elective abortions; tissues from fetuses whose mothers had known drug use were excluded from this study. To prepare human fetal liver (hFL) S9 fractions for metabolic experiments, 0.1-0.3 g tissue sample was weighed out and 300 µL homogenization buffer was added. Samples were homogenized in 2 mL Omni Hard Tissue Homogenizing tubes containing 1.4 mm ceramic beads using an Omni Bead Ruptor 24 containing dry ice in acetone (Omni International, Kennesaw, GA). The mixture was homogenized for 2 x 20 seconds. The aliquots were then placed in 1.7 mL capped

centrifuge tubes and spun at 9,000 g for 20 min. The supernatant (S9 fraction) was removed and stored at -80ºC until further use. Protein content was determined using a Pierce BCA Protein Assay (Thermo Fisher Scientific, Inc., Rockford IL) according to the manufacturer's instructions with albumin as the standard.

Detection of CYP26A1 and CYP26B1 in human fetal livers: To determine if CYP26A1 or CYP26B1 was present in (hFL) S9 fractions, samples from 4 donor fetal livers were blotted and probed using a rabbit polyclonal CYP26A1 antibody (1:2000) raised against a C-terminal peptide of CYP26A1 and a rabbit polyclonal CYP26B1 antibody (1:4000), both purified and validated as described previously (Thatcher et al., 2010; Topletz et al., 2012). Western blots were performed using the same procedure used to validate the antibodies. A calibration curve containing 0.1, 0.2, and 0.4 pmoles of CYP26A1 or CYP26B1 supersomes were included on each gel for reference. Sixty μg of each hFL S9 fraction was loaded per lane on each blot. Alexa Flour 680 rabbit anti-mouse antibody (1:4000, Invitrogen Corporation, Eugene, OR) was used as the secondary antibody.

All-trans-retinoic acid (atRA) metabolism in human fetal livers: The formation of 4-OH-RA and 4-oxo-RA from *at*RA was measured in hFL S9 fractions. As 4-oxo-RA is sequentially formed from 4-OH-RA, the additive formations were used to account for all 4-OH-RA formed. The ratio of 4-oxo-RA to 4-OH-RA formation from *at*RA was calculated to determine any gestational-age dependent changes in 4-oxo-RA formation. The time and protein linearity for 4-OH-RA + 4-oxo-RA formation from *at*RA in S9 fractions was determined and subsequent incubations performed within linear conditions. Incubations were performed as previously described (Thatcher et al., 2010), using 0.1 mg/mL hFL S9 protein and 500 nM *at*RA with a total incubation time of 10 min. Incubations were performed in 100 mM KPi buffer (pH 7.4) in an

oscillating water bath kept at 37ºC. Incubations were initiated with the addition of NADPH (1 mM final concentration) and incubated for 10 min. The reactions were quenched by the addition of 3 mL ethyl acetate. Extractions of a*t*RA, 4-oxo-RA, (4R)-OH-RA, (4S)-OH-RA, or 18-OH-RA were performed in 8 x 13 mm borosilicate glass test tubes as previously described (Thatcher et al., 2010). To extract retinoids, an internal standard (*at*RA-d_5, 50 nM) was added to each aliquot of sample in 100 mM KPi buffer (pH 7.4) containing 3 mL ethyl acetate, the organic layer removed and dried under nitrogen, and the sample residue reconstituted in 100 µL acetonitrile for MS/MS analysis.

Analytes were separated and analyzed using an Agilent Zorbax C18 column (3.5 µm, 2.1 mm x 100 mm) with an AB Sciex API 5500 Q/LIT mass spectrometer equipped with an Agilent 1290 Infinity UHPLC. Analytes were separated using a series of linear gradient changes over an 8.5 min total run time with a mobile phase flow of 0.3 mL/min. Initial conditions were 10:90 acetonitrile: aqueous 0.1% formic acid, percent organic increased to 50:50 over the first 0.5 min, then further increased linearly over 4 min to conditions of 85:15 acetonitrile: aqueous 0.1% formic acid. After 0.1 min, percent organic was increased further to 95:5 acetonitrile: aqueous 0.1% formic acid, held for 2.5 min, then reversed to initial conditions for a re-equilibration period of 1.5 min. Analytes were detected using negative ion electrospray; the parent-fragment MS/MS transitions of *m/z* 299 → 255 Da (*at*RA), *m/z* 315 → 253 Da (4-OH-RA), *m/z* 313 → 269 Da (4-oxo-RA), *m/z* 315 → 241 Da (16-OH-RA) and *m/z* 316 → 272 Da (4-oxo-RA-d_3) were monitored.

Inhibition of CYP3A7 and CYP26-mediated metabolism of atRA by fluconazole and talarazole in supersomes: Fluconazole has been shown to selectively inhibit CYP3A4 but not CYP26A1 or CYP26B1 at concentrations > 10 µM, indicating that fluconazole might be used as

a selective CYP3A7 inhibitor in hFL S9 fractions (Nelson, C., personal communication). Inhibition of CYP3A7-medated metabolism of *at*RA by fluconazole was determined by incubating CYP3A7 supersomes (5 pmoles/mL) and *at*RA (10 µM) with or without fluconazole (300 µM) for 10 minutes. Inhibition of CYP3A7 and CYP26A1-mediated metabolism of *at*RA by talarazole was determined by incubating CYP3A7 (5 pmoles/mL) or CYP26A1 (2 pmoles/mL + P450 reductase, 4 pmoles/mL) supersomes and *at*RA (500 nM) with or without talarazole (200 nM). Samples were incubated for either 2 (CYP26A1) or 10 (CYP3A7) minutes. Incubations and extractions were performed as previously described and reconstituted in 100 µL acetonitrile for HPLC-MS/MS analysis. Percent inhibition of *at*RA metabolism was calculated as the amount of 4-OH-RA formed in the presence of the inhibitor compared to the no-inhibitor controls.

Contribution of CYP3A7 and CYP26 to atRA metabolism in human fetal livers: Fluconazole, (200 µM, CYP3A7 inhibitor), talarozole (200 nM, CYP26 inhibitor), or ketoconazole (10 µM, P450 inhibitor), were co-incubated with *at*RA (500 nM) to determine the contributions of CYP3A7 or CYP26 to 4-OH-RA and 4-OH-RA+4-oxo-RA formation in hFL S9 fractions (n = 4). Incubations and extractions were performed as previously described and reconstituted in 100 µL acetonitrile for HPLC-MS/MS analysis. Percent activity remaining was calculated as compared to a no-inhibitor control.

Testosterone Metabolism in human fetal livers: To determine CYP3A7-mediated metabolism of testosterone (TST) by hFL S9 fractions, TST (100 µM, final concentration) was incubated for 10 min with 0.2 mg/mL hFL S9 protein in 100 mM KPi buffer (pH 7.4). All incubations were performed using 96-well plates with a total volume of 0.1 mL per well. The reaction was initiated by the addition of NAPDH (1 mM final concentration) after a 10 min pre-

incubation period and quenched by adding 80 µL of sample to 80 µL ice-cold acetonitrile in a fresh 96-well plate. Plates were then centrifuged for 20 min at 612g, 4ºC and 0.125 mL supernatant was removed and transferred into a fresh 96-well plate for UFLC-MS/MS (ultra-fast liquid chromatography-tandem mass spectrometry) analysis. All incubations were performed in triplicate. TST metabolism by CYP3A7 was determined by formation of 6βOH-TST; a standard curve for 6βOH-TST was constructed using concentrations from 10 to 500 nM. For incubations with testosterone, 6βOH-TST was separated using a zorbax column (SB-C_{18}; 5µm, 2.1 x 50 mm, Agilent Technologies, Palo Alto, CA) with a Shimadzu UFLC XR DGU-20A5 (Shimadzu Scientific Instruments, Columbia, MD) coupled to an AB Sciex 3200 Mass Spectrometer (AB Sciex, Framingham, MA). The UFLC gradient elution used a mobile phase flow of 0.3 mL/min, initial conditions of 5:95 acetonitrile: aqueous 0.1% formic acid. Initial conditions were held for 2 min then percent organic increased linearly to 100:0 acetonitrile: aqueous 0.1% formic acid over 2 min and held for 1.5 min before returning to initial conditions for a reequilibration period of 3.5 min. 6βOH-TST was detected using positive ion electrospray at 5500 V and 450ºC; *m/z* 305 → 287 Da was monitored.

Contribution of P450 enzymes to 4-oxo-RA formation from 4-OH-RA in human fetal livers: Formation of 4-oxo-RA was used to quantify 4-OH-RA metabolism in hFL S9 fractions (n = 3). To determine if the formation of 4-oxo-RA from 4-OH-RA was enzymatic, NADPH dependent, or P450-mediated, 4-OH-RA (100 nM) was incubated as described above using boiled hFL S9 fractions, +/- NAPDH, and ketoconazole (10 µM), respectively. To prepare boiled hFL S9 fractions, hFL S9 fractions to be used were aliquoted into a 1.7 mL capped centrifuge tube and boiled for 10 min to denature (inactivate) enzymes. Boiled hFL S9 samples were then added to incubations in the same concentration as active hFL S9 fractions (0.1 mg/mL)

before incubating with 4-OH-RA. Samples were incubated and extracted using previously described conditions (thesis chapter 2), then evaporated to dryness and reconstituted in 100 µL acetonitrile for HPLC-MS/MS analysis. Percent decrease of 4-oxo-RA formation using boiled hFL S9 fratctions, -NADPH, or ketoconazole was calculated in comparison to the +NADPH control with no inhibitor and active hFL S9 fractions.

Data and Statistical Analysis: Mass spectrometry data was analyzed using Analyst software. Peak heights were used to determine the ratio of substrate to the internal standard (4-oxo-RA-d_3). *at*RA and testosterone metabolite formation data were fitted using linear regression using Prism v.5 (GraphPad Software, Inc., La Jolla, CA). Regressions with *P* values < 0.05 were considered significant. One-way analyses of variance were performed using Prism v.5 (GraphPad) to determine statistical significance of differences in inhibition of *at*RA and 4-OH-RA metabolism in CYP3A7 supersomes and hFL S9 fractions compared to non-inhibited controls. A *P* value < 0.05 was considered significant. One-way analyses of variance coupled with Bonferroni's Multiple Comparison Test were used to determine significant differences in *at*RA metabolism between gestational weeks 10-12, 12-14, 14-16, and 16-20, gender of the fetus, and race.

The intrinsic clearances (Cl_{int}) of 4-OH-RA + 4-oxo-RA formation from *at*RA in the fetal livers were predicted by using equation 5.1 as described for the adult liver (Thatcher et al., 2010). The liver weight used for each gestational age is described in Table 5-1.

$$Cl_{int,FL} = Cl_{int\ per\ mg\ protein\ FL} \times \frac{mg\ protein_{FL}}{g_{FL}} \times total\ g_{FL} \qquad \text{equation 5.1}$$

The extraction ratio (ER_{FL}) of *at*RA for the fetal liver was then calculated using equation 5.2. Blood flow to fetal liver was calculated as half of the umbilical vein flow ($Q_{umbilical\ vein}$) per gestational age as described in Table 5-1, as half of the umbilical vein flow has been shown to go

to the fetal liver and the other half to the fetal heart (Whitaker, 1997). The unbound fraction of *at*RA in umbilical cord blood was estimated to be 0.01 as previously reported in calculations of hepatic clearance (Thatcher et al., 2010).

$$ER_{FL} = \frac{f_u * Cl_{int,FL}}{0.5 * Q_{umbilical\ vein} + f_u * Cl_{int,FL}}$$ equation 5.2

5.3 Results

5.3.1 Formation of 4-OH-RA and 4-oxo-RA from *at*RA in human fetal livers:

Qualitative analysis of the *at*RA metabolic profile in hFL S9 fractions showed formation of 4-OH-RA and 4-oxo-RA but not 18-OH-RA or 16-OH-RA (Figure 5.1). Formation rate of 4-OH-RA (Figure 5.3A) ranged from 24 ± 11 pmoles/min/mg protein (FL 18, GD 98) to 124 ± 7 pmoles/min/mg protein (FL 27, GD 98). 4-oxo-RA formation from *at*RA (Figure 5.3B) ranged from 1.6 ± 0.1 pmoles/min/mg protein (FL 26, GD 113) to 16 ± 1 pmoles/min/mg protein (FL 15, GD 101), accounting for 10% of all *at*RA metabolism in hFL S9 fractions. The additive formation rates of 4-OH-RA and 4-oxo-RA (Figure 5.3C) ranged from 28 ± 11 pmoles/min/mg protein (FL 18, GD 98) to 134 ± 8 pmoles/min/mg protein (FL 27, GD 98). Formation of 4-OH-RA (r^2 = 0.04, *P* = 0.33), 4-oxo-RA (r^2 = 0.02, *P* = 0.49), or 4-OH-RA+4-oxo-RA (r^2 = 0.04, *P* = 0.33) did not correlate to gestational age (Figure 5.3, Table 5-2). There were no significant differences in 4-OH-RA, 4-oxo-RA, or 4-OH-RA+4-oxo-RA formation between different fetal genders or maternal races (Table 5-2). The ratio of 4-oxo-RA to 4-OH-RA formation after *at*RA metabolism was not significantly different between gestational weeks 10-12, 12-14, 14-16, or 16-20 and differing fetal genders or maternal races (*P* > 0.05, Table 5-2).

5.3.2 Detection of CYP26A1 and CYP26B1 in human fetal livers: Western blots of CYP26A1 and CYP26B1 are shown in Figure 5.2A and B. Neither CYP26A1 nor CYP26B1

protein was detected in any of the four hFL S9 fractions tested, although CYP26A1 and CYP26B1 supersomes were detectable at 0.1 pmol per lane.

5.3.3 Prediction of *at*RA clearances in the fetal liver during the first and second trimesters of human gestation: The intrinsic clearance of 4-OH-RA+4-oxo-RA formation from *at*RA scaled up to the whole fetal liver during the first and second trimesters of human pregnancy are shown in Figure 5.3E. The Cl_{intFL} (Figure 5.3E) increased exponentially with gestational age, although the increase was in agreement with increased fetal liver volume (Table 5-1). The extraction ratios of *at*RA by the fetal livers at gestational ages 72-137 days were very low, ranging from 0.01 to 0.05 (Figure 5.3F).

5.3.4 Identification of P450s responsible for 4-OH-RA and 4-OH-RA+4-oxo-RA formation from *at*RA in human fetal livers: Fluconazole (300 μM) inhibited 70 % of 4-OH-RA formation from *at*RA (10 μM) in CYP3A7 supersomes (Figure 5.4A), suggesting that fluconazole could be used as a selective CYP3A7 inhibitor in incubations with hFL S9 fractions. Talarozole (200 nM) co-incubated with CYP26A1 supersomes inhibited > 70 % of 4-OH-RA formation from *at*RA (500 nM) compared to the no-inhibitor control (Figure 5.4A). Conversely, talarozole (200 nM) co-incubated with CYP3A7 supersomes inhibited less than 30 % of 4-OH-RA formation from *at*RA (500 nM) with CYP3A7 supersomes and was not significantly different from the no-inhibitor control, confirming talarozole (200 nM) to be a selective CYP26 inhibitor (Figure 5.4A). Formation of 4-OH-RA and the additive formation of 4-OH-RA and 4-oxo-RA from *at*RA by hFLs was > 95 % decreased ($P < 0.05$) when co-incubated with ketoconazole, indicating that 4-OH-RA formation from *at*RA was P450-mediated in hFL S9 fractions (Figure 5.4B). Inhibition of CYP3A7-mediated formation of 4-OH-RA and 4-OH-RA+4-oxo-RA by fluconazole ranged from 30-60%, ($P < 0.05$) while talarazole only inhibited

30-40% ($P < 0.05$) of 4-OH-RA and 4-OH-RA+4-oxo-RA formation (Figure 5.4B,C). In contrast, fluconazole (60%) inhibited 4-OH-RA formation from *at*RA thirty percent more than talarozole (30%) in hFL 15 and hFL 30. Ketoconazole inhibition was consistent (>90%) in all hFLs.

5.3.5 Testosterone metabolism and correlation with *at*RA metabolism in human fetal livers: The CYP3A7-mediated formation of 6βOH-TST in hFL S9 fractions was quantified. There was a significant correlation between 4-OH-RA + 4-oxo-RA formation from *at*RA and 6βOH-TST from testosterone (Figure 5.3D, $r^2 = 0.58$, $P < 0.05$). However, only 50 % (13 out of 27) of the data points fell within the 95 % confidence interval (Figure 5.3D)

5.3.6 Formation of 4-oxo-RA from 4-OH-RA in human fetal livers: No 4-oxo-RA was formed from 4-OH-RA by hFL S9 fractions that had been boiled, showing 4-oxo-RA formation to be enzyme-mediated (Figure 5.5, black bars). A small but significant inhibition (14-20 %, $P < 0.05$) of 4-oxo-RA formation was observed when 4-OH-RA was co-incubated with ketoconazole in hFLs (Figure 5.5, striped bars). Interestingly, formation of 4-oxo-RA in incubations without NADPH ranged from 20 to 60 % of the +NADPH controls, indicating that portion of 4-oxo-RA formation is NADPH dependent (Figure 5.5, grey bars).

5.4 Discussion

*at*RA is a key morphogen in mammalian development, and precise concentrations of *at*RA within the fetal target tissues during gestation are crucial for normal cellular differentiation (White and Schilling, 2008). We hypothesized that the fetal liver functions as a secondary barrier to protect the fetus from over-exposure to *at*RA via metabolism by CYP3A7 and CYP26 enzymes. The aim of our studies was to determine the relative importance of CYP26 and

CYP3A7 in *at*RA metabolism in the fetal liver and to predict the quantitative role of the fetal liver as a first pass barrier to fetal exposure to *at*RA.

Taken together all of the presented data support a predominant role of CYP3A7 in *at*RA metabolism in human fetal liver. Firstly, the metabolic profiles of *at*RA when incubated with hFLs were characteristic of the metabolic profile of *at*RA by CYP3A7 not that of CYP26A1 or CYP26B1 (Figure 5.1B, E, F). Both CYP26A1 and CYP26B1 form the 4-OH-RA and 16-OH-RA primary metabolites from *at*RA whereas CYP3A7 only forms 4-OH-RA (Figure 5.1B, C, D). The formation of 4-OH-RA but not that of 16-OH-RA was detected after *at*RA was incubated with hFLs (Figure 5.1E, F). Second, CYP26A1 or CYP26B1 protein was not detected in hFLs (Figure 5.2A,B). This is in contrast to studies which show the presence of CYP26 mRNA in individual human fetal livers (Trofimova-Griffin and Juchau, 1998; Xi and Yang, 2008). Third, CYP3A7-mediated formation of 6βOH-TST from testosterone in hFLs correlated significantly ($r^2 = 0.58$, $P < 0.001$) with 4-OH-RA+4-oxo-RA formation from *at*RA, suggesting that the same enzyme contributes to the two metabolic reactions. Fourth, fluconazole, a selective CYP3A7 inhibitor, inhibited the formation of 4-OH-RA 30-60 % (Figure 5.4). Interestingly, ketoconazole was the most effective inhibitor of 4-OH-RA formation, decreasing 4-OH-RA formation by > 95 % in hFLs. This may be due to the more efficient inhibition of CYP3A7 by ketoconazole or the inhibition of another, unknown P450 by ketoconazole.

The formation clearances of 4-OH-RA, 4-oxo-RA, or 4-OH-RA+4-oxo-RA from *at*RA per miligram of protein in hFLs did not change with gestational age (Figure 5.3E, $P > 0.05$), sex ($P > 0.05$, Table 5-2) or race ($P > 0.05$, Table 5-2). The lack of gestational stage dependency is in agreement with previously reported data showing that CYP3A7 mRNA and activity (testosterone metabolism) during the first and second trimesters are fairly constant (Leeder et al.,

2005) but is in contrast to the data from the smaller study with seven hFLs that showed increase *at*RA hydroxylation with gestational age. Due to the observed variability in 4-OH-RA formation between hFLs the previous gestational stage dependency is likely due to the small samples size of the study.

While the intrinsic clearance of *at*RA was unchanged with increasing gestational age the organ clearance for fetal liver increased with gestational age due to the increase in the liver size. Interestingly, the extraction ratio of *at*RA by the fetal liver was predicted to be very low (0.01-0.05) suggesting that fetal liver does not provide any barrier for fetal exposure to maternally available *at*RA. The low extraction ratio indicates that the total organ clearance is dependent on the unbound intrinsic clearance by the fetal liver ($Cl_{int,FL} \bullet f_u$) and not the umbilical blood flow. The lack of CYP26A1 or CYP26B1 in the fetal liver may account for the low $Cl_{int,FL}$ of *at*RA during the first and second trimesters of human gestation (Figure 5.2).

It is interesting that CYP26A1 is expressed in the adult liver and has been shown to be the main enzyme responsible for the hepatic clearance of *at*RA (Thatcher et al., 2010), yet no expression of CYP26A1 protein in the fetal liver was detected. This suggests that the expression patterns of CYP26 enzymes are different during fetal development and adult life (Thatcher et al., 2010). It is possible that since CYP26A1 expression is regulated by *at*RA exposure (Yamamoto et al., 2000; Tay et al., 2010), the fetal liver *at*RA concentrations are lower than adult liver resulting in undetectable CYP26A1 expression. CYP26A1 mRNA was previously undetected in human fetal liver tissues from gestational ages 57-110 (Trofimova-Griffin et al., 2000). CYP26A1 and CYP26B1 were both also undetected in the fetal mouse liver, suggesting that there is species agreement with regards to CYP26 expression in the fetal liver (Abu-Abed et al., 2002).

The active retinoid 4-oxo-RA was formed from *at*RA by all of the fetal livers tested, but not by recombinant CYP3A7, CYP26A1, or CYP26B1 (Figure 5.1). Thus, we sought to characterize the formation of 4-oxo-RA from *at*RA in fetal livers. Formation of 4-oxo-RA from 4-OH-RA was shown to be enzyme dependent in hFLs, although ketoconazole only minimally inhibited 4-oxo-RA formation from 4-OH-RA, indicating that formation of 4-oxo-RA is predominantly non-P450 mediated in hFLs (Figure 5.5). Interestingly, the reduced 4-oxo-RA formation in the absence of NADPH suggests that the enzyme forming 4-oxo-RA from 4-OH-RA (4-OH-RA oxidase) is partially NADPH-dependent or utilizes $NADP^+$ generated in situ from exogenous NADPH. The formation ratio of 4-oxo-RA to 4-OH-RA after *at*RA metabolism in fetal livers did not change during the first and second trimesters of human pregnancy, which suggests that expression of 4-OH-RA oxidase may not fluctuate in the fetal liver between 10-20 weeks of gestation (Table 5-2).

In conclusion, the fetal liver does not play a major role in *at*RA clearance from the umbilical vein flow and CYP3A7 appears to be the main P450 enzyme responsible for atRA metabolism in the fetal liver. Additionally, the presence of the 4-OH-RA oxidase that forms 4-oxo-RA suggests that 4-oxo-RA formation may be important during fetal development.

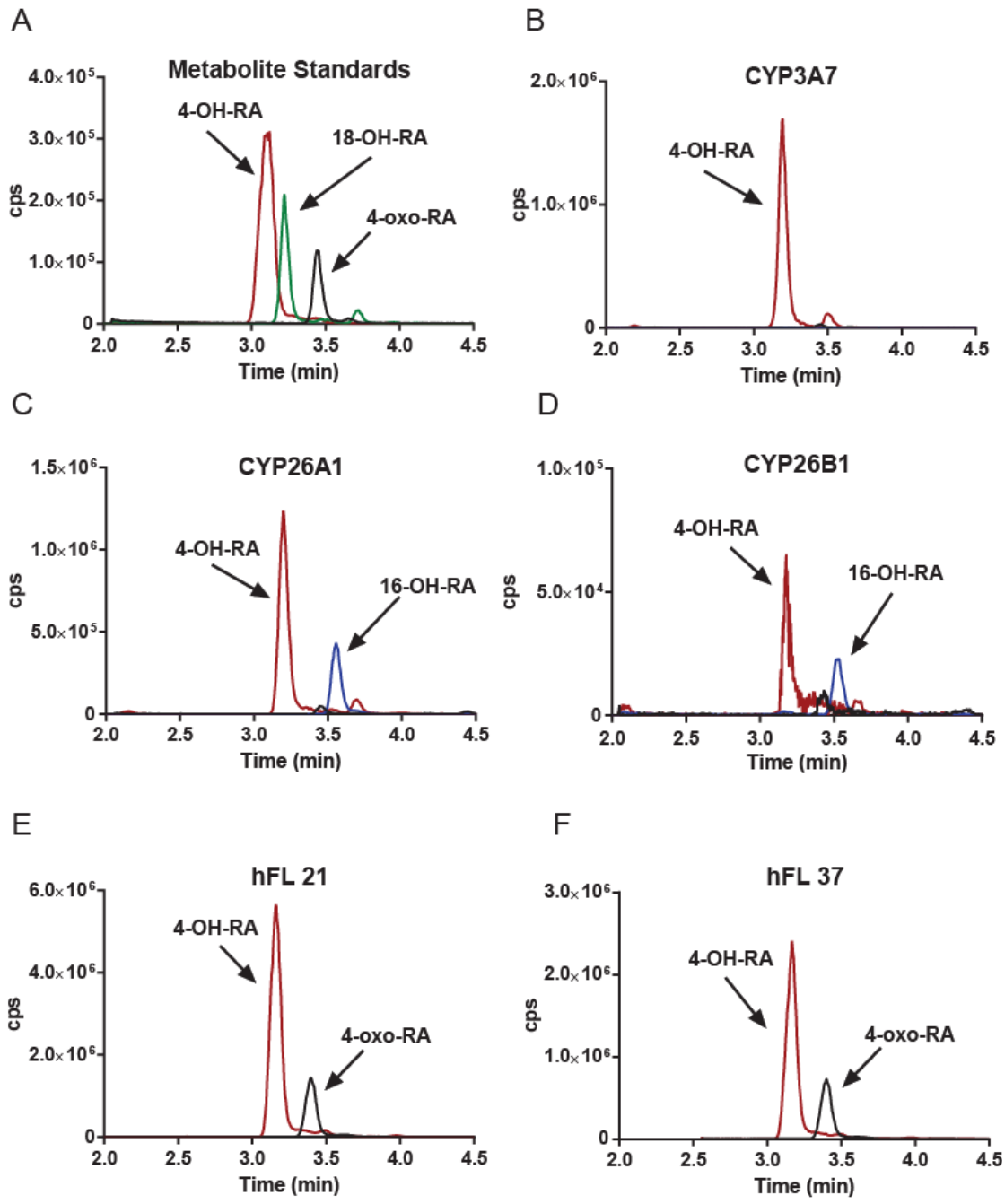

Figure 5.1: Qualitative characterization of *at*RA metabolism by CYP3A7, CYP26A1, CYP26B1 and human fetal livers (hFL 21 and hFL 37) using negative ion electrospray HPLC-MS/MS. *m/z* transitions of 315 > 253 Da (red line, inset), 313 > 269 Da (blue line), and 315 > 241 Da (data not shown) were monitored. Qualitative analysis showed that 4-OH-RA and 4-oxo-RA but not 18-OH-RA or 16-OH-RA was formed by hFL S9 fractions.

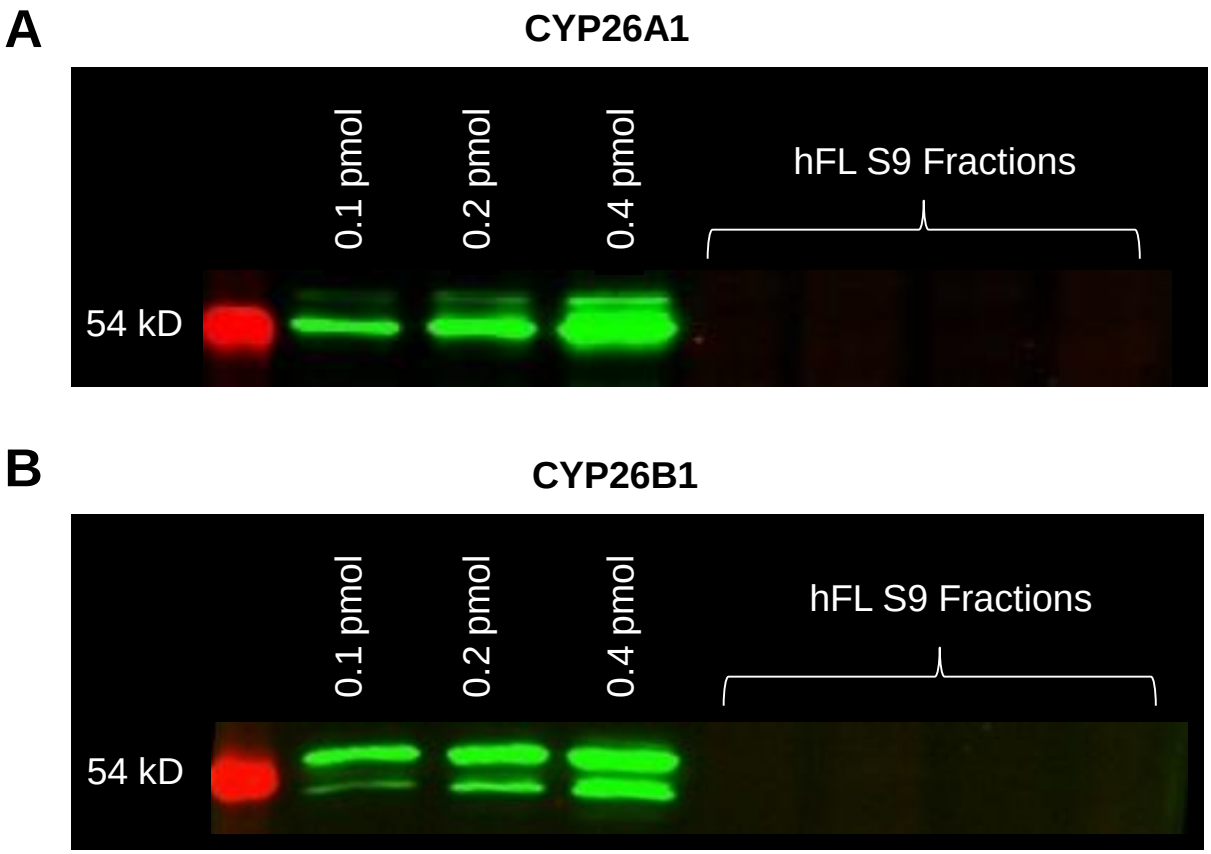

Figure 5.2: Western blots of CYP26A1 (A) and CYP26B1 (B) in human fetal livers. Neither CYP26A1 nor CYP26B1 protein was detected in human fetal liver S9 fractions.

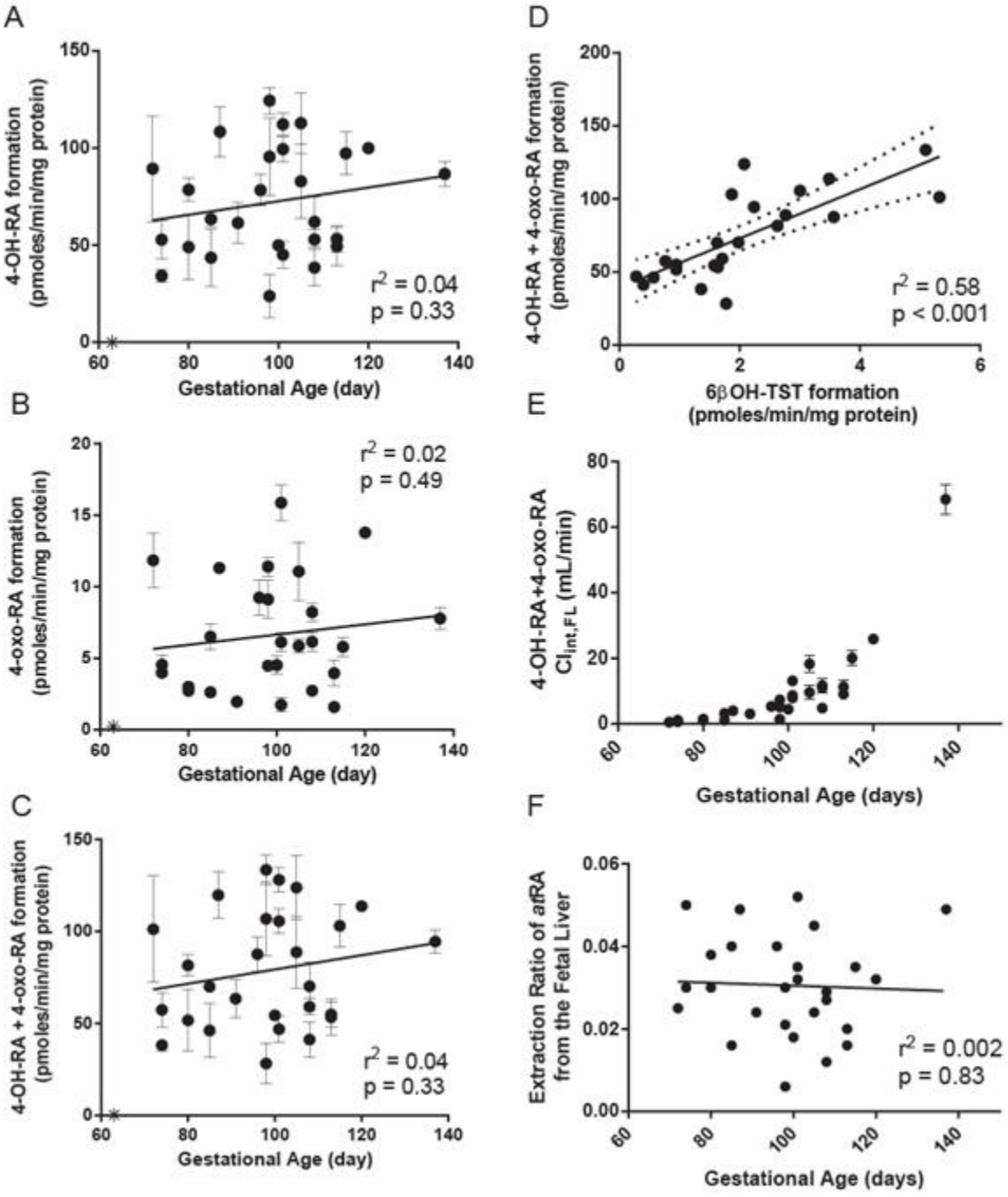

Figure 5.3: Metabolism of *at*RA and TST in hFL S9 Fractions. Formation of 4-OH-RA (A), 4-oxo-RA (B), and combined formation of 4-OH-RA and 4-oxo-RA (C) from *at*RA by hFL S9 fractions during the first and second trimesters of human pregnancy. (D) Correlation between 4-OH-RA+4-oxo-RA from *at*RA and 6βOH-TST from TST by hFL S9 fractions. Unbound $Cl_{int,FL}$ (E) of 4-OH-RA+4-oxo-RA formation from *at*RA scaled up to the total fetal liver volume and extraction ratio (F) of *at*RA by the fetal liver.

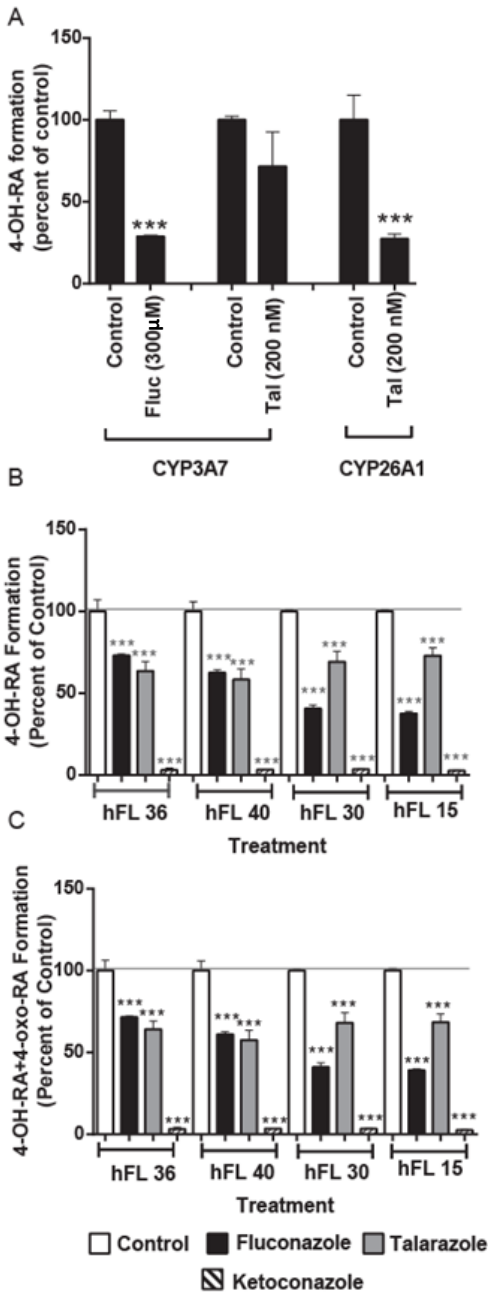

Figure 5.4: Inhibition of *at*RA metabolism in CYP3A7 supersomes, CYP26A1 supersomes, and hFL S9 fractions. (A) Selective inhibition of 4-OH-RA formation from *at*RA (10 μM and 500 nM) in CYP3A7 and CYP26A1 supersomes by fluconazole (300 μM) and talarazole (200 nM). Inhibition of 4-OH-RA (B) and 4-OH-RA+4-oxo-RA (C) formation from *at*RA in hFL S9 fractions by fluconazole (200 μM, CYP3A7, black bars), talarazole (200 nM, CYP26, grey bars), and ketoconazole (10 μM, P450s, striped bars) from no inhibitor controls (white bars).

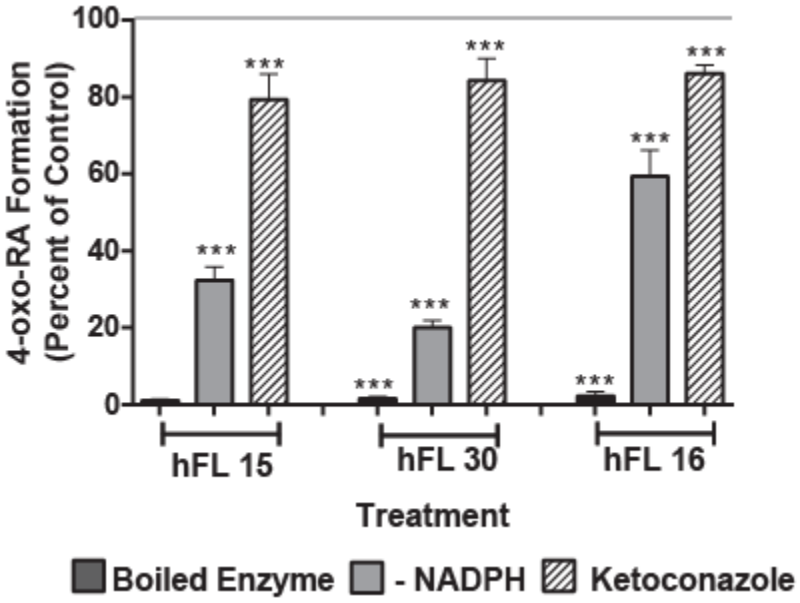

Figure 5.5: Inhibition of 4-oxo-RA formation from 4-OH-RA (100 nM) in hFL S9 fractions using boiled enzyme (black bars), no NADPH (grey bars), or with ketoconazole (striped bars, 10 µM) compared to a +NADPH control.

Table 5-1: Fetal livers (FL) and their corresponding gestational ages and mg protein per gram of fetal liver homogenized. Corresponding [a]fetal liver volumes and [b]umbilical vein blood flows were calculated using previously reported values.

Fetal Liver	Gestational Age (Day)	Sex	Race	mg protein/g fetal liver	Fetal Liver Volume (g)	Umbilical Vein Flow (mL/min)
FL 30	72	M	n/a	27	0.4	0.45
FL 20	74	M	n/a	70	0.5	0.45
FL 21	74	n/a	Asian	79	0.5	0.45
FL 36	80	n/a	Caucasian	43	0.9	0.78
FL 39	80	F	Asian/Hispanic	53	0.9	0.78
FL 24	85	n/a	Asian	75	1.2	1.6
FL 37	85	M	n/a	43	1.2	1.6
FL 14	87	F	n/a	47	1.4	1.6
FL 12	91	F	Asian	52	1.9	2.6
FL 31	96	M	Caucasian	46	2.6	2.6
FL 13	98	M	n/a	32	3.0	4.8
FL 27	98	F	Caucasian	36	3.0	4.8
FL 18	98	n/a	Asian	33	3.0	4.8
FL 34	100	M	n/a	48	3.4	4.8
FL 40	101	M	Caucasian	68	3.7	4.8
FL 33	101	M	n/a	93	3.7	4.8
FL 15	101	n/a	n/a	37	3.7	4.8
FL 23	105	M	Alaskan	46	4.7	7.8
FL 38	105	F	Caucasian	63	4.7	7.8
FL 19	108	F	Hispanic	60	5.6	7.8
FL 28	108	F	Asian	67	5.6	7.8
FL 29	108	F	n/a	42	5.6	7.8
FL 26	113	n/a	n/a	44	7.4	11.1
FL 25	113	M	n/a	57	7.4	11.1
FL 17	115	n/a	n/a	47	8.3	11.1
FL 16	120	M	Caucasian	42	10.7	15.6
FL 22	137	M	Alaskan	62	23.2	26.8

[a]Fetal liver volumes from gestational days 72-137 were calculated from previously reported values (Gielchinsky et al., 2011; Schiessl et al., 2011).
[b]Umbilical blood flow (mL/min) calculated using average value of 111.7 mL/min/(kg fetal weight) as described in (Sutton et al., 1990)

Table 5-2: Differences in *at*RA metabolite formation rates between weeks 10-20 during human gestation, and with respect to gender and race. There were no significant differences between gestational week, sex, or race in the formation of 4-OH-RA, 4-oxo-RA, their additive formations, or the ratio of 4-oxo-RA to 4-OH-RA formation.

	4-OH-RA formation (pmoles/min/mg protein)	**4-oxo-RA formation (pmoles/min/mg protein)**	**4-OH-RA + 4-oxo-RA formation (pmoles/min/mg protein)**	**4-oxo-RA/ 4-OH-RA (ratio)**
gestational week 10-12 (n =5)	61 ± 23	5.2 ± 3.8	66 ± 25	0.09 ± 0.04
gestational week 12-14 (n = 8)	75 ± 34	7.1 ± 3.7	82 ± 37	0.10 ± 0.05
gestational week 14-16 (n = 9)	73 ± 30	6.9 ± 4.3	80 ± 33	0.09 ± 0.03
gestational week 16-20 (n= 5)	77 ± 24	6.6 ± 4.6	84 ± 28	0.08 ± 0.04
Female Fetus (n = 8)	80 ± 25	7.5 ± 3.6	87 ± 28	0.09 ± 0.03
Male Fetus (n = 11)	75 ± 27	7.4 ± 4.7	83 ± 31	0.10 ± 0.05
Alaskan (n = 2)	106 ± 9	14.8 ± 1.5	121 ± 10	0.14 ± 0.00
Asian (n = 6)	76 ± 35	6.4 ± 3.6	82 ± 38	0.09 ± 0.04
Caucasian (n = 6)	73 ± 21	5.7 ± 3.1	79 ± 24	0.08 ± 0.03

Chapter 6 Conclusions

Relative differences in the catalytic efficiency and metabolite profiles of *at*RA and its metabolites by CYP26A1 and CYP26B1, the biological activity of *at*RA metabolites, and the regulation of *at*RA metabolism during pregnancy, both in the maternal mouse liver and in the human fetal liver were explored in this thesis.

Clear differences were observed in the metabolic profiles and catalytic efficiencies of *at*RA and its metabolites between CYP26A1 and CYP26B1. The *at*RA metabolites, (4S)-OH-RA, (4R)-OH-RA, 4-oxo-RA and 18-OH-RA were found to be substrates of both CYP26A1 and CYP26B1 and CYP26 enzymes mostly formed dihydroxylated products except from (4R)-OH-RA, from which 4-oxo-RA was formed by CYP26A1. CYP26A1 metabolized all substrates tested faster than CYP26B1, although CYP26B1 preferred (4R)-OH-RA over (4S)-OH-RA as a substrate, conversely to CYP26A1. CYP26B1 appeared to be less stereospecific than CYP26A1 though it preferentially oxidized *at*RA at the C-4 position whereas CYP26A1 oxidized *at*RA at the C-4, C-16, and C-18 positions.

CYP26A1 was induced in HepG2 cells by *at*RA, 4-oxo-RA, (4R)-OH-RA, (4S)-OH-RA and 18-OH-RA. Together, the relative CYP26A1 induction and the inducer exposures within the cells showed that 4-oxo-RA was the most potent retinoid tested. (4S)-OH-RA and (4R)-OH-RA were rapidly depleted to form 4-oxo-RA within the first twelve hours after treatment (before CYP26A1 activity was shown to increase), suggesting that 4-oxo-RA formation was due to an enzyme other than CYP26A1. The formation of 4-oxo-RA was shown to be non-P450 mediated in both HepG2 cells and fetal livers. Co-treatment of 4-OH-RA with alcohol dehydrogenase (4-methylpyrrazole, cimetidine), aldo-ketoreductase (testosterone), and retinol dehydrogenase (carbenoxolone) inhibitors in HepG2 cells showed no inhibitory effect on the formation of 4-oxo-RA. Based on this data, the enzyme responsible for 4-oxo-RA formation in vivo remains to

be identified. As 4-oxo-RA was shown to be an active retinoid that was formed both in HepG2 cells and in fetal livers, the enzyme that forms 4-oxo-RA from 4-OH-RA may play a major biological role both during development and in adult life.

In the mouse liver, Cyp26a1 mRNA increased during pregnancy as well as the formation of 16-OH-RA from *at*RA, a metabolite specifically formed by CYP26A1. Interestingly, increased mRNA of Cyp2d enzymes correlated to increased Cyp26a1 mRNA during murine gestation, and an RARE-2D promoter was found on Cyp2d40, suggesting that *at*RA signaling may play a role in Cyp2d and CYP2D6 regulation during pregnancy.

We hypothesize that fetal exposure to *at*RA is via synthesis of *at*RA from retinol in the fetal tissues, not *at*RA distributed from the maternal plasma into the fetal compartment. The placenta and fetal liver have been shown to express enzymes that metabolize *at*RA. We detected CYP3A7 but not CYP26A1 or CYP26B1 in the fetal livers during the first and second trimestsers of human gestation, although an unknown P450 enzyme as well as CYP3A7 likely is involved in *at*RA metabolism in the fetal liver. However, we determined the fetal liver to have a low extraction ratio of *at*RA (0.01-0.05) suggesting that the human fetal liver plays a minimal role in regulating fetal exposure to *at*RA. Further studies in the placenta may be useful in determining the role of the placenta as the primary barrier for regulating fetal exposure to *at*RA in the maternal plasma.

In conclusion, the results of this thesis show that CYP26A1 and CYP26B1 are important enzymes regulating *at*RA clearance during pregnancy and adult life, CYP26A1 and CYP26B1 have specific kinetic characteristics that likely explain their different roles in *at*RA clearance, and that *at*RA as well as its metabolites are active inducers of CYP26A1. We also conclude that the enzyme that forms 4-oxo-RA may be biologically important and warrants further study.

BIBLIOGRAPHY

Abu-Abed S, MacLean G, Fraulob V, Chambon P, Petkovich M, and Dolle P (2002) Differential expression of the retinoic acid-metabolizing enzymes CYP26A1 and CYP26B1 during murine organogenesis. *Mech Dev* **110:**173-177.

Abu-Abed SS, Beckett BR, Chiba H, Chithalen JV, Jones G, Metzger D, Chambon P, and Petkovich M (1998) Mouse P450RAI (CYP26) expression and retinoic acid-inducible retinoic acid metabolism in F9 cells are regulated by retinoic acid receptor gamma and retinoid X receptor alpha. *J Biol Chem* **273:**2409-2415.

Alder A, Bigler P, Werck-Reichhart D, and Al-Babili S (2009) In vitro characterization of Synechocystis CYP120A1 revealed the first nonanimal retinoic acid hydroxylase. *FEBS J* **276:**5416-5431.

Anderson GD (2005) Pregnancy-induced changes in pharmacokinetics: a mechanistic-based approach. *Clin Pharmacokinet* **44:**989-1008.

Andrade SE, Gurwitz JH, Davis RL, Chan KA, Finkelstein JA, Fortman K, McPhillips H, Raebel MA, Roblin D, Smith DH, Yood MU, Morse AN, and Platt R (2004) Prescription drug use in pregnancy. *Am J Obstet Gynecol* **191:**398-407.

Arens JF and Van Dorp DA (1946) Activity of vitamin A-acid in the rat. *Nature* **158:**622.

Arnold SL, Amory JK, Walsh TJ, and Isoherranen N (2012) A sensitive and specific method for measurement of multiple retinoids in human serum with UHPLC-MS/MS. *J Lipid Res* **53:**587-598.

Bollag W (1972) Prophylaxis of chemically induced papillomas and carcinomas of mouse skin by vitamin A-acid. *Experientia* **28:**1219-1220.

Cairns W, Smith CA, McLaren AW, and Wolf CR (1996) Characterization of the human cytochrome P4502D6 promoter. A potential role for antagonistic interactions between members of the nuclear receptor family. *J Biol Chem* **271:**25269-25276.

Carcillo JA, Adedoyin A, Burckart GJ, Frye RF, Venkataramanan R, Knoll C, Thummel K, Roskos L, Wilson JW, Sereika S, Romkes M, Bebia Z, and Branch RA (2003) Coordinated intrahepatic and extrahepatic regulation of cytochrome p4502D6 in healthy subjects and in patients after liver transplantation. *Clin Pharmacol Ther* **73:**456-467.

Chambon P (1996) A decade of molecular biology of retinoic acid receptors. *FASEB J* **10:**940-954.

Chang KS, Trujillo JM, Ogura T, Castiglione CM, Kidd KK, Zhao SR, Freireich EJ, and Stass SA (1991) Rearrangement of the retinoic acid receptor gene in acute promyelocytic leukemia. *Leukemia* **5:**200-204.

Chen H, Fantel AG, and Juchau MR (2000) Catalysis of the 4-hydroxylation of retinoic acids by cyp3a7 in human fetal hepatic tissues. *Drug Metab Dispos* **28:**1051-1057.

Chithalen JV, Luu L, Petkovich M, and Jones G (2002) HPLC-MS/MS analysis of the products generated from all-trans-retinoic acid using recombinant human CYP26A. *J Lipid Res* **43:**1133-1142.

Clagett-Dame M and DeLuca HF (2002) The role of vitamin A in mammalian reproduction and embryonic development. *Annu Rev Nutr* **22:**347-381.

Corchero J, Granvil CP, Akiyama TE, Hayhurst GP, Pimprale S, Feigenbaum L, Idle JR, and Gonzalez FJ (2001) The CYP2D6 humanized mouse: effect of the human CYP2D6 transgene and HNF4alpha on the disposition of debrisoquine in the mouse. *Mol Pharmacol* **60:**1260-1267.

Creech Kraft J, Lofberg B, Chahoud I, Bochert G, and Nau H (1989) Teratogenicity and placental transfer of all-trans-, 13-cis-, 4-oxo-all-trans-, and 4-oxo-13-cis-retinoic acid after administration of a low oral dose during organogenesis in mice. *Toxicol Appl Pharmacol* **100:**162-176.

Dai G, Bustamante JJ, Zou Y, Myronovych A, Bao Q, Kumar S, and Soares MJ (2011) Maternal hepatic growth response to pregnancy in the mouse. *Exp Biol Med (Maywood)* **236:**1322-1332.

Davis Ma (1913) The Necessity of Certain Lipins in the Diet During Growth. *J Biol Chem* **15:**167-175.

Dickmann LJ, Tay S, Senn TD, Zhang H, Visone A, Unadkat JD, Hebert MF, and Isoherranen N (2008) Changes in maternal liver Cyp2c and Cyp2d expression and activity during rat pregnancy. *Biochem Pharmacol* **75:**1677-1687.

Dixit V, Hariparsad N, Li F, Desai P, Thummel KE, and Unadkat JD (2007) Cytochrome P450 enzymes and transporters induced by anti-human immunodeficiency virus protease inhibitors in human hepatocytes: implications for predicting clinical drug interactions. *Drug Metab Dispos* **35:**1853-1859.

Duester G (2008) Retinoic acid synthesis and signaling during early organogenesis. *Cell* **134:**921-931.

Emerick RJ, Zile M, and DeLuca HF (1967) Formation of retinoic acid from retinol in the rat. *Biochem J* **102:**606-611.

Fiorella PD, Giguere V, and Napoli JL (1993) Expression of cellular retinoic acid-binding protein (type II) in Escherichia coli. Characterization and comparison to cellular retinoic acid-binding protein (type I). *J Biol Chem* **268:**21545-21552.

Frolik CA, Roberts AB, Tavela TE, Roller PP, Newton DL, and Sporn MB (1979) Isolation and identification of 4-hydroxy- and 4-oxoretinoic acid. In vitro metabolites of all-trans-retinoic acid in hamster trachea and liver. *Biochemistry* **18:**2092-2097.

Frolik CA, Tavela TE, Newton DL, and Sporn MB (1978) In vitro metabolism and biological activity of all-trans-retinoic acid and its metabolites in hamster trachea. *J Biol Chem* **253:**7319-7324.

Ghyselinck NB, Dupe V, Dierich A, Messaddeq N, Garnier JM, Rochette-Egly C, Chambon P, and Mark M (1997) Role of the retinoic acid receptor beta (RARbeta) during mouse development. *Int J Dev Biol* **41:**425-447.

Gielchinsky Y, Zvanca M, Minekawa R, Persico N, and Nicolaides KH (2011) Liver volume in trisomy 21 and euploid fetuses at 11 to 13 weeks. *Prenat Diagn* **31:**28-32.

Glover DD, Amonkar M, Rybeck BF, and Tracy TS (2003) Prescription, over-the-counter, and herbal medicine use in a rural, obstetric population. *Am J Obstet Gynecol* **188:**1039-1045.

Hanni R and Bigler F (1977) Isolation and identification of three major metabolites of retinoic acid from rat feces. *Helv Chim Acta* **60:**881-887.

Hanni R, Bigler F, Meister W, and Englert G (1976) Isolation and identification of three urinary metabolites of retinoic acid in the rat. *Helv Chim Acta* **59:**2221-2227.

Hebert MF, Easterling TR, Kirby B, Carr DB, Buchanan ML, Rutherford T, Thummel KE, Fishbein DP, and Unadkat JD (2008) Effects of pregnancy on CYP3A and P-glycoprotein activities as measured by disposition of midazolam and digoxin: a University of Washington specialized center of research study. *Clin Pharmacol Ther* **84:**248-253.

Hewitt NJ, Lecluyse EL, and Ferguson SS (2007) Induction of hepatic cytochrome P450 enzymes: methods, mechanisms, recommendations, and in vitro-in vivo correlations. *Xenobiotica* **37:**1196-1224.

Hogarth CA, Amory JK, and Griswold MD (2011) Inhibiting vitamin A metabolism as an approach to male contraception. *Trends Endocrinol Metab* **22:**136-144.

Hogstedt S, Lindberg B, Peng DR, Regardh CG, and Rane A (1985) Pregnancy-induced increase in metoprolol metabolism. *Clin Pharmacol Ther* **37:**688-692.

Hogstedt S, Lindberg B, and Rane A (1983) Increased oral clearance of metoprolol in pregnancy. *Eur J Clin Pharmacol* **24:**217-220.

Idres N, Benoit G, Flexor MA, Lanotte M, and Chabot GG (2001) Granulocytic differentiation of human NB4 promyelocytic leukemia cells induced by all-trans retinoic acid metabolites. *Cancer Res* **61:**700-705.

Idres N, Marill J, Flexor MA, and Chabot GG (2002) Activation of retinoic acid receptor-dependent transcription by all-trans-retinoic acid metabolites and isomers. *J Biol Chem* **277:**31491-31498.

IOM IoM (2001) Dietary Reference Intakes: Vitamins.

Jover R, Bort R, Gomez-Lechon MJ, and Castell JV (2001) Cytochrome P450 regulation by hepatocyte nuclear factor 4 in human hepatocytes: a study using adenovirus-mediated antisense targeting. *Hepatology* **33:**668-675.

Kane MA, Folias AE, Wang C, and Napoli JL (2008) Quantitative profiling of endogenous retinoic acid in vivo and in vitro by tandem mass spectrometry. *Anal Chem* **80:**1702-1708.

Kawaguchi R, Yu J, Honda J, Hu J, Whitelegge J, Ping P, Wiita P, Bok D, and Sun H (2007) A membrane receptor for retinol binding protein mediates cellular uptake of vitamin A. *Science* **315:**820-825.

Kawanobe T (1984) New Synthesis of g-Homocyclogeranial, g-Dihydroionone and their derivatives. *Agric Biol Chem* **48:**461-464.

Kewn S, Hoggard PG, Sales SD, Johnson MA, and Back DJ (2000) The intracellular activation of lamivudine (3TC) and determination of 2'-deoxycytidine-5'-triphosphate (dCTP) pools in the presence and absence of various drugs in HepG2 cells. *Br J Clin Pharmacol* **50:**597-604.

Krust A, Kastner P, Petkovich M, Zelent A, and Chambon P (1989) A third human retinoic acid receptor, hRAR-gamma. *Proc Natl Acad Sci U S A* **86:**5310-5314.

Kuhnel K, Ke N, Cryle MJ, Sligar SG, Schuler MA, and Schlichting I (2008) Crystal structures of substrate-free and retinoic acid-bound cyanobacterial cytochrome P450 CYP120A1. *Biochemistry* **47:**6552-6559.

Langton S and Gudas LJ (2008) CYP26A1 knockout embryonic stem cells exhibit reduced differentiation and growth arrest in response to retinoic acid. *Dev Biol* **315:**331-354.

Lee HP, Casadesus G, Zhu X, Lee HG, Perry G, Smith MA, Gustaw-Rothenberg K, and Lerner A (2009) All-trans retinoic acid as a novel therapeutic strategy for Alzheimer's disease. *Expert Rev Neurother* **9:**1615-1621.

Leeder JS, Gaedigk R, Marcucci KA, Gaedigk A, Vyhlidal CA, Schindel BP, and Pearce RE (2005) Variability of CYP3A7 expression in human fetal liver. *J Pharmacol Exp Ther* **314:**626-635.

Lefebvre P, Gaub MP, Tahayato A, Rochette-Egly C, and Formstecher P (1995) Protein phosphatases 1 and 2A regulate the transcriptional and DNA binding activities of retinoic acid receptors. *J Biol Chem* **270:**10806-10816.

Logan WS (1972) Vitamin A and keratinization. *Arch Dermatol* **105:**748-753.

Lohnes D, Kastner P, Dierich A, Mark M, LeMeur M, and Chambon P (1993) Function of retinoic acid receptor gamma in the mouse. *Cell* **73:**643-658.

Loudig O, Babichuk C, White J, Abu-Abed S, Mueller C, and Petkovich M (2000) Cytochrome P450RAI(CYP26) promoter: a distinct composite retinoic acid response element underlies the complex regulation of retinoic acid metabolism. *Mol Endocrinol* **14:**1483-1497.

Loudig O, Maclean GA, Dore NL, Luu L, and Petkovich M (2005) Transcriptional co-operativity between distant retinoic acid response elements in regulation of Cyp26A1 inducibility. *Biochem J* **392:**241-248.

Lufkin T, Lohnes D, Mark M, Dierich A, Gorry P, Gaub MP, LeMeur M, and Chambon P (1993) High postnatal lethality and testis degeneration in retinoic acid receptor alpha mutant mice. *Proc Natl Acad Sci U S A* **90:**7225-7229.

Lutz JD, Dixit V, Yeung CK, Dickmann LJ, Zelter A, Thatcher JE, Nelson WL, and Isoherranen N (2009) Expression and functional characterization of cytochrome P450 26A1, a retinoic acid hydroxylase. *Biochem Pharmacol* **77:**258-268.

Lutz JD and Isoherranen N (2012) Prediction of relative in vivo metabolite exposure from in vitro data using two model drugs: dextromethorphan and omeprazole. *Drug Metab Dispos* **40:**159-168.

Maden M (1982) Vitamin A and pattern formation in the regenerating limb. *Nature* **295:**672-675.

Maden M (2007) Retinoic acid in the development, regeneration and maintenance of the nervous system. *Nat Rev Neurosci* **8:**755-765.

Marletaz F, Holland LZ, Laudet V, and Schubert M (2006) Retinoic acid signaling and the evolution of chordates. *Int J Biol Sci* **2:**38-47.

Mathias AA, Maggio-Price L, Lai Y, Gupta A, and Unadkat JD (2006) Changes in pharmacokinetics of anti-HIV protease inhibitors during pregnancy: the role of CYP3A and P-glycoprotein. *J Pharmacol Exp Ther* **316:**1202-1209.

McBurney MW (1993) P19 embryonal carcinoma cells. *Int J Dev Biol* **37:**135-140.

McCormick AM, Napoli JL, Schnoes HK, and DeLuca HF (1978) Isolation and identification of 5, 6-epoxyretinoic acid: a biologically active metabolite of retinoic acid. *Biochemistry* **17:**4085-4090.

Muindi J, Frankel SR, Miller WH, Jr., Jakubowski A, Scheinberg DA, Young CW, Dmitrovsky E, and Warrell RP, Jr. (1992a) Continuous treatment with all-trans retinoic acid causes a progressive reduction in plasma drug concentrations: implications for relapse and retinoid "resistance" in patients with acute promyelocytic leukemia. *Blood* **79:**299-303.

Muindi JR, Frankel SR, Huselton C, DeGrazia F, Garland WA, Young CW, and Warrell RP, Jr. (1992b) Clinical pharmacology of oral all-trans retinoic acid in patients with acute promyelocytic leukemia. *Cancer Res* **52:**2138-2142.

Muindi JR, Roth MD, Wise RA, Connett JE, O'Connor GT, Ramsdell JW, Schluger NW, Romkes M, Branch RA, and Sciurba FC (2008) Pharmacokinetics and metabolism of all-

trans- and 13-cis-retinoic acid in pulmonary emphysema patients. *J Clin Pharmacol* **48:**96-107.

Napoli JL (2012) Physiological insights into all-trans-retinoic acid biosynthesis. *Biochim Biophys Acta* **1821:**152-167.

Narimatsu S, Kazamori D, Masuda K, Katsu T, Funae Y, Naito S, Nakura H, Yamano S, and Hanioka N (2009) The mechanism causing the difference in kinetic properties between rat CYP2D4 and human CYP2D6 in the oxidation of dextromethorphan and bufuralol. *Biochem Pharmacol* **77:**920-931.

Nau H (1995) Chemical structure--teratogenicity relationships, toxicokinetics and metabolism in risk assessment of retinoids. *Toxicol Lett* **82-83:**975-979.

Nau H (2001) Teratogenicity of isotretinoin revisited: species variation and the role of all-trans-retinoic acid. *J Am Acad Dermatol* **45:**S183-187.

Niederreither K, Abu-Abed S, Schuhbaur B, Petkovich M, Chambon P, and Dolle P (2002) Genetic evidence that oxidative derivatives of retinoic acid are not involved in retinoid signaling during mouse development. *Nat Genet* **31:**84-88.

Niemi M, Backman JT, Fromm MF, Neuvonen PJ, and Kivisto KT (2003) Pharmacokinetic interactions with rifampicin : clinical relevance. *Clin Pharmacokinet* **42:**819-850.

Ozpolat B, Lopez-Berestein G, and Mehta K (2001) ATRA(ouble) in the treatment of acute promyelocytic leukemia. *J Biol Regul Homeost Agents* **15:**107-122.

Ozpolat B, Mehta K, Tari AM, and Lopez-Berestein G (2002) all-trans-Retinoic acid-induced expression and regulation of retinoic acid 4-hydroxylase (CYP26) in human promyelocytic leukemia. *Am J Hematol* **70:**39-47.

Pijnappel WW, Hendriks HF, Folkers GE, van den Brink CE, Dekker EJ, Edelenbosch C, van der Saag PT, and Durston AJ (1993) The retinoid ligand 4-oxo-retinoic acid is a highly active modulator of positional specification. *Nature* **366:**340-344.

Ray WJ, Bain G, Yao M, and Gottlieb DI (1997) CYP26, a novel mammalian cytochrome P450, is induced by retinoic acid and defines a new family. *J Biol Chem* **272:**18702-18708.

Renaud HJ, Cui JY, Khan M, and Klaassen CD (2011) Tissue distribution and gender-divergent expression of 78 cytochrome P450 mRNAs in mice. *Toxicol Sci* **124:**261-277.

Rhinn M and Dolle P (2012) Retinoic acid signalling during development. *Development* **139:**843-858.

Roberts AB, Lamb LC, and Sporn MB (1980) Metabolism of all-trans-retinoic acid in hamster liver microsomes: oxidation of 4-hydroxy- to 4-keto-retinoic acid. *Arch Biochem Biophys* **199:**374-383.

Rosenberger M (1982) Retinoic Acid Metabolites.3.Total Synthesis of (2E, 4E, 6E, 8E)-3,7-Dimethyl-9-[6,6-dimethyl-2-(hydroxymethyl)-1-cyclohexen-1-yl]-2,4,6,8-nonatetraenoic Acid. *J Org Chem* **47:**1782-1785.

Ross AC and Zolfaghari R (2011) Cytochrome P450s in the regulation of cellular retinoic acid metabolism. *Annu Rev Nutr* **31:**65-87.

Rothman KJ, Moore LL, Singer MR, Nguyen US, Mannino S, and Milunsky A (1995) Teratogenicity of high vitamin A intake. *N Engl J Med* **333:**1369-1373.

Samokyszyn VM, Gall WE, Zawada G, Freyaldenhoven MA, Chen G, Mackenzie PI, Tephly TR, and Radominska-Pandya A (2000) 4-hydroxyretinoic acid, a novel substrate for human liver microsomal UDP-glucuronosyltransferase(s) and recombinant UGT2B7. *J Biol Chem* **275:**6908-6914.

Scheer N, Kapelyukh Y, McEwan J, Beuger V, Stanley LA, Rode A, and Wolf CR (2012) Modeling human cytochrome P450 2D6 metabolism and drug-drug interaction by a novel panel of knockout and humanized mouse lines. *Mol Pharmacol* **81:**63-72.

Schiessl B, Fakler U, Vogt M, Friese K, Hess J, and Oberhoffer R (2011) 3-Dimensional sonographic volumetry of fetal brain, liver and myocardial mass--interdisciplinary clinical validation of the method and application in fetuses with and without structural heart disease. *Z Geburtshilfe Neonatol* **215:**60-68.

Schmidt CK, Volland J, Hamscher G, and Nau H (2002) Characterization of a new endogenous vitamin A metabolite. *Biochim Biophys Acta* **1583:**237-251.

Schuetz JD, Kauma S, and Guzelian PS (1993) Identification of the fetal liver cytochrome CYP3A7 in human endometrium and placenta. *J Clin Invest* **92:**1018-1024.

Scott O and Goez HR (2011) Three cases of cerebellar hypoplasia and vitamin a deficiency: a case report and a possible pathophysiology. *J Child Neurol* **26:**1311-1315.

Shimada T, Yamazaki H, Mimura M, Inui Y, and Guengerich FP (1994) Interindividual variations in human liver cytochrome P-450 enzymes involved in the oxidation of drugs, carcinogens and toxic chemicals: studies with liver microsomes of 30 Japanese and 30 Caucasians. *J Pharmacol Exp Ther* **270:**414-423.

Shimshoni JA, Roberts AG, Scian M, Topletz AR, Blankert SA, Halpert JR, Nelson WL, and Isoherranen N (2012) Stereoselective Formation and Metabolism of 4-hydroxy-Retinoic Acid Enantiomers by Cytochrome P450 Enzymes. *J Biol Chem*.

Sonneveld E, van den Brink CE, Tertoolen LG, van der Burg B, and van der Saag PT (1999) Retinoic acid hydroxylase (CYP26) is a key enzyme in neuronal differentiation of embryonal carcinoma cells. *Dev Biol* **213:**390-404.

Sutton MS, Theard MA, Bhatia SJ, Plappert T, Saltzman DH, and Doubilet P (1990) Changes in placental blood flow in the normal human fetus with gestational age. *Pediatr Res* **28:**383-387.

Swindell EC, Thaller C, Sockanathan S, Petkovich M, Jessell TM, and Eichele G (1999) Complementary domains of retinoic acid production and degradation in the early chick embryo. *Dev Biol* **216:**282-296.

Taimi M, Helvig C, Wisniewski J, Ramshaw H, White J, Amad M, Korczak B, and Petkovich M (2004) A novel human cytochrome P450, CYP26C1, involved in metabolism of 9-cis and all-trans isomers of retinoic acid. *J Biol Chem* **279:**77-85.

Takeuchi H, Yokota A, Ohoka Y, and Iwata M (2011) Cyp26b1 regulates retinoic acid-dependent signals in T cells and its expression is inhibited by transforming growth factor-beta. *PLoS One* **6:**e16089.

Tay S, Dickmann L, Dixit V, and Isoherranen N (2010) A comparison of the roles of peroxisome proliferator-activated receptor and retinoic acid receptor on CYP26 regulation. *Mol Pharmacol* **77:**218-227.

Thatcher JE, Buttrick B, Shaffer SA, Shimshoni JA, Goodlett DR, Nelson WL, and Isoherranen N (2011) Substrate Specificity and Ligand Interactions of CYP26A1, the Human Liver Retinoic Acid Hydroxylase. *Mol Pharmacol* **80:**228-239.

Thatcher JE and Isoherranen N (2009) The role of CYP26 enzymes in retinoic acid clearance. *Expert Opin Drug Metab Toxicol* **5:**875-886.

Thatcher JE, Zelter A, and Isoherranen N (2010) The relative importance of CYP26A1 in hepatic clearance of all-trans retinoic acid. *Biochem Pharmacol* **80:**903-912.

Topletz AR, Thatcher JE, Zelter A, Lutz JD, Tay S, Nelson WL, and Isoherranen N (2012) Comparison of the function and expression of CYP26A1 and CYP26B1, the two retinoic acid hydroxylases. *Biochem Pharmacol* **83:**149-163.

Tracy TS, Venkataramanan R, Glover DD, and Caritis SN (2005) Temporal changes in drug metabolism (CYP1A2, CYP2D6 and CYP3A Activity) during pregnancy. *Am J Obstet Gynecol* **192:**633-639.

Trofimova-Griffin ME, Brzezinski MR, and Juchau MR (2000) Patterns of CYP26 expression in human prenatal cephalic and hepatic tissues indicate an important role during early brain development. *Brain Res Dev Brain Res* **120:**7-16.

Trofimova-Griffin ME and Juchau MR (1998) Expression of cytochrome P450RAI (CYP26) in human fetal hepatic and cephalic tissues. *Biochem Biophys Res Commun* **252:**487-491.

Wadelius M, Darj E, Frenne G, and Rane A (1997) Induction of CYP2D6 in pregnancy. *Clin Pharmacol Ther* **62:**400-407.

Walker AA, Dickmann L, and Isoherranen N (2011) Pregnancy decreases rat CYP1A2 activity and expression. *Drug Metab Dispos* **39:**4-7.

Westerink WM and Schoonen WG (2007) Cytochrome P450 enzyme levels in HepG2 cells and cryopreserved primary human hepatocytes and their induction in HepG2 cells. *Toxicol In Vitro* **21:**1581-1591.

Whitaker KB (1997) *Comprehensive perinatal & pediatric respiratory care*. Delmar Publishers, Albany.

White JA, Beckett-Jones B, Guo YD, Dilworth FJ, Bonasoro J, Jones G, and Petkovich M (1997) cDNA cloning of human retinoic acid-metabolizing enzyme (hP450RAI) identifies a novel family of cytochromes P450. *J Biol Chem* **272:**18538-18541.

White JA, Ramshaw H, Taimi M, Stangle W, Zhang A, Everingham S, Creighton S, Tam SP, Jones G, and Petkovich M (2000) Identification of the human cytochrome P450, P450RAI-2, which is predominantly expressed in the adult cerebellum and is responsible for all-trans-retinoic acid metabolism. *Proc Natl Acad Sci U S A* **97:**6403-6408.

White RJ and Schilling TF (2008) How degrading: Cyp26s in hindbrain development. *Dev Dyn* **237:**2775-2790.

Xi J and Yang Z (2008) Expression of RALDHs (ALDH1As) and CYP26s in human tissues and during the neural differentiation of P19 embryonal carcinoma stem cell. *Gene Expr Patterns* **8:**438-442.

Yamamoto Y, Zolfaghari R, and Ross AC (2000) Regulation of CYP26 (cytochrome P450RAI) mRNA expression and retinoic acid metabolism by retinoids and dietary vitamin A in liver of mice and rats. *FASEB J* **14:**2119-2127.

Yashiro K, Zhao X, Uehara M, Yamashita K, Nishijima M, Nishino J, Saijoh Y, Sakai Y, and Hamada H (2004) Regulation of retinoic acid distribution is required for proximodistal patterning and outgrowth of the developing mouse limb. *Dev Cell* **6:**411-422.

Yu AM and Haining RL (2006) Expression, purification, and characterization of mouse CYP2d22. *Drug Metab Dispos* **34:**1167-1174.

Zhang H, Wu X, Wang H, Mikheev AM, Mao Q, and Unadkat JD (2008) Effect of pregnancy on cytochrome P450 3a and P-glycoprotein expression and activity in the mouse: mechanisms, tissue specificity, and time course. *Mol Pharmacol* **74:**714-723.

Zhang Y, Zolfaghari R, and Ross AC (2010) Multiple retinoic acid response elements cooperate to enhance the inducibility of CYP26A1 gene expression in liver. *Gene* **464:**32-43.

VITA

Ariel was born in Dallas, Texas and lived her early years in Panama before moving to Franklin, Indiana in 1993. She obtained her Bachelor of Science in Chemistry from Purdue University in 2003, and then worked in the Department of Clinical Pharmacology at the Indiana University School of Medicine where her research centered on the influence of CYP3A5 genetic differences on vincristine and vinorelbine therapies. She began as doctoral student under the guidance of Dr. Nina Isoherranen in the Department of Pharmaceutics at the University of Washington in 2008 where she studied the formation, elimination and biological activities of all-*trans*-retinoic acid metabolites.